12

DAHLGREN DIVISION
NAVAL SURFACE WARFARE CENTER
Dahlgren, Virginia 22448-5100

NSWCDD/TR-94/379

THE 1995 VERSION OF THE NSWC AEROPREDICTION CODE: PART I-SUMMARY OF NEW THEORETICAL METHODOLOGY

BY FRANK G. MOORE ROY M. MCINVILLE TOM HYMER

WEAPONS SYSTEMS DEPARTMENT

FEBRUARY 1995

Approved for public release; distribution is unlimited.

Transition Process for the 1995 Version of the Aeroprediction Code (AP95)

The AP95 consists of the AP93 extended in angle-of-attack above 30° to cover the flight envelope that most weapons fly from launch to impact. The AP95 will also consist of the pre- and post-processor software for use on personal computers, which is documented separately in a users guide.

Transition of the AP95 to U.S. Government agencies, U.S. contractors and universities will be free (like the AP93) to continue to encourage dual-use technology between government and industry and to encourage technology transition. To obtain a copy, please fill out the attached form and mail it to the address listed.

Foreign governments can also request copies of the Code by filling out the attached form and sending it to the address at the bottom of the form. A charge of $25,000 for the Code will be made. The rational for this charge to foreign countries is the fact that U.S. taxpayers have paid for the Code development, whereas foreign governments have not. The $25,000 is only a small fraction of the development cost of the Code.

Pre-approved countries for transition of the Code include NATO member nations plus Australia, Japan, Sweden, Switzerland, South Korea and Israel. Other countries requesting copies of the Code will be considered on a case by case basis by the sponsoring agency (Office of Naval Technology) and the Foreign Military Sales Office.

Since we are sending out a copy of the new code free of charge for most requests, we will not be able to provide the level of consulting that we would like to. However, we do request several things from the users. First, if you find an error in the Code, we would appreciate you bringing it to the attention of either Dr. Frank Moore at (703)663-8831, to Mr. Tom Hymer at (703)663-4164, or to Dr. Roy McInville at (703)663-4760. Secondly, if you find areas of success or areas of weakness, we would appreciate hearing from you. We use information such as this to help guide any future modifications. Thirdly, if you find areas where additional code capability would be desirable, again, we would like to hear from you. In all cases, a written letter is preferred, but a phone call is better than no communication at all. Also, if you use the Code for the purpose of comparing the results to other computations within the external literature, we would like you to use the terminology AP95. If you modify the AP95 to suit your own needs, you could refer to the Code as modified AP95. Finally, we request that you not send any copies of the Code to other agencies or even other activities in your company if it is at a different location. Please refer them to us so that we can keep track of copies of the Code. This is particularly true of foreign requests since they are now processed through the FMS Office and charged for copies of the Code.

AP95 Transition Request

NAME: _____

COMPANY NAME: _____

ADDRESS: _____

_____

_____

PHONE NUMBER: _____

GOVT CONTRACT NUMBER: _____

MEANS OF TRANSITION: 3.5" Diskettes plus User Guides

We agree to not give a copy of the AP95 to any other agency. We will refer them to NSWCDD at the address below for a copy.

Your Signature _____

Supervisor Signature _____

Please send this form completely filled out to:

Commander
Dahlgren Division
Naval Surface Warfare Center
Attn: Dr. Frank Moore (G04)
17320 Dahlgren Road
Dahlgren, VA 22448

We will try to get you a copy of the AP95 along with a user's guide within a month.

If the request is from a foreign country, please send a letter requesting a copy of the Code along with a copy of this form to:

Navy International Programs Office
Attn: IPO-02C (Mr. John Marini)
1111 Jefferson Davis Highway
Suite 701
Arlington, VA 22202-1111

A charge of $25,000 will be required before the Code is transitioned to a foreign country. This cost helps defray some of the R&D costs paid for by U.S. taxpayers.

FOREWORD

The 1993 version of the Aeroprediction Code (AP93) was limited to angles of attack (AOA) of 30 deg and to zero roll orientation ($\Phi = 0°$ for fins in plus-fin orientation). While this covers the flight conditions that some missiles fly, other weapons require a broader set of conditions. For example, during vertical launch from a ship or from an aircraft pulling maximum maneuvers, AOA can exceed 60 to 70 deg, at subsonic Mach numbers. During terminal maneuvers at supersonic speeds, AOA can approach 40 deg. This report documents new technology developed to extend the AP93 to AOA that cover all weapons in stable flight at zero roll. This new technology has been integrated into a user friendly, interactive, personal computer version of the Aeroprediction Code and will be transitioned to users during FY95 as AP95.

The work described in this report was supported through the Office of Naval Research (Mr. Dave Siegel) by the Air Launched Weapons Program managed at the Naval Air Warfare Center, China Lake, California, by Mr. Tom Loftus and Dr. Craig Porter and by the Surface Weapons Systems Technology Program managed at the Naval Surface Warfare Center, Dahlgren Division (NSWCDD) by Mr. Robin Staton and Mr. Gil Graff. Also, support was provided by the AEGIS LEAP Program Office at NSWCDD by Mr. George Long. The authors express their appreciation to these individuals for their support in this work.

Approved by:

David S. Malyevac

DAVID S. MALYEVAC, Deputy Head
Weapons Systems Department

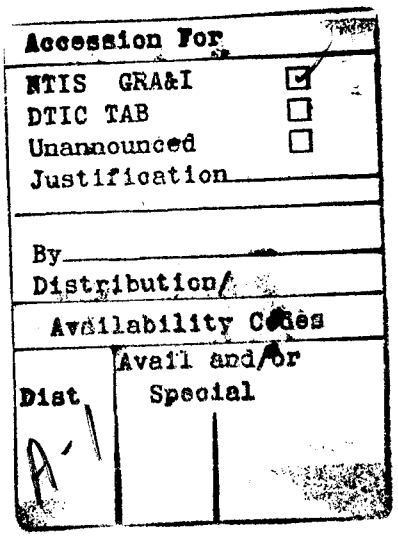

ABSTRACT

The NSWC Aeroprediction Code has been extended to angles of attack (AOA) greater than 30 deg. To accomplish this, several data bases were used to approximate the nonlinearities in individual missile component aerodynamics. Theoretical aerodynamic methods are used at small AOA. The new semiempirical model was applied to several configurations and the empirical constants adjusted to eliminate some of the errors associated with wind tunnel measurements of individual missile component loads.

The new version of the code (AP95) was then applied to several other missile configurations and estimates compared to data and other aerodynamic code calculations. Comparisons were made for Mach numbers 0.1 to 10.0 and AOA of 0 to 90 deg (not all data were available on any single configuration). In general, average accuracy levels of ±10 percent could be obtained for axial and normal force coefficient and ±4 percent of body length for center of pressure, using the AP95. An exception to this was at AOA above 30 deg and at high supersonic Mach numbers, where nonlinearities caused by internal shock interactions were not accounted for. While these accuracy levels are very encouraging for a semiempirical code, improvements in the AP95 methodology could be made by additional missile-component wind-tunnel data at high AOA.

CONTENTS

SECTION	Page
1.0 INTRODUCTION	1
2.0 ANALYSIS	2
2.1 BODY ALONE	6
2.2 WING ALONE	13
2.3 INTERFERENCE FACTORS	15
2.3.1 Data Bases Used	15
2.3.2 Accuracy Analysis	21
2.3.3 Wing-Body and Body-Wing Interference Due to AOA Experimental Results	24
2.3.4 Mathematical Model for $K_{W(B)}$ and $K_{B(W)}$	31
2.3.5 Interference Factor Due to Control Deflection and Wing-Tail Interference	45
2.3.6 Treatment of Linear Aerodynamics at High AOA	46
2.4 NONLINEARITIES NOT MODELED COMPLETELY	46
3.0 RESULTS AND DISCUSSION	50
3.1 CONFIGURATIONS WITHIN THE DATA BASE	51
3.2 CONFIGURATIONS OUTSIDE THE DATA BASE	52
4.0 SUMMARY AND RECOMMENDATIONS	79
5.0 REFERENCES	80
6.0 SYMBOLS AND DEFINITIONS	82
DISTRIBUTION	(1)

ILLUSTRATIONS

Figure		Page
1	DESIRED OPERATIONAL ENVELOPE FOR AEROPREDICTION CODE VERSUS AP93 CAPABILITY	2
2	CLASSIFICATION OF MISSILE AERODYNAMICS AS A FUNCTION OF M_∞ AND $\propto$	3
3	MODELING OF NONLINEARITIES IN MISSILE AERODYNAMICS	5
4	CROSSFLOW DRAG COEFFICIENT AS A FUNCTION OF EFFECTIVE REYNOLDS NUMBER	8
5	VARIATION OF CROSSFLOW DRAG COEFFICIENT WITH CROSSFLOW MACH NUMBER	9
6A	COMPUTED AND EXPERIMENTAL VALUES OF NORMAL FORCE COEFFICIENT AS A FUNCTION OF AOA	9
6B	COMPUTED AND EXPERIMENTAL VALUES OF NORMAL FORCE COEFFICIENT AS A FUNCTION OF AOA FOR A BODY-ALONE CONFIGURATION AT $M_\infty = 0.15$	10
7A	MODELS USED IN LANGLEY[9] WING-BODY TESTS	19
7B	MODELS USED IN STALLINGS AND LAMB[10] WING-ALONE TESTS	19
8	MODELS USED IN MEYER'S[16] WING-BODY TESTS	20
9	ACCURACY ESTIMATION ASSUMPTIONS FOR $K_{W(B)}$ AND $K_{B(W)}$	22
10	ACCURACY ESTIMATES FOR $K_{W(B)}$ AND $K_{B(W)}$ (IN PERCENT)	23
11	WING-BODY AND BODY-WING INTERFERENCE LIFT FACTORS AS A FUNCTION OF AOA ($M_\infty = 0.1$, r/s = 0.25)	25

ILLUSTRATIONS (Continued)

Figure		Page
12	WING-BODY AND BODY-WING INTERFERENCE FACTORS AS A FUNCTION OF AOA ($M_\infty = 0.6$)	26
13	WING-BODY AND BODY-WING INTERFERENCE FACTORS AS A FUNCTION OF AOA ($M_\infty = 0.8$)	26
14	WING-BODY AND BODY-WING INTERFERENCE FACTORS AS A FUNCTION OF AOA ($M_\infty = 1.2$)	27
15	WING-BODY AND BODY-WING INTERFERENCE FACTORS AS A FUNCTION OF AOA ($M_\infty = 1.5$)	27
16	WING-BODY AND BODY-WING INTERFERENCE FACTORS AS A FUNCTION OF AOA ($M_\infty = 2.0$)	28
17	WING-BODY AND BODY-WING INTERFERENCE FACTORS AS A FUNCTION OF AOA ($M_\infty = 2.5$)	28
18	WING-BODY AND BODY-WING INTERFERENCE FACTORS AS A FUNCTION OF AOA ($M_\infty = 3.0$)	29
19	WING-BODY AND BODY-WING INTERFERENCE FACTORS AS A FUNCTION OF AOA ($M_\infty = 3.5$)	29
20	WING-BODY AND BODY-WING INTERFERENCE FACTORS AS A FUNCTION OF AOA ($M_\infty = 4.5$)	30
21	WING-BODY AND BODY-WING INTERFERENCE FACTORS AS A FUNCTION OF AOA ($M_\infty = 0.6$)	32
22	WING-BODY AND BODY-WING INTERFERENCE FACTORS AS A FUNCTION OF AOA ($M_\infty = 0.8$)	32
23	WING-BODY AND BODY-WING INTERFERENCE FACTORS AS A FUNCTION OF AOA ($M_\infty = 1.2$)	33
24	WING-BODY AND BODY-WING INTERFERENCE FACTORS AS A FUNCTION OF AOA ($M_\infty = 1.5$)	33

ILLUSTRATIONS (Continued)

Figure		Page
25	WING-BODY AND BODY-WING INTERFERENCE FACTORS AS A FUNCTION OF AOA ($M_\infty = 2.0$)	34
26	WING-BODY AND BODY-WING INTERFERENCE FACTORS AS A FUNCTION OF AOA ($M_\infty = 2.5$)	34
27	WING-BODY AND BODY-WING INTERFERENCE FACTORS AS A FUNCTION OF AOA ($M_\infty = 3.0$)	35
28	WING-BODY AND BODY-WING INTERFERENCE FACTORS AS A FUNCTION OF AOA ($M_\infty = 3.5$)	35
29	WING-BODY AND BODY-WING INTERFERENCE FACTORS AS A FUNCTION OF AOA ($M_\infty = 4.5$)	36
30	GENERIC REPRESENTATION OF $K_{W(B)}$ WITH AOA ($\Phi = 0°$)	36
31	GENERIC REPRESENTATION OF $K_{B(W)}$ WITH AOA ($\Phi = 0°$)	40
32	MINIMUM VALUE OF BODY-WING INTERFERENCE FACTOR AT HIGH AOA	44
33	NONLINEAR WING-BODY INTERFERENCE MODEL FOR CONTROL DEFLECTION	47
34	LINEARIZED AERO TREATMENT AS $\propto$ INCREASES	48
35	ILLUSTRATION OF SOME INTERNAL SHOCK INTERACTIONS	50
36	COMPARISON WITH EXPERIMENTAL RESULTS INSIDE DATA BASE	51
37A	BUTLER, SEARS, AND PALLAS[22] WIND TUNNEL MODEL TESTED	53
37B	VARIATION OF FOREBODY AXIAL FORCE COEFFICIENT WITH MACH NUMBER FOR VARIOUS NOSES ON 10-CAL AFTERBODY (R_N/ft = 1.8 X 10^6, ℓ_N = 2 cal)	55

ILLUSTRATIONS (Continued)

Figure		Page
37C	VARIATION OF FOREBODY AXIAL FORCE COEFFICIENT WITH MACH NUMBER FOR VARIOUS NOSES ON 10-CAL AFTERBODY (R_N/ft = 1.8 X 10^6, ℓ_N = 4 cal)	56
38A	BODY-DORSAL-TAIL CONFIGURATION USED FOR COMPARING ZEUS, AP95, AND AP93 COMPUTATIONS	57
38B	NORMAL FORCE COEFFICIENT AND CENTER OF PRESSURE COMPARISONS OF THREE ANALYTICAL METHODS FOR BODY-TAIL OF FIGURE 38A	58
38C	NORMAL FORCE COEFFICIENT AND CENTER OF PRESSURE COMPARISONS OF THREE ANALYTICAL METHODS FOR CONFIGURATION OF FIGURE 38A	59
39A	WING-BODY AND WING-BODY-TAIL CONFIGURATIONS USED FOR COMPARING AP95 TO EXPERIMENT AND AP93	60
39B	NORMAL FORCE COEFFICIENT COMPARISONS FOR BODY-TAIL CONFIGURATION OF FIGURE 39A	61
39C	NORMAL FORCE COEFFICIENT AND CENTER OF PRESSURE COMPARISONS FOR CONFIGURATION OF FIGURE 39A	62
40A	CANARD-CONTROLLED MISSILE CONFIGURATION[24]	64
40B	COMPARISON OF AXIAL, NORMAL AND PITCHING MOMENT COEFFICIENTS BETWEEN EXPERIMENT, MISSILE DATCOM AND AP95 FOR FIGURE 40A CONFIGURATION (δ = -20°)	65
40C	COMPARISON OF AXIAL, NORMAL AND PITCHING MOMENT COEFFICIENTS BETWEEN EXPERIMENT, MISSILE DATCOM AND AP95 FOR FIGURE 40A CONFIGURATION (δ = 0°)	66
40D	COMPARISON OF AXIAL, NORMAL AND PITCHING MOMENT COEFFICIENTS BETWEEN EXPERIMENT, MISSILE DATCOM AND AP95 FOR FIGURE 40A CONFIGURATION (δ = +20°)	67

ILLUSTRATIONS (Continued)

Figure		Page
41A	MMPT CONFIGURATION TESTED AT $M_\infty = 0.2$ (FROM SMITH, SALAZAR, ET AL.[25])	68
41B	COMPARISON OF STATIC AERODYNAMIC COEFFICIENTS BETWEEN EXPERIMENT AND PREDICTIONS FOR CONFIGURATION OF FIGURE 41A	69
42	NORMAL FORCE COEFFICIENT COMPARISONS OF HOWARD AND DUNN[26] CONFIGURATION	70
43A	AIR-TO-AIR MISSILE CONFIGURATION USED IN VALIDATION PROCESS[27,28]	72
43B	STATIC AERODYNAMIC COEFFICIENT COMPARISONS FOR FIGURE 43A CONFIGURATION ($M_\infty = 1.5$)	73
43C	STATIC AERODYNAMIC COEFFICIENT COMPARISONS FOR FIGURE 43A CONFIGURATION ($M_\infty = 2.0$)	74
43D	STATIC AERODYNAMIC COEFFICIENT COMPARISONS FOR FIGURE 43A CONFIGURATION ($M_\infty = 2.87$)	75
43E	STATIC AERODYNAMIC COEFFICIENT COMPARISONS FOR FIGURE 43A CONFIGURATION ($M_\infty = 3.95$)	76
43F	STATIC AERODYNAMIC COEFFICIENT COMPARISONS FOR FIGURE 43A CONFIGURATION ($M_\infty = 2.3$)	77
43G	STATIC AERODYNAMIC COEFFICIENT COMPARISONS FOR FIGURE 43A CONFIGURATION ($M_\infty = 4.6$)	78

TABLES

Table		Page
1	SHIFT IN BODY-ALONE CENTER OF PRESSURE AS A FUNCTION OF MACH NUMBER AND AOA (AS A FRACTION OF BODY LENGTH)	12
2	VALUES OF $(C_{N_w})_{\alpha=15°}$	16
3	VALUES OF $(C_{N_w})_{\alpha=35°}$	17
4	VALUES OF $(C_{N_w})_{\alpha=60°}$	18
5	DATA FOR $[\Delta K_{W(B)}]_{\alpha=0}$	37
6	DATA FOR α_C (deg)	37
7	DATA FOR $[K_{W(B)}]_{\alpha=\alpha_D}$	38
8	DATA FOR α_D (deg)	38
9	DATA FOR α_M (deg)	39
10	DATA FOR $[\Delta K_{B(W)}]_{\alpha=0}$	42
11	DATA FOR $dK_{B(W)}/d\alpha$ (per deg)	42
12	DATA FOR α_1 (deg)	43
13	DATA FOR α_2 (deg)	43

1.0 INTRODUCTION

Estimating missile aerothermodynamics over the flight regime where missiles fly is quite important in all phases of design. These aerodynamics are used by the flight dynamicist to estimate range performance and miss distance; the heating information is used to perform heat transfer analysis; and the aerodynamic and thermodynamic loads are used by the structural engineer to estimate structural integrity of the configuration. Missiles that are launched from a vertical launcher can experience Angles of Attack (AOA) approaching 90 deg if a strong crosswind is present. Missiles that are launched from aircraft undergoing maneuvers can also experience AOA approaching 60 deg. Finally, terminally guided missiles undergoing maneuvers in the endgame can anticipate AOA as high as 40 deg. Hence, it is necessary to have aerodynamics estimates above 30 deg AOA to cover the flight regime for all possible conditions. Figure 1 is an operational envelope for an aeroprediction code that, hopefully, will cover all possible conditions in AOA and Mach number for missiles in stable flight.

The recent version of the NSWCDD Aeroprediction Code (AP93) released to the public[1-3] was limited to AOA of about 30 deg because the wing-alone, wing-body, and body-wing interference aerodynamics were developed only to about 30 deg AOA (dotted line in Figure 1). In some cases, the accuracy degraded at an AOA of 25 deg. The wing-alone methodology was recently extended by Moore and McInville[4] to AOA of 180 deg by developing a new fourth-order method versus a second-order technique used in the AP93. The fourth-order method was shown to give improved accuracy over the second-order technique in the AOA range 0 to 30 deg, in addition to extending the AOA range to 180 deg.[4] This report develops the complementary extension of the body-alone and interference factor methodology above AOA of 30 deg. This new technology, along with that in the Moore and McInville study, will allow the AP93 code to be extended in AOA capability so the entire AOA boundary of Figure 1 can be covered. This new version of the code will be called AP95 since it will be transitioned to users during Fiscal Year 1995.

While the extension to higher AOA represents a significant step forward in modeling nonlinearities in an engineering version of an aeroprediction code, it should be emphasized that there are still several nonlinearities not modeled or modeled only approximately in AP95. These include roll-dependent or cross-coupling aerodynamics effects; asymmetric body-shed vortices, which occur for $M_\infty < 2$ and AOA between about 20 and 60 deg; and internal shock interactions from the nose to the tail or wing, or from the wing to the tail. These latter effects typically occur above AOA of about 30 deg and at supersonic or hypersonic Mach numbers. These phenomena will be discussed more fully in the section that follows.

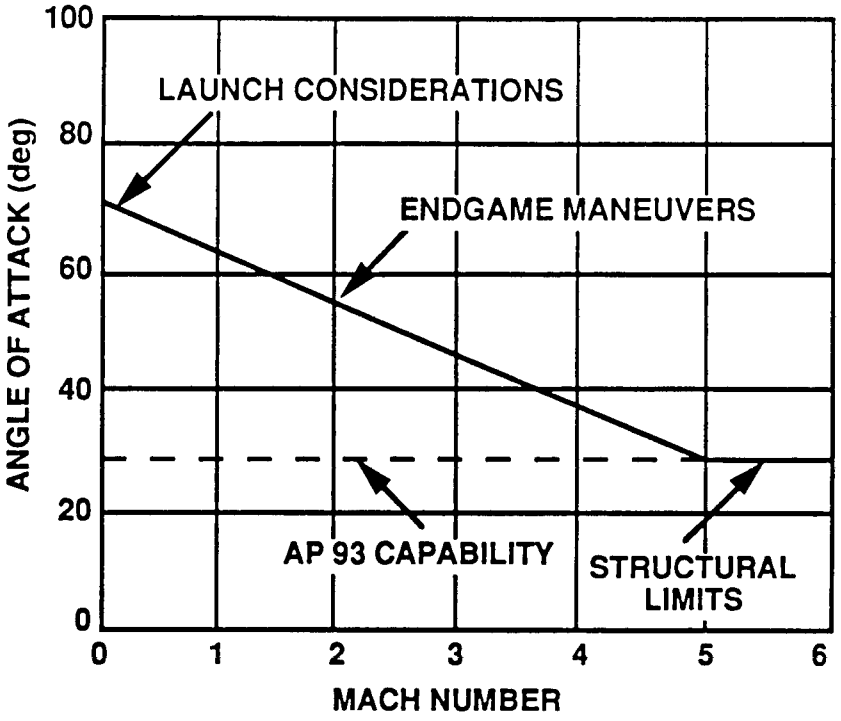

FIGURE 1. DESIRED OPERATIONAL ENVELOPE FOR AEROPREDICTION CODE VERSUS AP93 CAPABILITY

2.0 ANALYSIS

The physical phenomena involved in missile aerodynamics should be examined before proceeding with the development of nonlinear methods for high AOA. Figure 2 attempts to describe missile aerodynamics in a generic way as a function of the AOA and Mach number regions desired from an operational standpoint in Figure 1. At low AOA, the aerodynamics are mostly linear (except for transonic flow), and linearized and slender-body aerodynamic methods prove very effective in providing acceptable accuracy for approximate aerodynamic prediction codes.[5] As AOA increases above 10 deg, the nonlinearities associated with AOA become increasingly important at all Mach numbers, and the nonlinear compressibility effects become important above $M_\infty \approx 0.6$. Linearized codes can still be used in the range $10° < \alpha < 20°$, but with degraded accuracy. As AOA increases above 20 deg, the flow becomes strongly nonlinear but still reasonably well behaved in terms of static aerodynamics as a function of AOA. At these AOA, nonlinear aerodynamic methods are required for reasonable accuracy. For approximate aerodynamic codes, these nonlinear methods are typically empirical or semiempirical.[1,6,7]

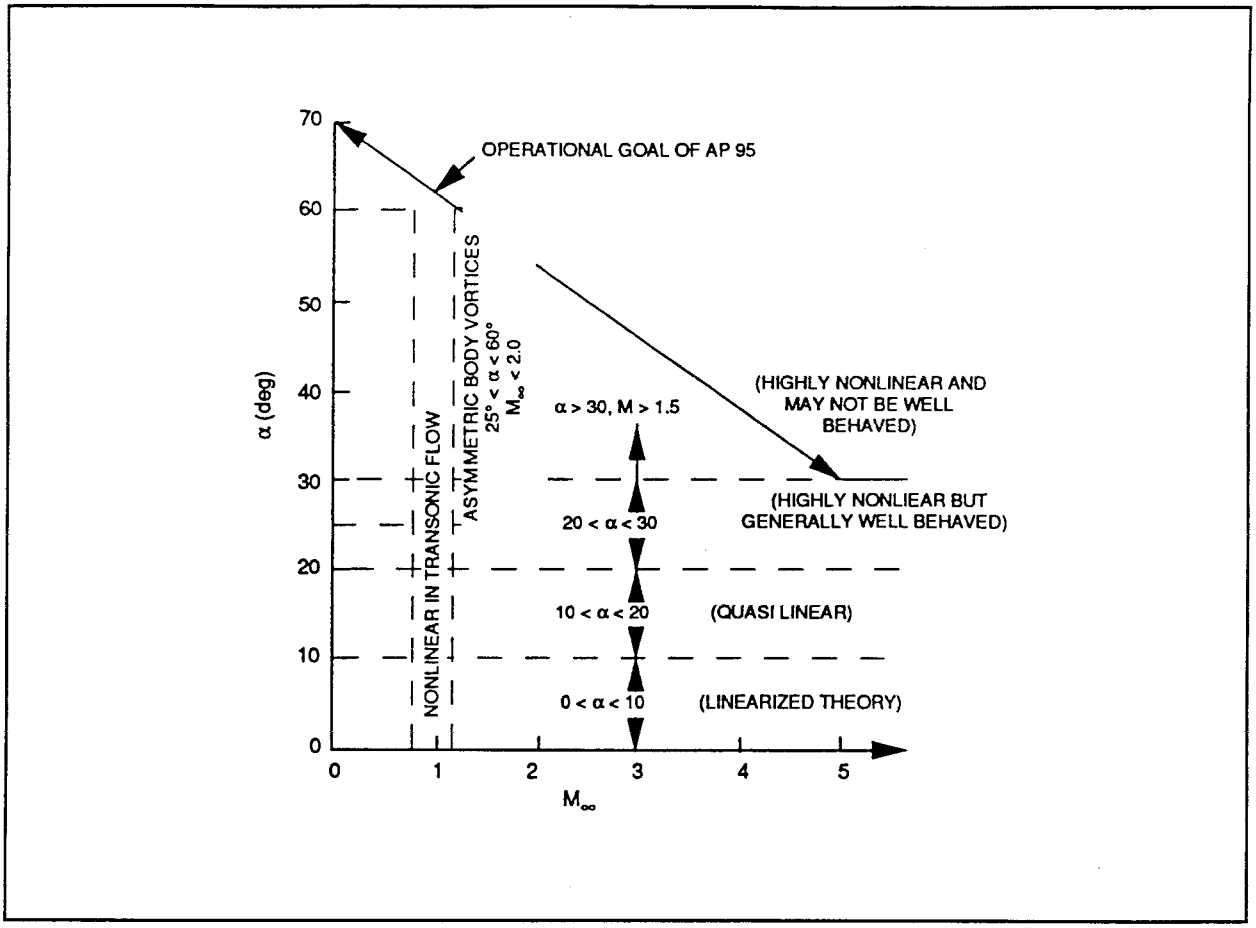

FIGURE 2. CLASSIFICATION OF MISSILE AERODYNAMICS AS A FUNCTION OF M_∞ AND α

Above α of about 25 deg and below M_∞ of about 2, another nonlinear phenomenon occurs on many configurations because of the asymmetric shedding of body vortices. This phenomenon is the strongest in the subsonic Mach number range and starts to dissipate at crossflow Mach numbers of about 0.5.[8] While the phenomenon is reasonably well understood, it is predictable in the general sense only in terms of upper bounds on side forces created by the shedding. Forward placed fins or control surfaces tend to minimize the effect.

Above α of about 30 deg and $M_\infty \approx 2.0$, strong shock interactions can cause very strong effects on the aerodynamics. These effects exhibit themselves in the form of loss of static stability and normal force. Typical shocks of interest are the bow shock intersecting a control surface or a forward lifting surface shock intersecting a tail surface. The latter problem appears to be more critical since the moment arm to the tail is generally longer than to the wing or canard. Aerodynamics in this region may not be well behaved in terms of either monotonically increasing or decreasing.

The question arises as to whether the databases that will be used to estimate the nonlinear aerodynamic phenomena will provide acceptable results. For a body-alone configuration at low Mach numbers, the normal force will vary somewhat because of the presence of the side force, but basically can be estimated with reasonable accuracy if boundary layer transition in the crossflow plane is predicted accurately. For Mach numbers approaching 2 and greater, past attempts have

shown the methods used in AP93 to be directly applicable at higher AOA with few changes.[1] However, these methods were based on empirical approximations to the nonlinearities occurring to the wing, body, and wing-body interference based on a component build-up data base.[9,10] This data base had various size wings with a single body. Hence, no wing-tail shock interactions or wing-tail interference could be estimated directly. In summary, it is anticipated that all the nonlinearities in missile aerodynamics except the internal shock interaction of the wing and tail and wing-tail interference can be approximately accounted for using the available data bases. The body side force at low Mach number will not be approximated since only in-plane aerodynamics ($\Phi = 0$) are being considered. The high AOA canard or wing-shed vortex and control-deflection effects can be approximately modeled with empirical experiments compared to other data bases.[1]

Figure 3 is a summary of the nonlinear phenomena and the way they are modeled in the AP93. The analysis sections that follow will expand upon these methods to allow the AOA boundaries of Figure 1 to be available for flow computations. It should be pointed out at the outset, however, that by extending the flow computations into the "highly nonlinear, may-not-be-well-behaved" region of Figure 2, the accuracy available in the AP93 for the $\alpha \leq 30$ deg cases may be somewhat degraded. On average, these accuracy levels were ±10 percent on C_A and C_N and ±4 percent ℓ on X_{CP}. There were cases where these accuracy bounds were exceeded at a given α and M. However, when all α and M cases were averaged for a given configuration, these accuracy bounds were found to hold.

The total normal force equation[12] for a wing-body-tail configuration at a given AOA, control deflection, and Mach number is

$$C_N = C_{N_B} + \left[\left(K_{W(B)} + K_{B(W)}\right) \alpha + \left(k_{W(B)} + k_{B(W)}\right) \delta_W \right] \left(C_{N_\alpha}\right)_W$$

$$+ \left[\left(K_{T(B)} + K_{B(T)}\right) \alpha + \left(k_{T(B)} + k_{B(T)}\right) \delta_T \right] \left(C_{N_\alpha}\right)_T + C_{N_{T(V)}} \qquad (1)$$

The first term in Equation (1) is the normal force of the body alone including the linear and nonlinear components; the second term is the contribution of the wing (or canard) including interference effects and control deflection; the third term is the contribution of the tail including interference effects and control deflection; and the last term is the negative downwash effect on the tail resulting from wing-shed or body-shed vortices. The uppercase K represents the interference of the configuration with respect to AOA, and the lowercase k represents the interference with respect to control deflection. The subscripts W(B) and T(B) represent the change (or interference effect) of the wing and tail in the presence of the body, whereas the subscripts B(W) and B(T) indicate the additional lift (or interference effect) on the body because of the presence of wings or tails. When Equation (1) was originally defined, it was associated with the linear aerodynamics only.[12]

NONLINEAR PHENOMENA	METHOD OF MODELING ANALYTICAL	EMPIRICAL	NOT MODELED
1. LOW α COMPRESSIBILITY EFFECTS	X	X (TRANSONIC ONLY)	
2. BASE DRAG		X	
3. LOW α CANARD SHED VORTICES	X		
4. HIGH α CANARD SHED VORTICES		X	
5. BODY ALONE NONLINEAR LIFT	X		
6. WING ALONE NONLINEAR LIFT		X	
7. WING BODY AND BODY WING INTERFERENCE DUE TO α			
• LOW α	X		
• HIGH α		X	
8. WING BODY INTERFERENCE DUE TO CONTROL DEFLECTION			
• LOW / α + δ /	X		
• HIGH / α + δ /		X	
9. ROLL DEPENDENT AND CROSS COUPLING EFFECTS			X
10. LOSS OF NONLINEAR LIFT OF WINGS IN TRANSONIC FLOW		X	
11. BODY VORTEX EFFECTS AT HIGH α		X	
12. HIGH MACH INTERNAL SHOCK INTERACTIONS		ONLY PARTLY IN $K_{W(B)}$ AND $K_{B(W)}$	ASYMMETRIC BODY VORTICES

FIGURE 3. MODELING OF NONLINEARITIES IN MISSILE AERODYNAMICS

The way Equation (1) is implemented in the AP93 is similar, except each of the terms has a linear and a nonlinear component.[1] The nonlinear components of the wing and tail lift and interference factors are calculated based on a local AOA of $\propto + \delta$ as opposed to $\propto$ or δ alone. Also, the derivatives are simply secant slopes; i.e.,

$$C_{N_{\propto}} = C_N/\propto$$

Hence, for ease of implementation into an existing code, actual force terms are computed and the secant slopes computed.

The remaining discussion in this section will deal with the modifications to each of the nonlinear components of the terms in Equation (1) that allow extension of this equation above $\propto = 30$ deg. Because of inaccuracies in the component data bases, the wing-alone and interference terms had to be adjusted when the overall nonlinear mathematical model was applied to several complete missile configurations. For this reason, a discussion of errors in the data bases is included later in this section. Also, in the discussion of each aerodynamic component, mention will be made when the component data bases had to be modified to allow accurate estimation of overall missile configuration static aerodynamics.

In summary, the overall analysis approach to the development of a nonlinear high AOA aeroprediction code is as follows:

a) Use linear theory (LT)/slender-body theory (SBT)/second-order methods primarily for low AOA ($\propto \leq 10$ deg).
b) Use missile component data bases to develop empirical estimates of component aerodynamics.
c) Develop mathematical models for these empirical, high AOA methods when feasible.
d) Apply the methods to overall missile configurations outside the data base and adjust the parameters in the mathematical model to try to minimize errors in the data bases.

2.1 BODY ALONE

The primary focus in the body-alone work has been an attempt to improve the modeling of the nonlinear normal force at crossflow Mach numbers (M_C) below 0.6, to include compressibility effects in the laminar-skin friction drag computation and to improve upon the center of pressure caused by the nonlinear aerodynamics. Each of these improvements will be considered separately.

The nonlinear contribution to the normal force is generally expressed as

$$C_{N_{NL}} = \eta C_{D_C} A_P/A_{REF} \sin^2 \propto \qquad (2)$$

where C_{D_C} is the crossflow drag coefficient; A_P and A_{REF} are the body longitudinal planform area and the reference area, respectively; $\propto$ is the AOA; and η is a parameter used to compensate for the fact that the body is not an infinite cylinder, but has a finite length. As explained in detail in a study by Ericsson and Reding[8] and one by Jorgenson,[13] C_{D_C} varies in a complex fashion for $M_C < 0.5$. Below a certain critical Reynolds number (Re_{CRIT}), the body boundary layer is laminar and the flow separates at about the 90- to 100-deg circumferential location (where $\Phi = 0$ deg is the leeward plane) producing a large wake region and a relatively constant value of C_{D_C}. At Re_{CRIT}, the separated boundary layer transitions to turbulent and reattaches, remaining attached until approximately the 40-deg circumferential location (140 deg from the windward plane). The resulting smaller wake produces a sudden decrease in the value of C_{D_C}. As the Reynolds number increases further, transition moves forward and the laminar separation bubble disappears leading to an eventual stabilization of C_{D_C} as the turbulent separation becomes fixed at about the 80-deg location. At crossflow Mach numbers greater than 0.5, localized supersonic regions develop as the flow expands around the body. The shocks that are produced by these supersonic pockets are strong enough to separate the boundary layer regardless of its laminar or turbulent state, and the "drag bucket" disappears, leaving C_{D_C} virtually independent of the state of the boundary layer.

As pointed out in the Ericsson and Reding study,[8] the observed value of Re_{CRIT} can vary drastically from test to test and from one wind tunnel to another because of a number of factors including tunnel turbulence, wall and model roughness, and model vibration. In fact, over an order-of-magnitude difference has been found using the same model in different wind tunnels.

The C_{D_c} model that has been incorporated into AP95 was developed primarily using the data from a NASA Langley Research Center study[9] with added input from the Jorgenson study.[13] The Langley body-alone data were obtained using a model with a 3.0-cal tangent ogive nose and an overall length of 12.33 cal. Body diameter was 3.0 in. The Jorgenson data represent measurements on two configurations. One has a 2.5-cal ogive nose and a total length of 9.5 cal. The other has a 3.5-cal ogive nose and a total length of 10.5 cal. The body diameter in both cases is 1.5 in. Freestream Mach numbers ranged from 0.6 to 1.2 and AOA varied from 5 deg up to 60 deg. Since only total C_N values were given, C_{D_c} was extracted by first subtracting the linear component as determined by SBT, for simplicity. Equation (2) was then used to compute C_{D_c}, with the value of η coming from Jorgenson.

The resulting C_{D_c} values were plotted in two different fashions. First, a plot showing their relationship to Reynolds number was generated. Instead of the crossflow Reynolds number, an effective value intended to produce superior correlation of data was used.[8] This Reynolds number was defined by

$$Re_{EFF} = \frac{1}{2} Re_D \left\{ \frac{\cos\alpha\cot\alpha + 2\sin\alpha}{2} \right\} \left\{ \frac{1 + [1 + (1/2\cot\alpha)^2]^{1/2}}{[1 + (1/2\cot\alpha)^2]^{1/2}} \right\} \tag{3}$$

where Re_D is the Reynolds number based on the body diameter. This plot is shown in Figure 4. With the exception of the Jorgenson[13] data for the 2.5-cal nose case, there is fairly good correlation, as indicated by the superimposed dashed curve, to a critical Reynolds number of approximately 400,000. The degree of scatter present is not unexpected given the conditions discussed previously. The lack of general agreement of the one data set could be an extreme case of the expected scatter or it could be the result of errors in the C_{D_c} extraction process. The available information[13] was sketchy and some assumptions were made which may not have been correct. In any event, the Re_{CRIT} value of 400,000 is higher than that indicated in Ericsson and Reding[8] by a factor of 4 and about twice that shown in Jorgenson. It is, however, well within the possible order-of-magnitude variation referenced previously. In addition, it is fairly close to the theoretical two-dimensional value of 330,000. Thus, it would seem that the extracted C_{D_c} values represent a reasonable data base from which to work.

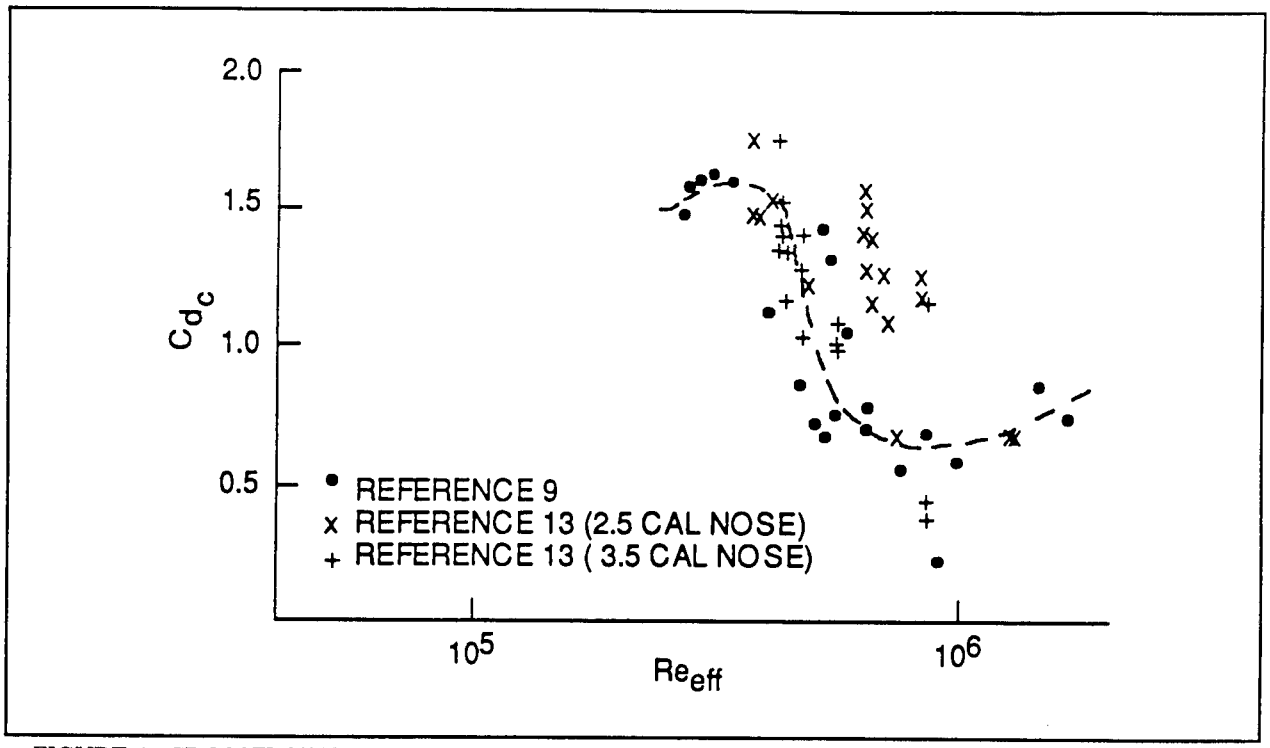

FIGURE 4. CROSSFLOW DRAG COEFFICIENT AS A FUNCTION OF EFFECTIVE REYNOLDS NUMBER

The second plot of the extracted C_{D_c} values shows their variation with crossflow Mach number and is shown in Figure 5. Note the presence of a well-defined "drag bucket" at the lower crossflow Mach numbers. There is little, if any, data from the present cases to define the upper branch of the C_{D_c} curve since it applies only for subcritical Reynolds numbers, and the conditions of the Langley[9] and Jorgenson[13] studies produced, for the most part, supercritical situations. The upper branch of the C_{D_c} curve can be drawn on the plot with reasonable certainty because it is known to be basically a constant value of 1.2 for crossflow Mach numbers below 0.4. When plotting the dashed curve through the data points, emphasis was given to the Langley information since it seemed to be better organized. This resulted in a location for the lower branch of the curve that is shifted slightly toward lower M_C values, more so than that shown in Jorgenson, extending from $0.03 \leq M_C \leq 0.4$ rather than from $0.1 \leq M_C \leq 0.5$. In addition, the lowest C_{D_c} values are about 0.55 as opposed to 0.25 in the Jorgenson study. (Note that the dashed curve in Figure 5 does not simply represent a best fit through the data points. It has been adjusted to give minimum errors for the Langley data in the computational procedure described below.)

The methodology incorporated into AP95 for computing nonlinear body-alone normal force for $M_C < 0.5$ is based on Figure 5. First the flow is determined to be subcritical or supercritical by computing the equivalent Reynolds number using Equation (3). If this Re_{EQ} is above a specified critical value, Re_{CRIT}, then the lower branch of Figure 5 is used to determine C_{D_c} at the given M_C. If Re_{EQ} is below Re_{CRIT}, the upper branch of the curve is used. As mentioned in the previous paragraph, the final form of the C_{D_c} curve in Figure 5 was obtained by setting up this procedure in AP95 and using it to compute the normal force for the Langley[9] cases. The curve was then adjusted to give the best fit to the data at freestream Mach numbers of 0.6, 0.8, and 1.2. Above crossflow Mach numbers of 0.5, the curves are basically unchanged from the AP93 version of the code. The

final computed results along with the experimental data are shown in Figure 6A. The agreement is good, with deviations being less than 10 percent in almost all instances.

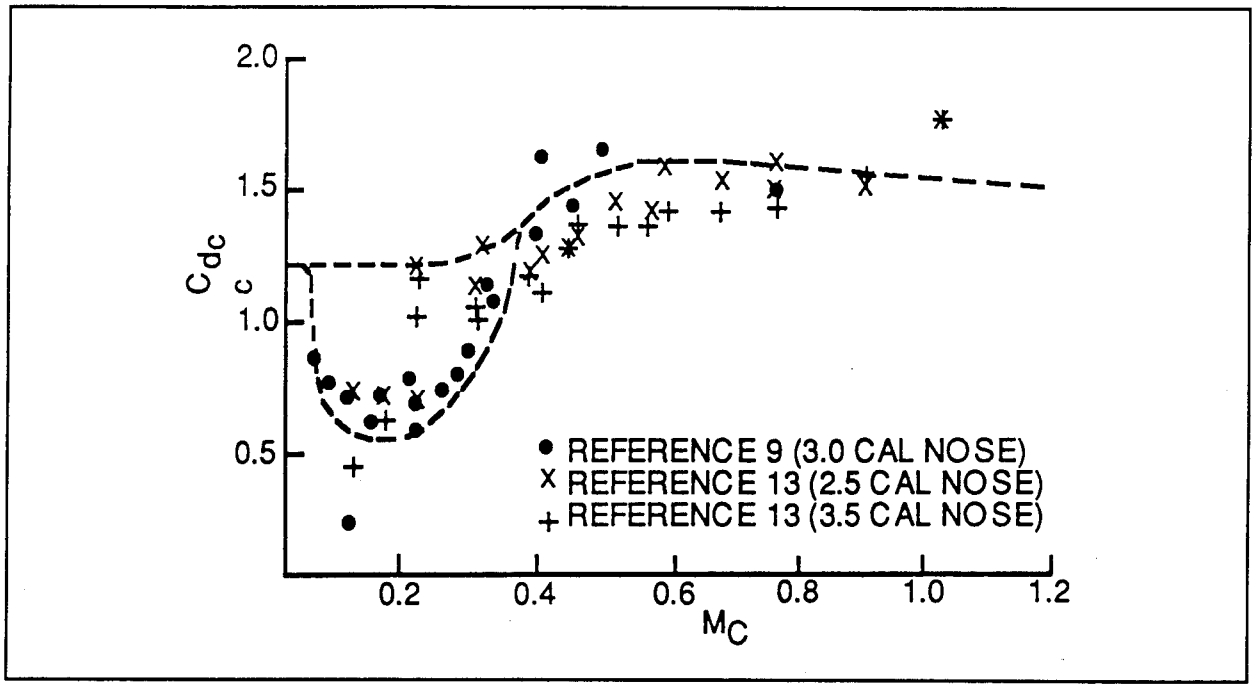

FIGURE 5. VARIATION OF CROSSFLOW DRAG COEFFICIENT WITH CROSSFLOW MACH NUMBER

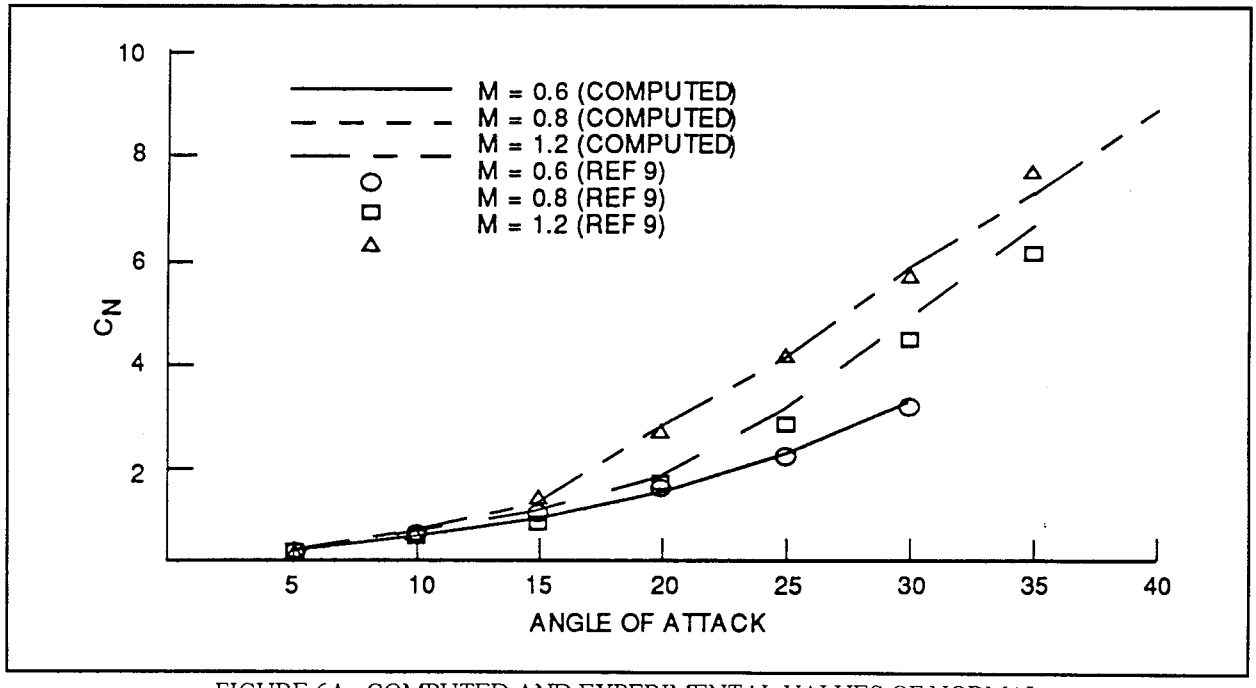

FIGURE 6A. COMPUTED AND EXPERIMENTAL VALUES OF NORMAL FORCE COEFFICIENT AS A FUNCTION OF AOA

Because of the variation of transition-linked phenomena with test conditions, Re_{CRIT} can be adjusted in the AP95 input file. Its default value is the theoretical two-dimensional cylinder result of 330,000. In addition, the location of the "drag bucket" can be shifted horizontally by specifying a second input parameter. The results of this procedure can be seen in Figure 6B where the new method is applied to the body-alone configuration which has a 2.7-cal tangent ogive nose and a total length of 20.0 cal.[14] If the baseline C_{D_c} curve is used, the results are much too low, as shown by the dashed line. If the lower branch is shifted to the right by 0.1 on the M_C axis, the very good results shown by the solid line are obtained. In this instance, the crossflow Mach number is apparently low enough to stay on the upper supercritical branch of the shifted drag curve. The required shift to a higher M_C limit for subcritical flow in this instance could be the result of an exceptionally smooth model or a very quiet wind tunnel or a combination of both. Figure 6B illustrates the extreme sensitivity of body-alone normal force for low Mach number, low crossflow Mach number, and different wind tunnel effects.

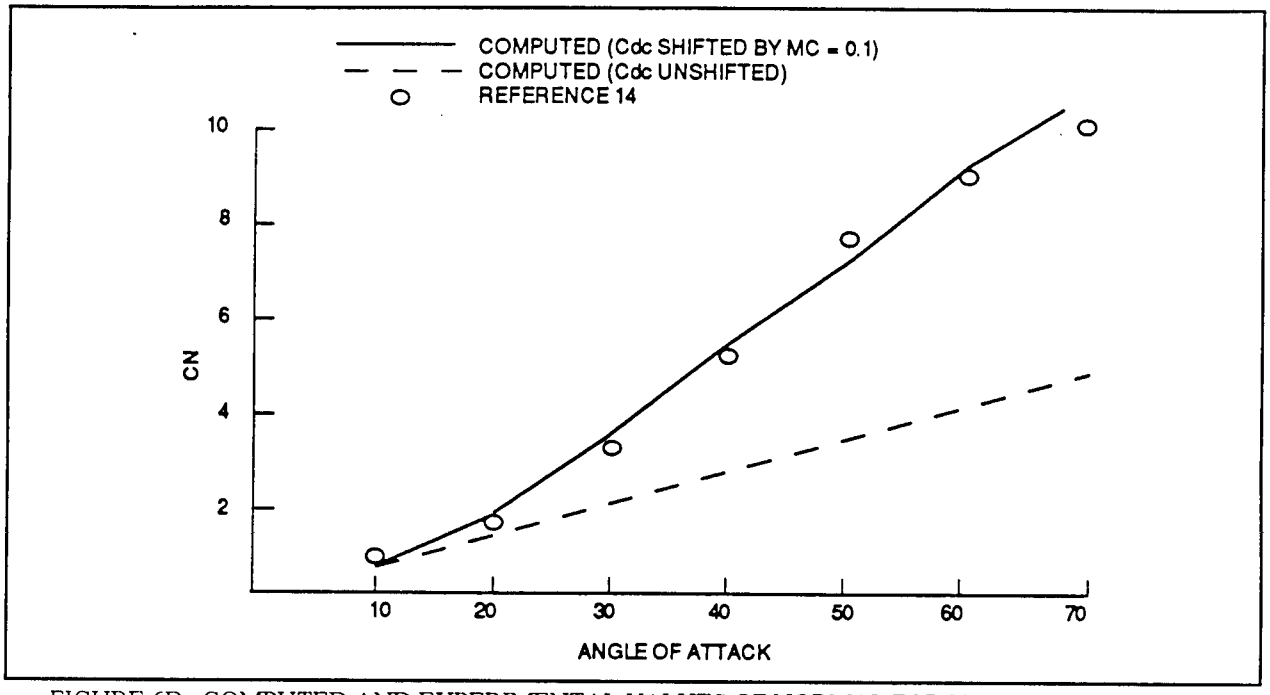

FIGURE 6B. COMPUTED AND EXPERIMENTAL VALUES OF NORMAL FORCE COEFFICIENT AS A FUNCTION OF AOA FOR A BODY-ALONE CONFIGURATION AT $M_\infty = 0.15$

In all of the above results, the method of determining the linear component of normal force has been modified from AP93. For AOA up to 30 deg, the same procedure is used, but beyond that point, the 30-deg value is computed and then forced to go to zero at $\alpha = 90$ deg in a linear fashion as shown below.

$$C_{N_L} = (C_{N_L})_{\alpha=30°}\left(1 - \frac{\alpha - 30°}{60°}\right) \tag{4}$$

The body-alone center of pressure is determined by summing the separately determined linear and nonlinear contributions to the total moment and then dividing by the combined normal force; i.e.,

$$X_{CP} = \frac{C_{N_L}(X_{CP})_L + C_{N_{NL}}(X_{CP})_{NL}}{C_{N_L} + C_{N_{NL}}} \tag{5}$$

For purposes of this computation, the center of pressure for nonlinear normal force is assumed to always lie at the centroid of the body planform area. This method was employed in AP93. At supersonic Mach numbers, the center of pressure of the linear component of normal force is also determined as in AP93 by summing the individual local pressure contributions to the total normal force and moment. At subsonic and transonic Mach numbers, however, a change has been made. Rather than the AP93 approach of using SBT to determine the linear term of the normal-force center of pressure of the nose, an improved methodology[14] has been implemented as shown below.

$$\frac{(X_{CP})_L}{\ell_N} = \frac{1}{2}\left[\frac{50(M+18) + 7M^2C_P(5M-18)}{40(M+18) + 7M^2C_P(4M-3)}\right] \tag{6}$$

where the pressure coefficient is defined by

$$C_P = \left(0.083 + \frac{0.096}{M^2}\right)\left(\frac{\theta}{10}\right)^{1.69}$$

and

$$\theta = 2\tan^{-1}\left[1/(2\,\ell_N/d)\right]$$

In these equations, the length, ℓ_N, is the body nose length. Equation (6) determines the value of $(X_{CP})_L$ for Mach numbers between 0.4 and 1.2. Below M = 0.4, the $(X_{CP})_L$ value computed at Mach 0.4 is used.

The second modification in the body-alone methodology of the AP93 is in the center-of-pressure change with AOA. Two nonlinear phenomena are present that Equation (5) does not fully account for. One phenomenon is the shift in center of pressure which occurs as a result of the asymmetric body vortices which typically occur above AOA = 25 deg and below $M_\infty = 2.0$. This phenomenon appears to affect the normal force only slightly but shifts the center of pressure forward. The second phenomenon occurs in the transonic flow range where a shock forms on the body as the flow approaches sonic conditions. The center of pressure shift tends to be forward from this phenomenon as well.

To estimate the center of pressure shifts, two different data bases[9,11] were used and were nondimensionalized with respect to body length. In implementing these results into complete missile configurations, the shifts in the transonic region were found to be slightly too large and were somewhat reduced. Also, an upper bound on maximum allowable shift was used based on a 15-cal body length. In other words, if a 20-cal body were being considered, the maximum allowable shift in the center of pressure is based on a 15-cal body. The final tabulation of shifts in the body-alone center of pressure as a function of AOA and Mach number is given in Table 1. Again, Table 1 is in percent of body length with an upper body length shift based on a 15-cal body. Positive values in the table indicate a shift toward the body base, and negative values, a shift toward the nose.

TABLE 1. SHIFT IN BODY-ALONE CENTER OF PRESSURE AS A FUNCTION OF MACH NUMBER AND AOA (AS A FRACTION OF BODY LENGTH)

M \ α	0	10	20	30	40	50	60	70	80	90
0.00	0.00	0.01	0.01	0.000	-0.025	-0.040	-0.040	-0.030	-0.010	0.00
0.20	0.00	0.02	0.02	0.010	-0.025	-0.040	-0.045	-0.030	-0.010	0.00
0.40	0.00	0.03	0.03	0.010	-0.025	-0.040	-0.050	-0.030	-0.015	0.00
0.60	0.00	0.03	0.03	0.010	-0.035	-0.055	-0.070	-0.050	-0.030	0.00
0.80	0.00	0.02	0.02	-0.015	-0.050	-0.070	-0.070	-0.050	-0.015	0.00
0.90	0.00	0.00	0.00	-0.015	-0.050	-0.070	-0.070	-0.040	-0.015	0.00
1.00	0.00	0.00	0.00	-0.015	-0.040	-0.040	-0.040	-0.030	-0.005	0.00
1.15	0.00	0.00	0.00	-0.015	-0.020	-0.025	-0.030	-0.025	-0.005	0.00
1.30	0.00	0.00	0.00	-0.005	-0.010	-0.010	-0.010	-0.005	0.000	0.00
1.50	0.00	0.00	0.00	0.000	0.000	0.000	-0.010	-0.005	0.000	0.00
2.00	0.00	0.02	0.02	0.020	0.015	0.010	0.005	0.000	0.000	0.00
2.50	0.00	0.03	0.03	0.030	0.015	0.010	0.005	0.000	0.000	0.00
5.99	0.00	0.03	0.03	0.030	0.015	0.010	0.005	0.000	0.000	0.00
≥6.00	0.00	0.00	0.00	0.00	0.00	0.00	0.00	0.000	0.000	0.00

In examining Table 1, two other points are worth noting. One point is that at low AOA, most of the shifts are in the positive direction. It is speculated that this is because the center of pressure of the linear term of normal force is assumed constant, whereas it probably moves rearward like the nonlinear component of normal force. The second point is that because of different methods of predicting pressure on the body alone, a shift is required for moderate supersonic to low hypersonic Mach numbers ($M \leq 5.99$), but no shift is required where a different pressure prediction method for hypersonic Mach numbers ($M \geq 6.0$) is used.

The other modification in the body-alone solution has to do with adding compressibility effects into the laminar-skin friction drag calculation.

The current method used to calculate skin-friction drag is based on the Van Driest II method for the turbulent portion of the boundary layer. This method takes into account compressibility and has shown reasonable levels of accuracy. The laminar portion of the flow is based on incompressible flow over a flat plate. The mean skin-friction coefficient is given by the formula

$$C_{F_\ell} = \frac{1.328}{Re_\infty}$$

where Re_∞ is the Reynolds number based on the point where transition occurs. A more accurate approach is to take into account compressibility for higher-Mach-number, higher-altitude flight where a large portion of the boundary layer is laminar. Assuming a Prandtl number of 1.0, ratio of specific heats of 1.4, and exponent in the Sutherland Viscosity Law of 0.8, an improved formula can be derived based on Schlichting's Boundary Layer Theory (page 348, Figure 15.7).[15] The mean skin-friction coefficient for laminar compressible boundary layers then becomes

$$C_{F_\ell} = \frac{1}{Re_\infty}[1.328 - 0.0236M_\infty - 0.00335M_\infty^2 + 0.000349M_\infty^3 - 8.54 \times 10^{-6}M_\infty^4] \quad (7)$$

The skin-friction drag is simply the mean skin-friction coefficient multiplied by the ratio of wetted area to reference area; i.e.,

$$C_{A_F} = C_{F_\ell}\frac{(A_{WETTED})_\ell}{A_{REF}} + C_{F_T}\frac{(A_{WETTED})_T}{A_{REF}} \quad (8)$$

Equation (7) will reduce the laminar-skin friction drag over the incompressible case. The higher the Mach number, the greater the reduction.

2.2 WING ALONE

A brief summary of the new wing-alone methodology[4] will be presented here for completeness. In essence, several alternative fourth-order methods for computing wing-alone lift were investigated.[4] The AP93[1] methodology used a second-order method. However, above AOA of 25 to 30 deg, this second-order technique began to degrade in accuracy, and higher order methods were required. The new higher order method is defined by

$$C_{N_W} = a_0 + a_1 \alpha_W + a_2 \alpha_W^2 + a_3 \alpha_W^3 + a_4 \alpha_W^4 \quad (9)$$

where $\alpha_W = |\alpha + \delta|$.

The constants a_i in Equation (9) are defined by

$$a_0 = 0 \text{ (from symmetry)} \tag{10a}$$

$$a_1 = \left(C_{N_\alpha}\right)_{\alpha=0} \text{ (from LT)} \tag{10b}$$

$$a_2 = 34.044(C_N)_{\alpha=15°} - 4.824(C_N)_{\alpha=35°} + 0.426(C_N)_{\alpha=60°} - 6.412a_1 \tag{10c}$$

$$a_3 = -88.240(C_N)_{\alpha=15°} + 23.032(C_N)_{\alpha=35°} - 2.322(C_N)_{\alpha=60°} + 11.464a_1 \tag{10d}$$

$$a_4 = 53.219(C_N)_{\alpha=15°} - 17.595(C_N)_{\alpha=35°} + 2.661(C_N)_{\alpha=60°} - 5.971a_1 \tag{10e}$$

The terms $(C_N)_{\alpha=15°}$, $(C_N)_{\alpha=35°}$, and $(C_N)_{\alpha=60°}$, are defined[4] by tables of data from several sources.[6,10,11] Equations (9) and (10) are used for $\alpha_W \leq 60$ deg. Above $\alpha_W = 60$ deg, extrapolations are used based on the value of $(C_N)_{\alpha=60°}$. These extrapolations are defined as follows:

For $M_\infty \leq 1.2$, $60° < \alpha_W \leq 90°$,

$$C_{N_W} = (C_{N_W})_{\alpha_W} = 60° \left(\frac{\sin \alpha_W}{\sin 60°} \right)^{1/3} \tag{11}$$

For $M_\infty \geq 2.0$, $60° < \alpha_W \leq 90°$,

$$C_{N_W} = (C_{N_W})_{\alpha_W} = 60° \frac{\sin \alpha_W}{\sin 60°} \tag{12}$$

For Mach numbers between the values of 1.2 and 2.0, linear interpolation is used.

Moore and McInville[4] provide detailed comparisons of the new method with data. The new fourth-order technique proved to be more accurate than the second-order method used in AP93 over the AOA range up to 30 deg. Of greater importance, the fourth-order technique predicted wing-alone aerodynamics to 60 deg AOA with the same level of accuracy. On the negative side, there was a lack of confidence in data for $M_\infty \leq 1.2$ and above AOA of 30 deg.[4] Hence, additional accurate wind-tunnel data could help refine the tables used in Equations (9) and (10).

Several modifications were required of the tables for $(C_N)_{\alpha=15°}$, $(C_N)_{\alpha=35°}$, and $(C_N)_{\alpha=60°}$ on complete missile configurations.[4] One modification consisted of defining a wing-alone data base for very low aspect ratio wings (AR = 0.1), since the data bases that were the sources of the tables[6,10,11] were limited to AR = 0.5. A second modification was increasing the higher Mach

number wing-alone data of Stallings and Lamb[10] (the primary basis of the Moore and McInville tables) closer to that of Nielsen, Hemsch, and Smith data.[6] The $(C_N)_{\alpha=15°}$ table was changed very little, but the $(C_N)_{\alpha=35°}$, and $(C_N)_{\alpha=60°}$ were increased as much as 15 percent in some cases. None of the increases exceeded the Nielsen, Hemsch, and Smith data bases. It can only be speculated that there were sting interference effects in the Stallings and Lamb[10] data that caused it to be somewhat low at higher AOA. The basis for this speculation was that in using the modified tables on several configurations, consistently better results at high AOA are obtained. The Moore and McInville tables[4] were also adjusted at lower Mach numbers as well. Here, aspect ratio one data were increased slightly and data for aspect ratio two and higher were decreased slightly. This change was also more consistent with the Nielsen, Hemsch, and Smith data base. The final modified tables for wing-alone data used in Equation (10) are given in Tables 2 through 4.[4]

2.3 INTERFERENCE FACTORS

Referring to Equation (1), several interference factors must be defined as a function of α, M, and wing geometry (as required). These include $K_{W(B)}$, $K_{B(W)}$, $k_{W(B)}$, $k_{B(W)}$, and $C_{N_{T(V)}}$. Another interference term $C_{N_{B(V)}}$ (negative lift on body resulting from wing-shed vortex) is not explicitly shown in Equation (1). This term is inherently included in the $K_{B(W)}$ and $C_{N_{T(V)}}$ terms. The $K_{B(W)}$ term is computed directly based on the Langley[9] wind tunnel data base. The $C_{N_{T(V)}}$ term is determined by empirically modifying the mathematical model based on available wind tunnel data of configurations with two sets of lifting surfaces. The reason for this approach is because the $C_{N_{B(V)}}$ term is inherently included in the data base measurements and cannot be extracted except through an analytical approximation. This approximation in itself introduces errors, and the approach of combining it with the $C_{N_{T(V)}}$ and $K_{B(W)}$ terms was thought to be better. In the interference factor discussion, the wing is assumed to be interchangeable with the tail for the first four factors. The $C_{N_{T(V)}}$ term is actually a normal-force coefficient component, but is considered an interference term since it is strictly dependent on the vortices shed from a forward lifting surface. Before these factors are considered, however, the data bases used for the nonlinear interference factor derivations, along with their accuracy, are discussed.

2.3.1 Data Bases Used

Three primary data bases have tested a body alone, and then the body close to a wing, with separate measurements for the wing and body. The largest and most complete of these data bases are defined by the Langley[9] and Baker[11] studies. The body tested in the Langley study was a 12.33-cal long tangent ogive cylinder with a 3.0-cal sharp nose, whereas that in the Baker study was a 10-cal body with a 2.5-cal nose. The wings tested include aspect ratios from 0.5 to 4.0 and taper ratios of 0, 0.5, and 1.0. Mach numbers included 0.6 to 4.6, AOA 0 to 40 deg, and roll angles, 0 to 90 deg. Not all conditions were tested at the maximum AOA ($M \leq 1.2$, for example).

TABLE 2. VALUES OF $(C_{N_w})_{\alpha = 15°}$

ASPECT RATIO	TAPER RATIO	MACH NUMBER									
		0	0.6	0.8	1.0	1.2	1.6	2.0	3.0	4.5	≥6.
≤0.1	0.0	.23	.23	.23	.225	.22	.21	.19	.17	.15	.11
	0.5	.23	.23	.23	.225	.22	.21	.19	.17	.15	.11
	1.0	.23	.23	.23	.225	.22	.21	.19	.17	.15	.11
0.5	0.0	.28	.29	.30	.32	.33	.33	.32	.24	.175	.16
	0.5	.39	.41	.415	.42	.43	.42	.39	.28	.22	.20
	1.0	.34	.34	.36	.40	.42	.42	.40	.30	.23	.22
1.0	0.0	.43	.44	.46	.49	.53	.50	.43	.33	.26	.23
	0.5	.47	.50	.60	.62	.625	.55	.50	.39	.29	.26
	1.0	.46	.48	.52	.58	.60	.55	.51	.39	.29	.26
2.0	0.0	.55	.59	.65	.67	.68	.58	.51	.36	.26	.24
	0.5	.56	.59	.66	.76	.80	.66	.54	.40	.31	.29
	1.0	.56	.59	.66	.76	.70	.62	.55	.38	.29	.28
≥4.0	0.0	.65	.66	.71	.83	.86	.73	.59	.43	.30	.28
	0.5	.69	.71	.75	.88	.92	.75	.62	.45	.34	.33
	1.0	.69	.71	.75	.88	.92	.75	.62	.45	.34	.33

TABLE 3. VALUES OF $(C_{N_w})_{\alpha = 35°}$

ASPECT RATIO	TAPER RATIO	MACH NUMBER									
		0	0.6	0.8	1.0	1.2	1.6	2.0	3.0	4.5	≥6.
≤0.1	0.0	.97	1.0	1.0	1.0	.97	.91	.8	.74	.68	.65
	0.5	.97	1.0	1.0	1.0	.97	.91	.8	.74	.68	.65
	1.0	.97	1.0	1.0	1.0	.97	.91	.8	.74	.68	.65
0.5	0.0	.89	.91	.93	.95	.98	.95	.88	.78	.71	.69
	0.5	1.10	1.13	1.16	1.25	1.20	1.09	1.0	.84	.76	.74
	1.0	1.06	1.08	1.13	1.16	1.19	1.12	1.03	.86	.76	.74
1.0	0.0	1.18	1.20	1.22	1.24	1.18	1.11	1.04	.90	.80	.78
	0.5	1.20	1.22	1.24	1.33	1.40	1.20	1.15	.95	.82	.80
	1.0	1.10	1.11	1.16	1.26	1.36	1.20	1.16	.95	.82	.80
2.0	0.0	.95	1.01	1.13	1.20	1.28	1.20	1.08	.93	.85	.80
	0.5	1.00	1.07	1.18	1.30	1.40	1.32	1.21	1.00	.90	.87
	1.0	.98	1.05	1.17	1.27	1.39	1.32	1.21	1.00	.90	.87
≥4.0	0.0	.97	1.05	1.17	1.21	1.34	1.22	1.10	.95	.86	.84
	0.5	1.03	1.09	1.22	1.32	1.44	1.35	1.25	1.05	.96	.94
	1.0	1.03	1.09	1.21	1.32	1.44	1.35	1.25	1.05	.96	.94

TABLE 4. VALUES OF $(C_{N_w})_{\alpha = 60°}$

ASPECT RATIO	TAPER RATIO	MACH NUMBER									
		0	0.6	0.8	1.0	1.2	1.6	2.2	3.0	4.5	≥6.
≤0.5	0.0	1.22	1.23	1.28	1.40	1.48	1.52	1.48	1.4	1.34	1.34
	0.5	1.26	1.27	1.30	1.40	1.54	1.64	1.54	1.44	1.39	1.39
	1.0	1.26	1.27	1.30	1.40	1.51	1.58	1.54	1.46	1.40	1.40
1.0	0.0	1.44	1.46	1.49	1.53	1.56	1.63	1.58	1.50	1.45	1.44
	0.5	1.40	1.42	1.45	1.53	1.58	1.70	1.64	1.54	1.48	1.47
	1.0	1.33	1.34	1.35	1.44	1.62	1.72	1.67	1.57	1.50	1.49
2.0	0.0	1.26	1.27	1.34	1.48	1.59	1.74	1.68	1.54	1.48	1.46
	0.5	1.30	1.31	1.37	1.48	1.63	1.84	1.80	1.63	1.57	1.56
	1.0	1.30	1.31	1.37	1.48	1.63	1.76	1.73	1.64	1.57	1.56
≥4.0	0.0	1.27	1.28	1.37	1.50	1.64	1.80	1.70	1.56	1.50	1.48
	0.5	1.31	1.32	1.40	1.52	1.70	1.89	1.82	1.66	1.60	1.59
	1.0	1.31	1.32	1.40	1.52	1.70	1.78	1.75	1.66	1.60	1.59

The third wing-body data base is from a more recent study by Meyer,[16] and complements the Langley[9] data base. Meyer tested a 10-cal long tangent ogive cylinder with a 2-cal nose and three different sets of fins. Body-alone, body in proximity to the fins, and fins in proximity to the body measurements were made. Data were taken for AOA to 80 deg for various roll positions and at $M_\infty = 0.1$. Since the lower limit of the Langley data base was only M = 0.6 and α = 40 deg, the Meyer data base should provide insight into the interference factor behavior above α = 40 deg for subsonic speeds, as well as insight into the previously[1] extrapolated Mach number range of M < 0.6.

Wing-alone data were obtained as already discussed. Figures 7 and 8 show geometrical sketches of the configurations tested for wing-alone and wing-body data.[9,10,16]

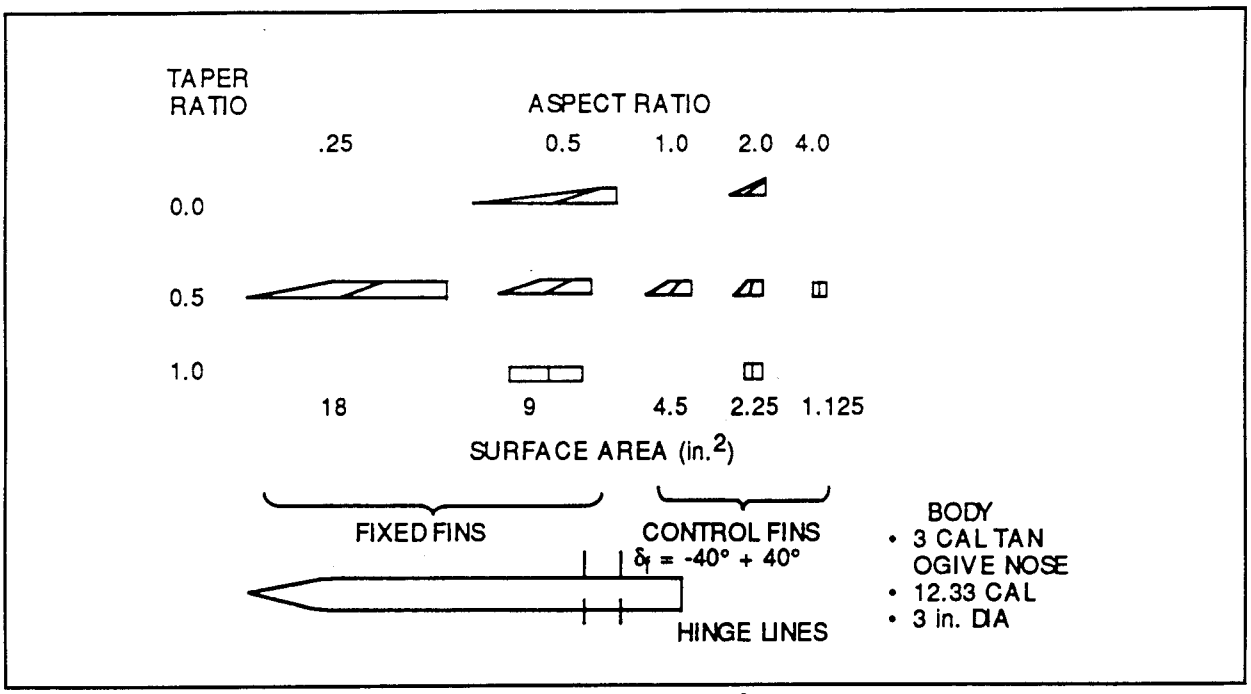

FIGURE 7A. MODELS USED IN LANGLEY[9] WING-BODY TESTS

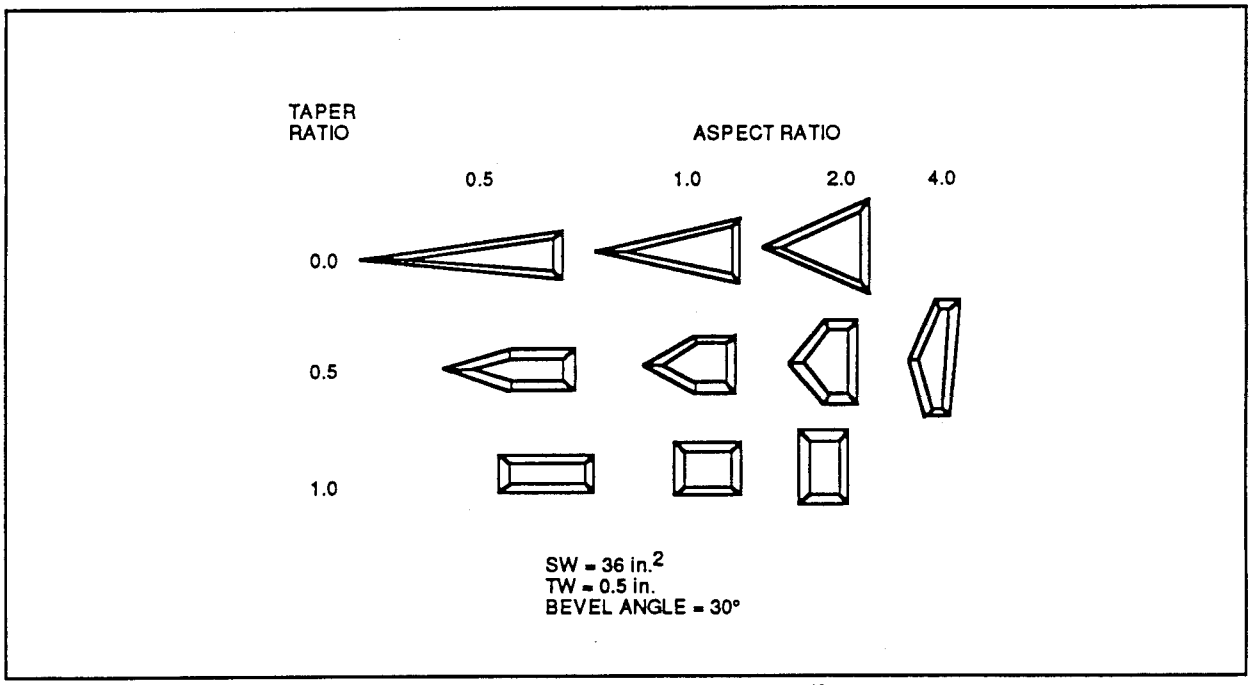

FIGURE 7B. MODELS USED IN STALLINGS AND LAMB[10] WING-ALONE TESTS

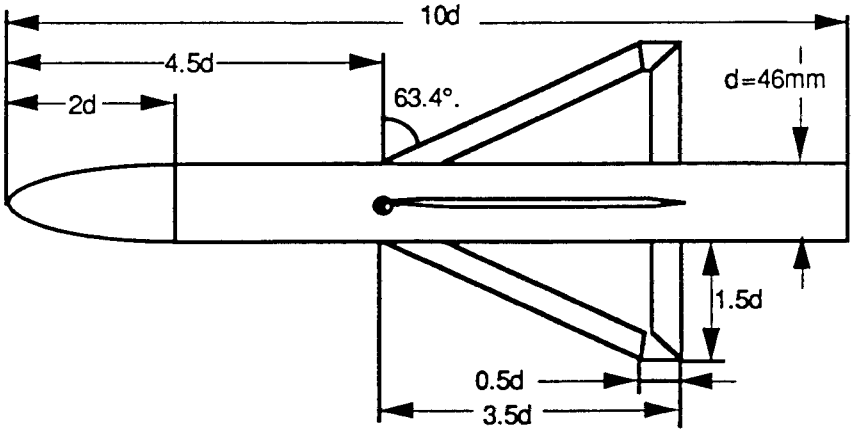

WING B - MID POSITION CONFIGURATION

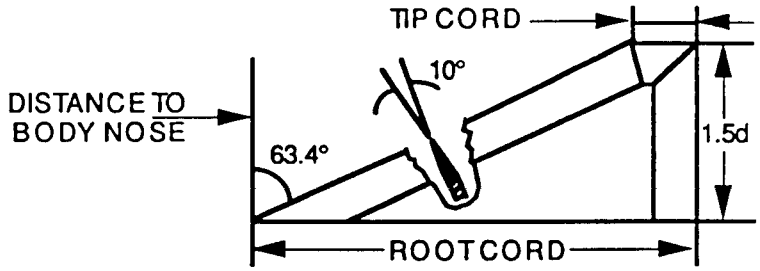

CONIGURATION	DISTANCE TO NOSE	ROOT CHORD	TIP CHORD
WING A - MID POSITION	4.5d	3.0d	0.0
WING B - FORE POSITION	2.4d	3.5d	0.5d
WING B - MID POSITION	4.5d	3.5d	0.5d
WING B - BACK POSITION	6.0d	3.5d	0.5d
WIND C - MID POSITION	4.5d	4.0d	1.0d

FIGURE 8. MODELS USED IN MEYER'S[16] WING-BODY TESTS

2.3.2 Accuracy Analysis

This section attempts to put in perspective the estimates of $K_{W(B)}$ and $K_{B(W)}$, which will be given later. Since three completely different data sets are used in the calculation process, errors associated with each of these data sets will be discussed individually and then in combination. It should be emphasized that this error analysis is based on experience from previous wind tunnel tests and on Missile Aerodynamics in general, because the Langley data[9] is not documented; Stallings and Lamb[10] measured pressures, but not forces and moments; and Meyer[16] gave errors for forces and moments, but apparently did not correct for body-sting carryover effects.

The Langley study provides a comprehensive wing-body data base measuring body-alone aerodynamics, and then wing-body and fin in conjunction with the body aerodynamics, all separately.[9] The sting balance will be assumed to give normal force accuracy within 0.5 percent at maximum load, the same as documented in another test in the same tunnel.[16] The Langley study also kept r/s constant at a value of 0.5 throughout the test.[9] This meant that the area of the fins changed significantly for aspect ratio to vary. If A_P is the planform area of the body in the crossflow plane, the ratio of the body planform area (A_P) to the wing area varies from 4.1 to 32.8 as aspect ratio increases from 0.5 to 4.0. Looked at in another way, for aspect ratios of 0.5, 1.0, 2.0, and 4.0, the wing planform is 24, 12, 6, and 3 percent, respectively, of the body planform area.

The Stallings and Lamb wing-alone data base kept the wing planform area constant and varied aspect ratio and taper ratio.[10] Since pressures were measured along the wing airfoil sections, and these pressures were integrated to get forces and moments, the wings were probably slightly thicker than normal. This extra thickness may cause a slightly lower value of normal force than in the Langley[9] data for some configurations. Also at moderate to high AOA, there could be some sting effects present. However, the Stallings and Lamb data base[10] was the main focus of the new wing-alone methodology used in this report. By and large, the airfoil differences between the tests[9,10] will be neglected, except as accounted for in Moore and McInville.[4]

A summary of the accuracy assumptions for $K_{W(B)}$ and $K_{B(W)}$, from Langley[9] and Stallings and Lamb[10] data, is given in Figure 9. Since $C_{N_{W(B)}}$ and C_{N_W} were direct measurements, $K_{W(B)}$ will be a more accurately estimated parameter than $K_{B(W)}$. That is because

$$K_{W(B)} = \frac{C_{N_{W(B)}}}{C_{N_W}} \tag{13}$$

On the other hand, $C_{N_{B(W)}}$ must be calculated by subtracting numbers of the same order of magnitude from other numbers that were measured in different tests; i.e.,

$$\Delta C_{N_{B(W)}} = C_N - C_{N_B} - C_{N_{W(B)}} \tag{14}$$

1. ASSUME STING BALANCES GIVE 1/2% OF C_N AT MAXIMUM LEVEL

2. C_N AND $C_{N_{W(B)}}$ MEASURED SIMULTANEOUSLY IN SAME TEST RUN. C_{N_B} AND C_{N_W} MEASURED IN DIFFERENT TEST OR RUN

3. $C_{N_{B(W)}}$, $K_{W(B)}$, $K_{B(W)}$ CALCULATED BASED ON MEASUREMENTS FROM 3 SEPARATE TESTS OR W/T RUNS

4. A_W CONSTANT IN C_{N_W}
   $A_p/A_W \cong 4.1, 8.3, 16.4, 32.8$ FOR AR = 0.5, 1.0, 2.0, 4.0 WING-BODY MEASUREMENTS

5. NEGLECT AIRFOIL PROFILE DIFFERENCES IN C_{N_W} AND $C_{N_{W(B)}}$ TESTS
   (THIS MAKES ACCURACY A BEST CASE ESTIMATE)

FIGURE 9. ACCURACY ESTIMATION ASSUMPTIONS FOR $K_{W(B)}$ AND $K_{B(W)}$

As long as there is a significant magnitude to $\Delta C_{N_{B(W)}}$, its value can be computed with reasonable accuracy. This is possible when Mach number is low and the percent of wing planform area to body planform area is fairly high (AR = 0.5, M < 2). However, as this percent gets low or Mach number gets high, $\Delta C_{N_{B(W)}}$ gets small, and the accuracy of $K_{B(W)}$, which is defined by

$$K_{B(W)} = \frac{\Delta C_{N_{B(W)}}}{C_{N_W}} \tag{15}$$

gets progressively worse. Using the assumptions of Figure 9, Figure 10 gives the accuracy estimates of $K_{W(B)}$ and $K_{B(W)}$ using Langley[9] and Stallings and Lamb[10] data. Note that a Mach number limit has been placed on $K_{B(W)}$ at each aspect ratio. If Mach numbers greater than these limits are chosen, the accuracy is worse. As a result, Figure 10 draws a couple of conclusions for using the data[9,10] for computing $K_{W(B)}$ and $K_{B(W)}$ and includes a recommendation for any future follow-on tests.

ESTIMATED MEASUREMENT ERRORS						ESTIMATED MAXIMUM ERRORS IN COMPUTED TERMS							
						AR = 0.5		AR = 1.0		AR = 2.0		AR = 4.0	
AOA RNG (deg)	C_N	C_{N_B}	$C_{N_{W(B)}}$	C_{N_W}	$C_{N_{B(W)}}$	$K_{W(B)}$	$K_{B(W)}$ M≤3.0	$K_{W(B)}$	$K_{B(W)}$ M≤2.0	$K_{W(B)}$	$K_{B(W)}$ M≤1.5	$K_{W(B)}$	$K_{B(W)}$ M≤1.5
0-20	±.02	±.02	±.004	±.008	±.044	±7.5	±25	±14	±36	±19	±33	±32	±49
20-40	±.06	±.06	±.012	±.008	±.132	±1.5	±29	±1	±41	±6	±24	±9	±30
40-60	-------	-------	-------	±.008	-------	-------	-------	-------	-------	-------	-------	-------	-------

Conclusions: $K_{W(B)}$ estimates reasonable for AR ≤ 1.0 at all M and ∝. More scatter for AR > 1.0.

$K_{B(W)}$ estimates usable for lower AR and M. Best guess judgement needed for other conditions.

Recommendations: Any future component test data for engineering codes should have $A_P/A_W \leq 4.1$ and wing mounted in mid-body region to capture most of afterbody carryover lift.

FIGURE 10. ACCURACY ESTIMATES FOR $K_{W(B)}$ AND $K_{B(W)}$ (IN PERCENT)

Based on the Meyer[16] discussion, two of the possible error sources noted above appear to have been eliminated. This is because $C_{N_{B(W)}}$ and $C_{N_{W(B)}}$ and C_{N_B} were all measured directly on a wing that had a fairly large planform area relative to the body planform area. For the wing used in the present analysis, the percent area ratio was about 63, which is 2.6 times as large as the largest percent area ratio (24) in the Langley data base.[9] $\Delta C_{N_{B(W)}}$ from the Meyer data is then

$$\Delta C_{N_{B(W)}} = C_{N_{B(W)}} - C_{N_B} \tag{16}$$

Because of the large wing and direct measurements, $K_{W(B)}$ and $K_{B(W)}$ calculated from Meyer's data is believed to be as good as or better than the best errors shown in Figure 10. This is fortunate for three reasons. First, Meyer's data is for M = 0.1, whereas the Langley data base had a lower Mach number of 0.6. Second, Meyer used AOA to 80 deg, whereas in the Langley study, AOA went only to 40 deg (and only 25 deg in some cases). Hence, Meyer's data can be used to help define the extension of $K_{W(B)}$ and $K_{B(W)}$ past the α = 40 deg data limit of the Langley data. Finally, Meyer's data had an r/s of 0.25, versus an r/s of 0.5 in the Langley data. Hence, some assessment of the influence r/s has on the nonlinear term of the interference factors may be made.

The major sources of error in computing the interference factors using Meyer's[16] data is expected to be the use of different airfoil sections in the numerator and denominator of Equations (13) and (15) (since the wing alone was not tested) and the lack of an accounting for body-sting interference. This latter problem is expected to be primarily a problem in the body-alone forces. Since the body measurement occurs in both terms of Equation (16), these errors will tend to cancel in the interference factor calculations. However, the body-alone measurements could be substantially in error.[17,18]

Keeping in mind the comments on possible errors in the interference factor computations, the next two sections will discuss these interference factors. While no error boundaries are shown on the charts in these sections, the reader should keep in mind the maximum error numbers of Figure 10 and the judgement required in formulating these curves. As more data become available, these figures and mathematical models for the interference factors can be refined.

2.3.3 Wing-Body and Body-Wing Interference Due to AOA Experimental Results

A report by Moore, Hymer, and Devan[19] gave the wing-body and body-wing interference factors using data bases[6,9,10,11] up to AOA of 30 deg. The interference factors presented here are similar to those of the Moore, Hymer, Devan report, except the wing-alone data may have been modified slightly and all Langley[9] data available for Φ = 0 deg have been utilized, as opposed to limiting the computations to α = 30 deg. In addition, the Meyer[16] data have since become available, allowing more definition of the interference methodology below M_∞= 0.6. As a result, the earlier Moore, Hymer, et al. methodology[1,3,19] will be modified to account for these differences, and an improved mathematical model will be developed for $K_{W(B)}$ and $K_{B(W)}$.

Figure 11 presents the results at M = 0.1 from Meyer.[16] Note that these results are for r/s = 0.25, whereas all the results from Langley[9] are for r/s values of 0.50. The trends of both $K_{W(B)}$ and $K_{B(W)}$ follow the general model of the AP93. That is, for $K_{W(B)}$, the experimental values are higher than SBT at low AOA and, at some AOA, start decreasing. The AOA where the data start decreasing is higher than that predicted with AP93, indicating that for low Mach numbers, the AP93 model needs to be refined. Also, the amount that $K_{W(B)}$ exceeds SBT is slightly higher than predicted by the AP93 model, again indicating refinements. It is interesting to note that the minimum value of $K_{W(B)}$ is 0.92 versus 1.0. It is not clear whether this is a true value of the wing-body interference lift at subsonic speeds and high α, or if the wing-alone lift curves[4] are slightly high at this AOA. The representation of the data assumes a value of 1.0 at α = 40 deg for $K_{W(B)}$. The $K_{B(W)}$ data of Figure 11 also follow closely the trends as predicted by the AP93 model for α = 30 deg. Above 30 deg, $K_{B(W)}$ decreases to a minimum value of about half the SBT value at α = 90 deg.

Figures 12 through 20 present the aspect ratio 0.5 interference factor results from Langley along with SBT or LT and an approximate representation of the data. The approximate representation of the data is used to define the nonlinear models of the interference factors in terms of deviation from SBT results. Also recall that the AR = 0.5 results are believed to be the most reliable of the Langley data base, according to the accuracy analysis in Figures 9 and 10. Also note that the r/s values of these figures, along with those for AR = 1.0 and 2.0, is 0.5.

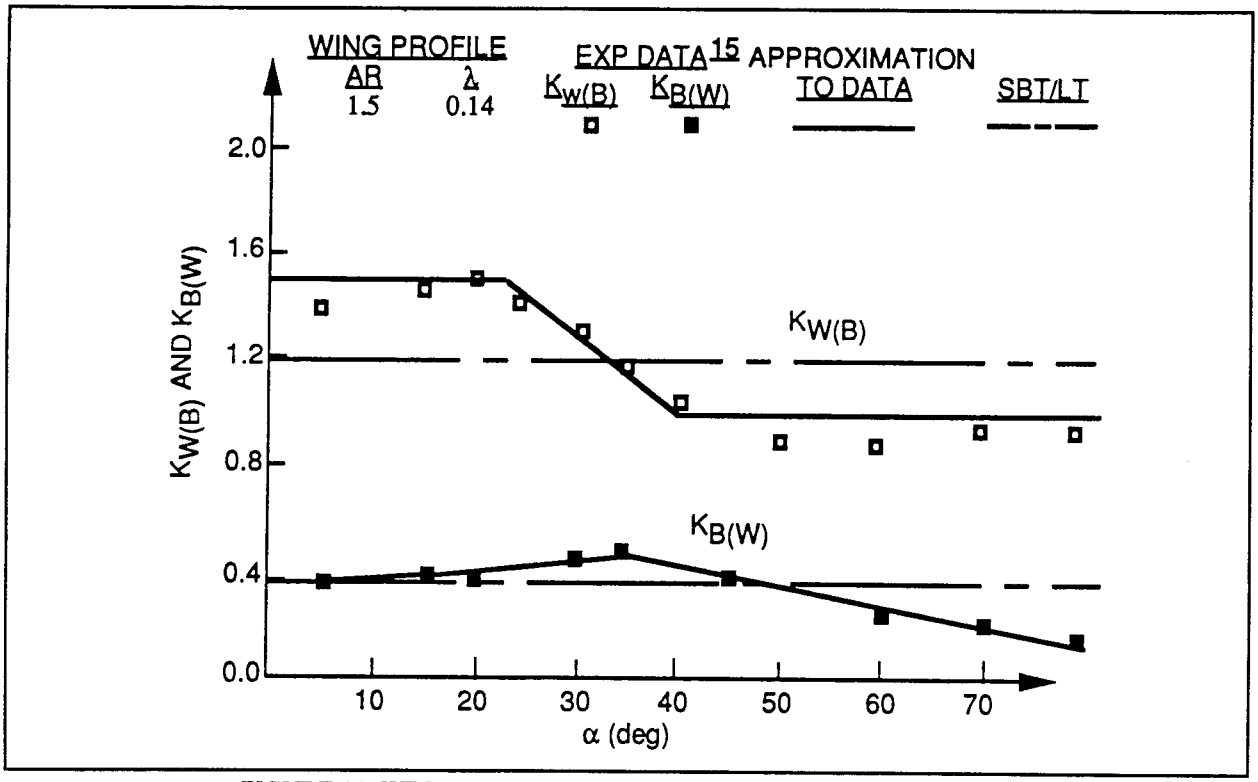

FIGURE 11. WING-BODY AND BODY-WING INTERFERENCE LIFT FACTORS AS A FUNCTION OF AOA (M_∞ = 0.1, r/s = 0.25)

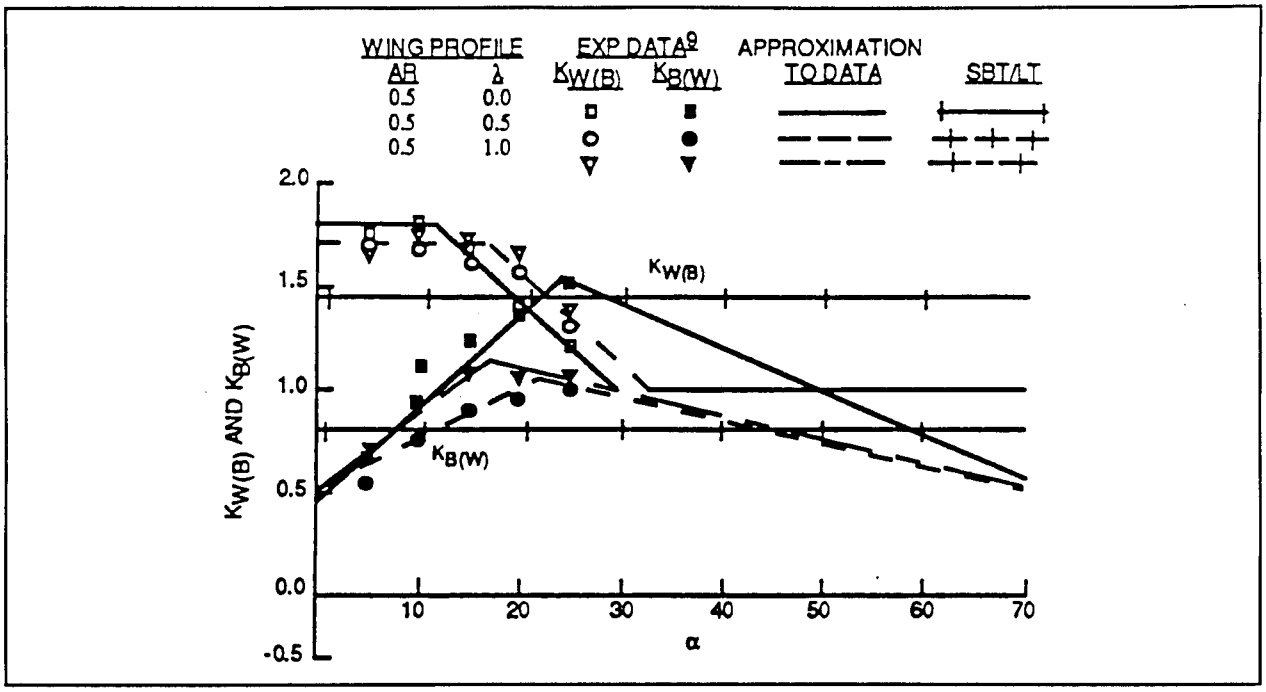

FIGURE 12. WING-BODY AND BODY-WING INTERFERENCE FACTORS AS A FUNCTION OF AOA ($M_\infty = 0.6$)

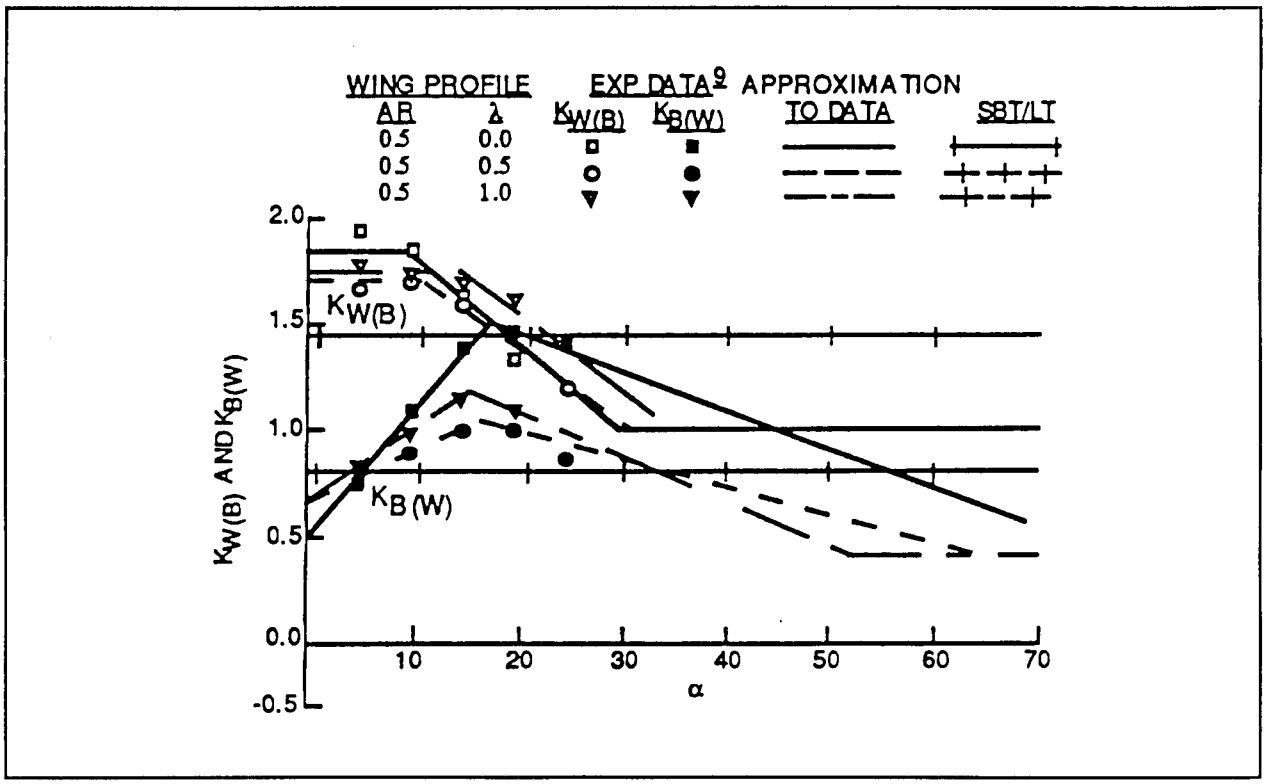

FIGURE 13. WING-BODY AND BODY-WING INTERFERENCE FACTORS AS A FUNCTION OF AOA ($M_\infty = 0.8$)

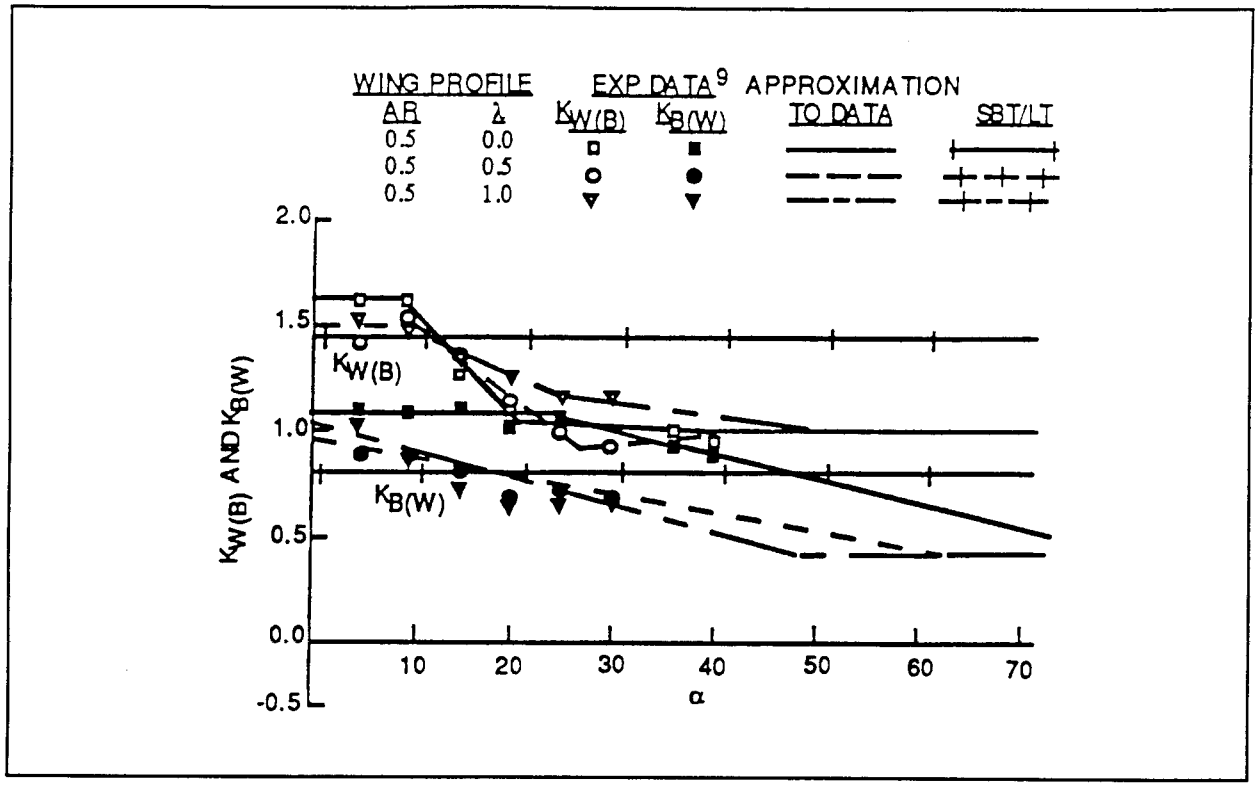

FIGURE 14. WING-BODY AND BODY-WING INTERFERENCE FACTORS AS A FUNCTION OF AOA (M_∞ = 1.2)

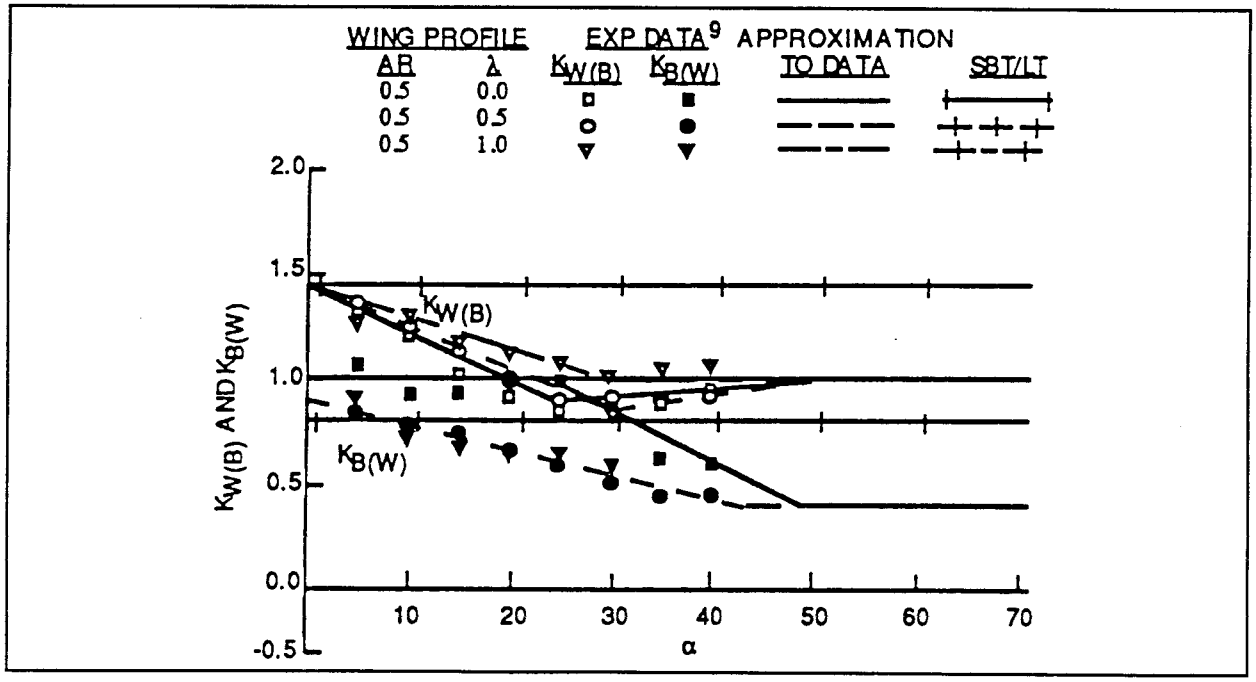

FIGURE 15. WING-BODY AND BODY-WING INTERFERENCE FACTORS AS A FUNCTION OF AOA (M_∞ = 1.5)

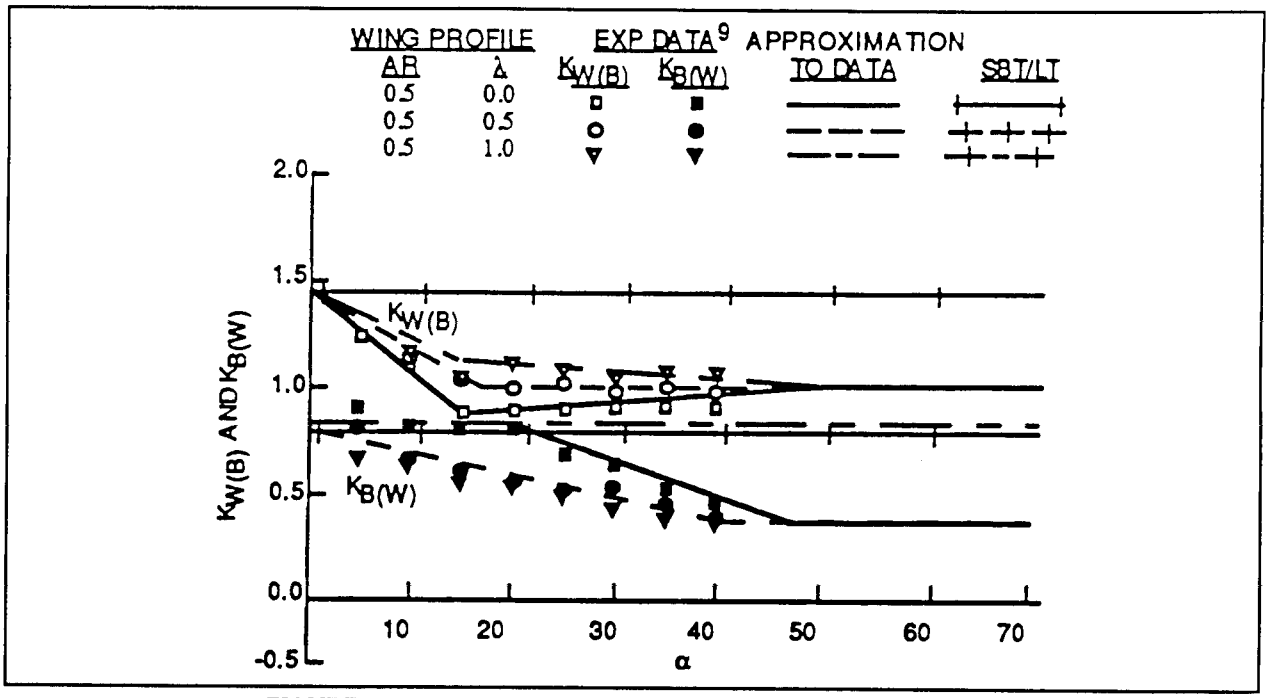

FIGURE 16. WING-BODY AND BODY-WING INTERFERENCE FACTORS AS A FUNCTION OF AOA ($M_\infty = 2.0$)

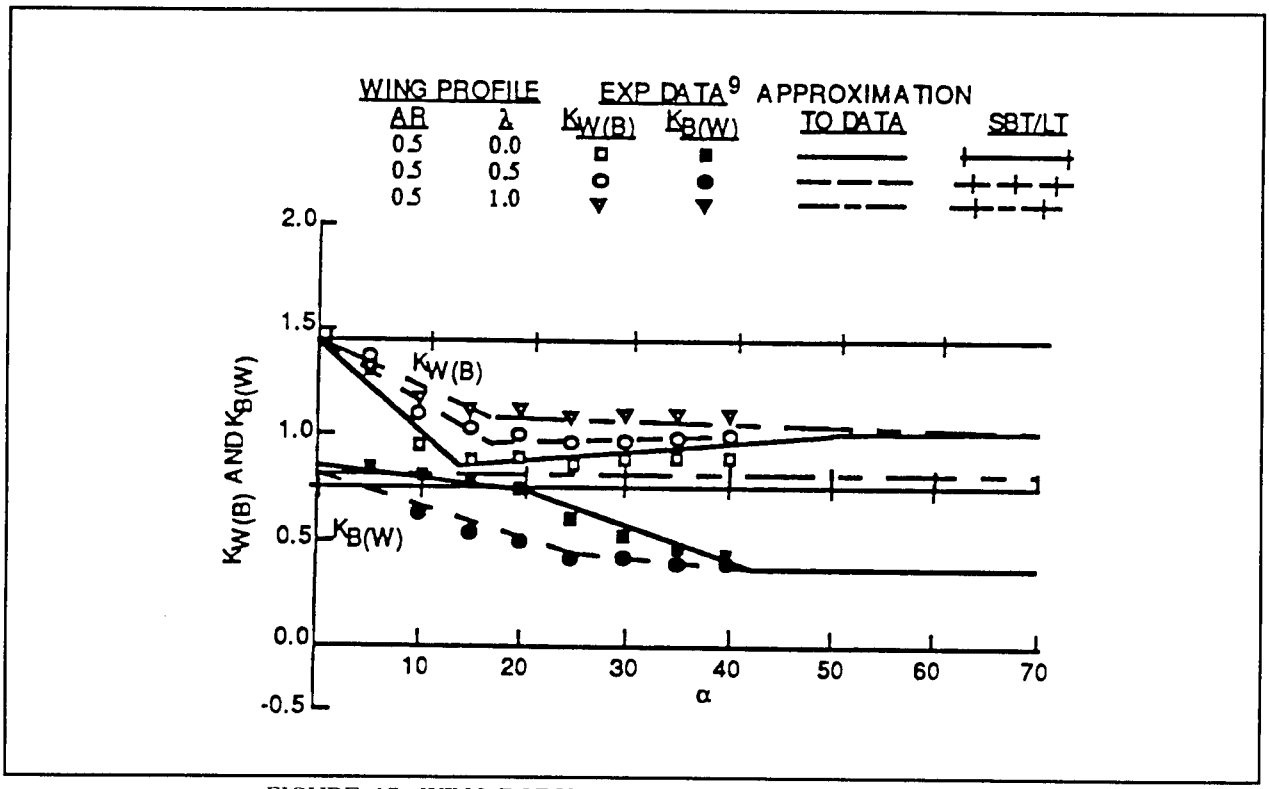

FIGURE 17. WING-BODY AND BODY-WING INTERFERENCE FACTORS AS A FUNCTION OF AOA ($M_\infty = 2.5$)

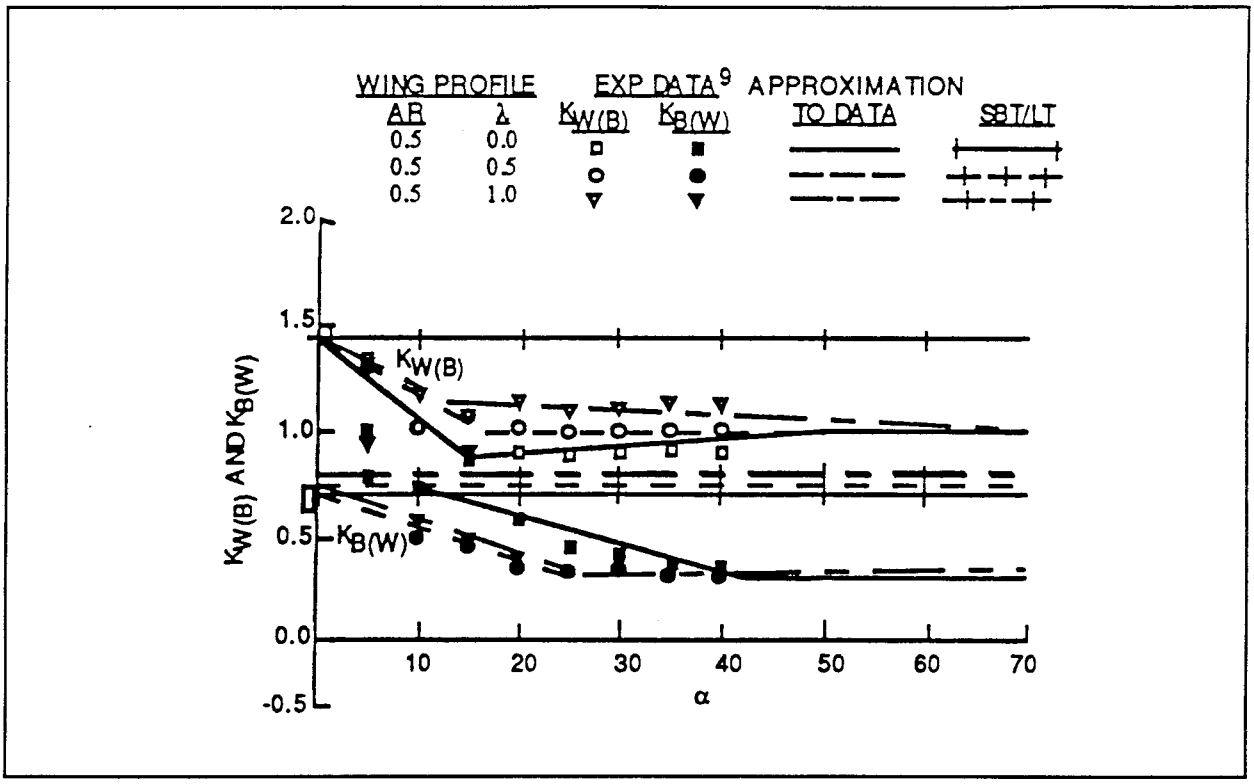

FIGURE 18. WING-BODY AND BODY-WING INTERFERENCE FACTORS AS A FUNCTION OF AOA ($M_\infty = 3.0$)

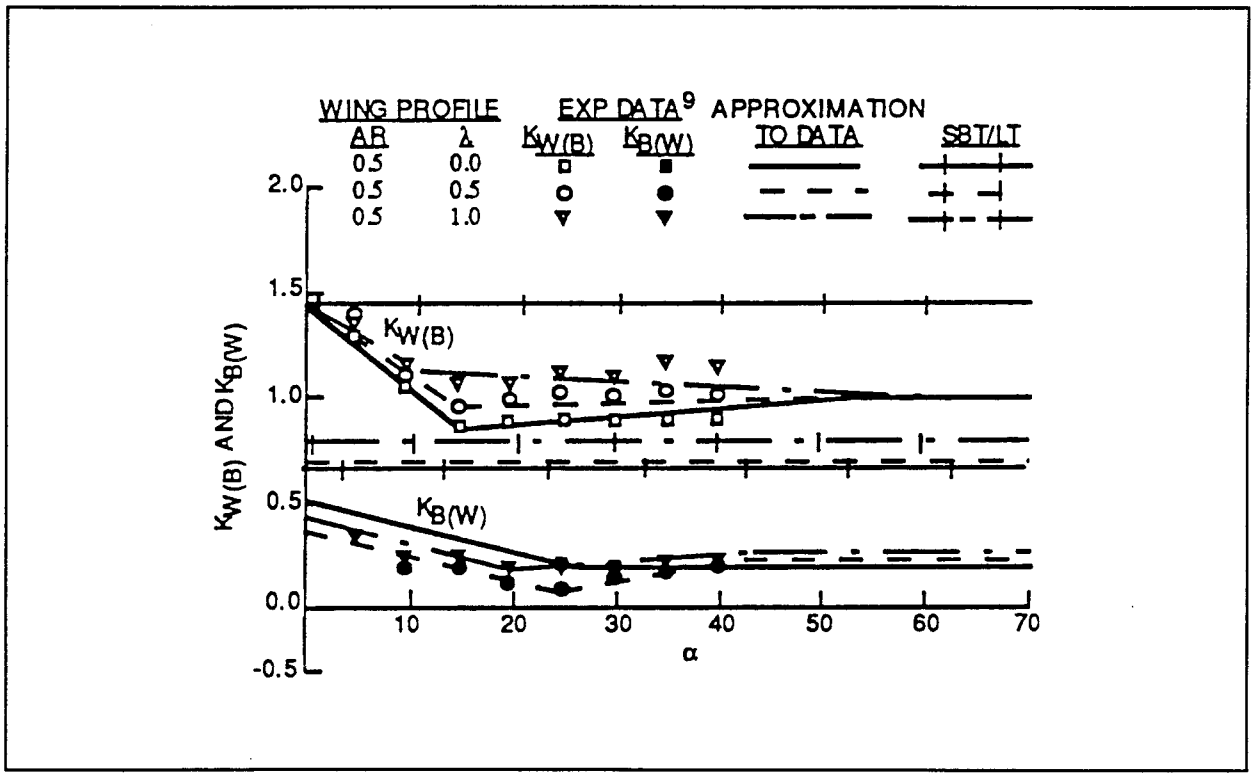

FIGURE 19. WING-BODY AND BODY-WING INTERFERENCE FACTORS AS A FUNCTION OF AOA ($M_\infty = 3.5$)

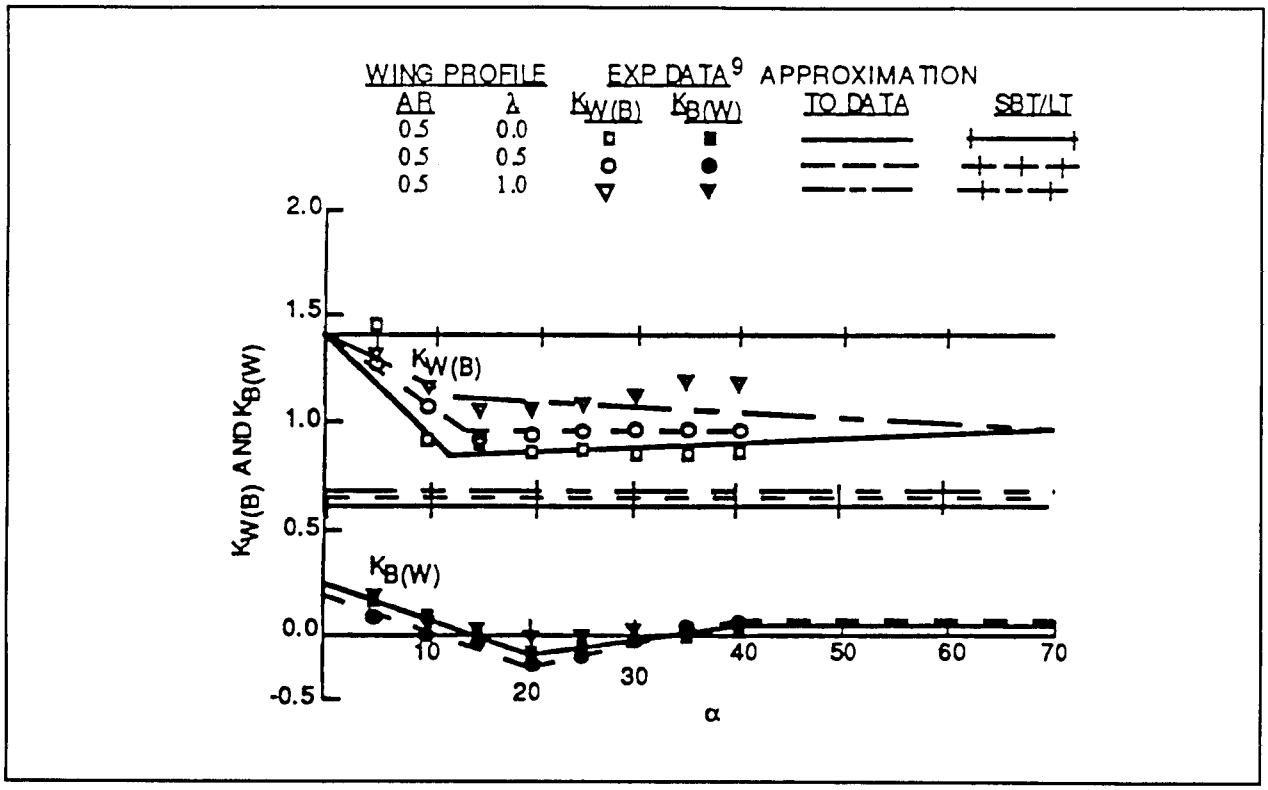

FIGURE 20. WING-BODY AND BODY-WING INTERFERENCE FACTORS AS A FUNCTION OF AOA ($M_\infty = 4.5$)

Examination of the M = 0.6 results of Figure 12 shows that $K_{W(B)}$ and $K_{B(W)}$ follow the general trends of being respectively greater or lower than SBT at low α. At some AOA, $K_{W(B)}$ and $K_{B(W)}$ start decreasing. Since there are no data above α = 25 deg, it is assumed that $K_{W(B)}$ decreases to 1.0 and that $K_{B(W)}$ decreases to 50 percent of the SBT value, analogous to the data of Figure 11. It is also worth noting that there appears to be a taper ratio effect (λ) on these results. As is obvious from this figure, additional data above α = 25 deg would help refine the model used to approximate the data.

Figures 13 through 20 present the remainder of the Langley study[9] results at AR = 0.5 for M_∞= 0.8, 1.2, 1.5, 2.0, 2.5, 3.5 and 4.5. Also shown with the experimental data is the SBT/LT along with an approximation to the data. It is interesting to note the trends in both $K_{W(B)}$ and $K_{B(W)}$ with Mach number. Examining $K_{W(B)}$ first, note that at low Mach number and low α, $K_{W(B)}$ is greater than SBT. At some AOA, this value starts decreasing and is assumed to go to 1.0 at some higher value of AOA. At high Mach number, the AOA where $K_{W(B)}$ starts decreasing is 0 deg. $K_{W(B)}$ decreases until it reaches a minimum, which is sometimes less than one. In many cases, $K_{W(B)}$ will increase again towards a value of 1.0.

$K_{B(W)}$ near α = 0 is lower than SBT at low M_∞, is higher than SBT at low supersonic M_∞, and is lower than LT at high M_∞. At low M_∞, $K_{B(W)}$ increases initially with increasing AOA until a maximum is reached. It then decreases until a minimum value is reached, which is 50 percent or less of the SBT. At high Mach number and α, $K_{B(W)}$ approaches zero, similar to what Newtonian impact theory predicts.

Figures 21 through 29 present the Langley[9] experimental data for the aspect ratio 1.0 and 2.0 cases. While some aspect ratio 4.0 data are available, none are shown because of the error analysis concerns of Figures 9 and 10. The same general trends are found in the AR = 1.0 and AR = 2.0 data as described in the AR = 0.5 data. However, there is considerably more scatter in the $K_{B(W)}$ data at high Mach number, as expected from Figure 10. SBT/LT results, along with an approximate representation of the data, are shown in the figures.

2.3.4 Mathematical Model for $K_{W(B)}$ and $K_{B(W)}$

The mathematical model developed by Moore, Hymer, and Devan[19] for both $K_{W(B)}$ and $K_{B(W)}$ for α up to 30 deg appears to work reasonably well based on many comparisons with experimental data to date. The objective here will be to refine those models based on a) Meyer's more recent data,[16] b) the Langley higher AOA data[9] not previously used by Moore, Hymer, and Devan,[19] and c) the modified wing-alone data bases[4] included in this report.

The model for $K_{W(B)}$ for $\alpha \leq 30$ deg[19] was based on SBT, as a baseline, and a change from SBT as a function of AOA, Mach number, and wing planform. This change was based on experimental data and was defined in terms of several parameters; i.e.,

$$[\Delta K_{W(B)}]_{\alpha=0},\ \alpha_C,\ \frac{dK_{W(B)}}{d\alpha},\ \alpha_D$$

Here, $[\Delta K_{W(B)}]_{\alpha=0}$ is the value that the experimental $K_{W(B)}$ exceeds SBT at $\alpha = 0$ deg; α_C is the AOA where the experimental value of $K_{W(B)}$ starts decreasing; $dK_{W(B)}/d\alpha$ is the rate at which $K_{W(B)}$ decreases; and α_D is the AOA where an initial minimum is obtained.

In Moore, Hymer, and Devan's work, analytical equations were developed for the four parameters defined above based on an average of the data available.[19] This had the advantage of smoothing out some of the experimental variations, but had the disadvantage of not being quite as accurate because of the smoothing out of some of the physics in the data. When the Langley[9] data for $\alpha > 30$ deg is used, the approximate equations would need to be modified and a new parameter added. The present approach will be to use tables to define the four parameters mentioned, along with one other parameter, α_M. These five parameters are shown in Figure 30. These parameters, based on Figures 11 through 29, are given in Tables 5 through 9 as a function of aspect and taper ratios, and Mach number. The parameter $dK_{W(B)}/d\alpha$ is replaced with $[K_{W(B)}]_{\alpha=\alpha_D}$ in the tables and the slope is computed. The approach used here is to linearly interpolate between these parameters for a given value of AR, λ, and M.

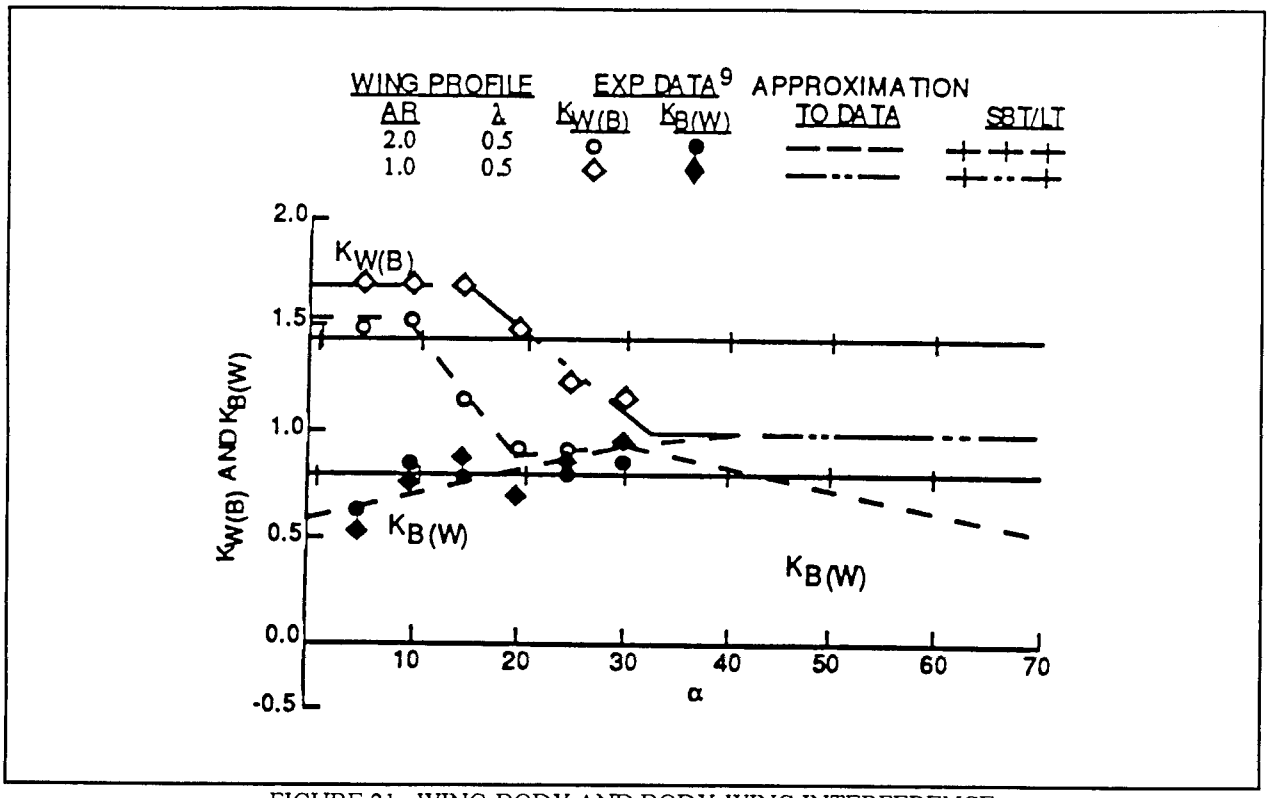

FIGURE 21. WING-BODY AND BODY-WING INTERFERENCE FACTORS AS A FUNCTION OF AOA ($M_\infty = 0.6$)

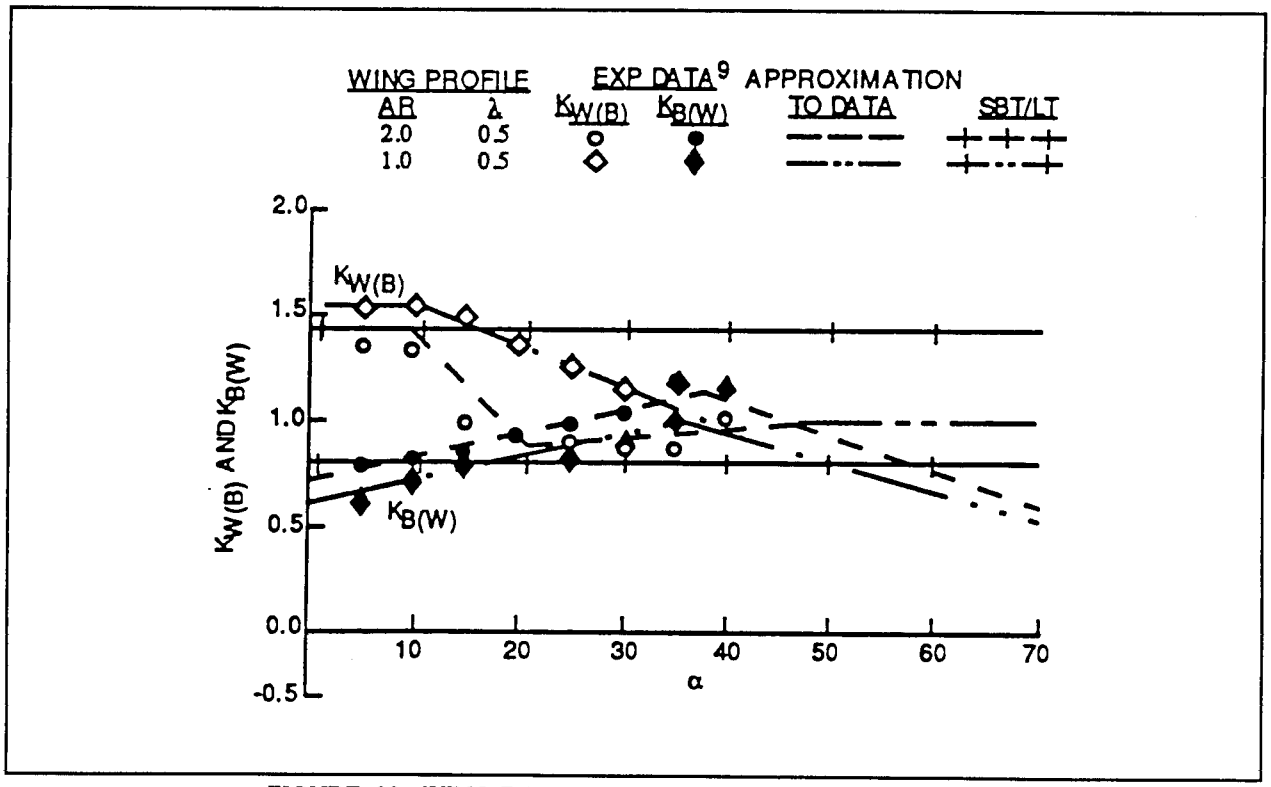

FIGURE 22. WING-BODY AND BODY-WING INTERFERENCE FACTORS AS A FUNCTION OF AOA ($M_\infty = 0.8$)

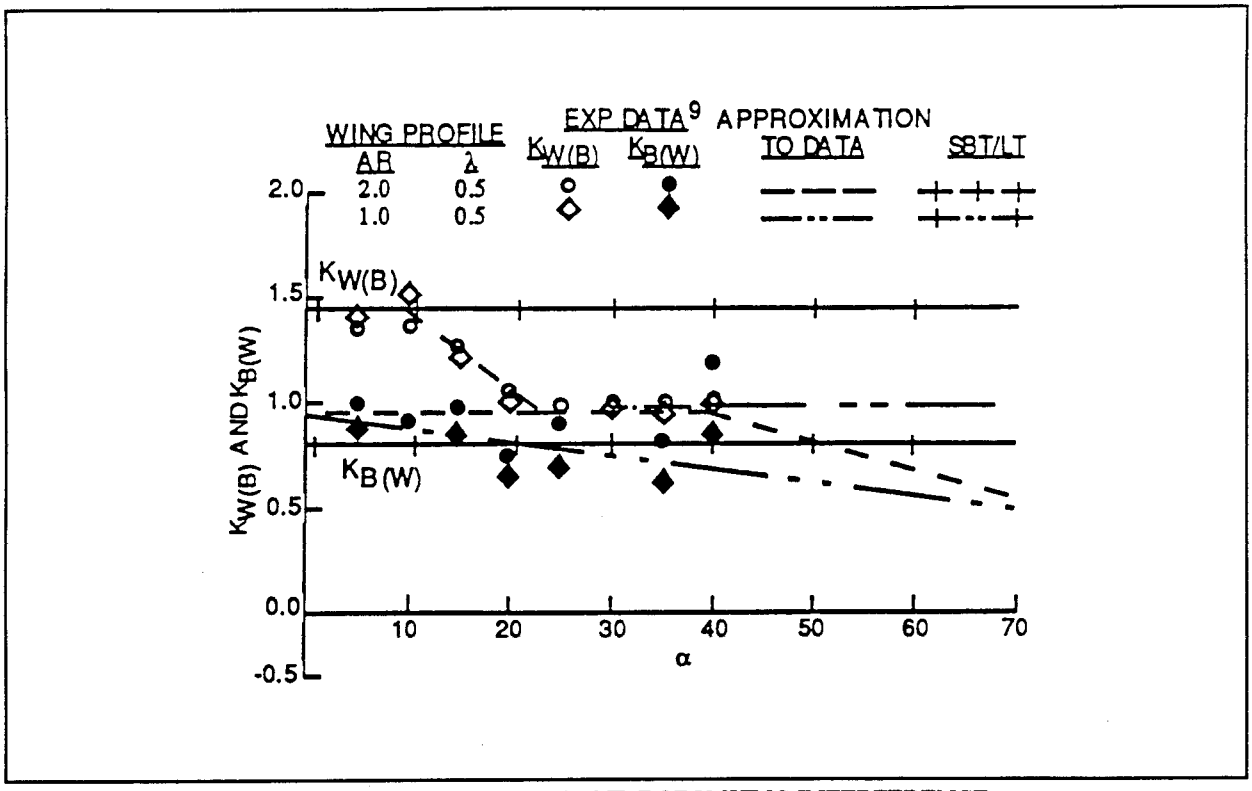

FIGURE 23. WING-BODY AND BODY-WING INTERFERENCE FACTORS AS A FUNCTION OF AOA (M_∞ = 1.2)

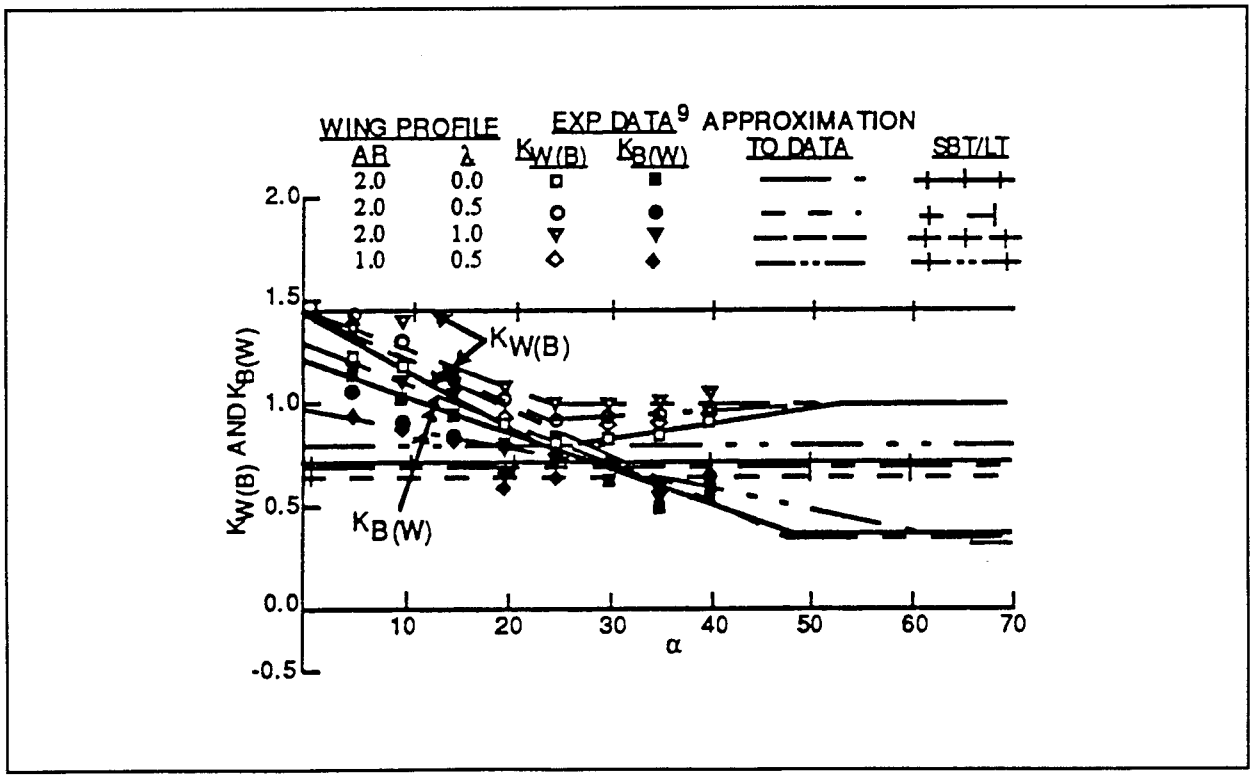

FIGURE 24. WING-BODY AND BODY-WING INTERFERENCE FACTORS AS A FUNCTION OF AOA (M_∞ = 1.5)

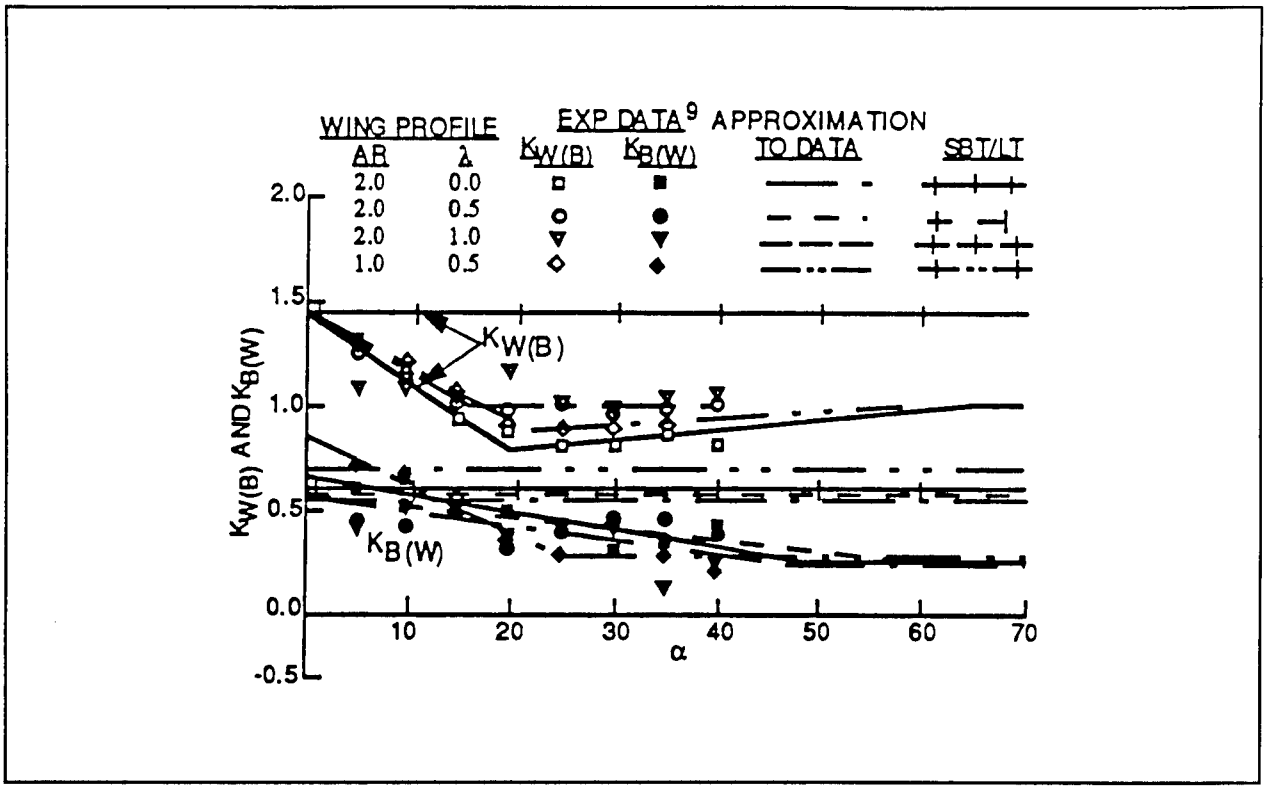

FIGURE 25. WING-BODY AND BODY-WING INTERFERENCE FACTORS AS A FUNCTION OF AOA ($M_\infty = 2.0$)

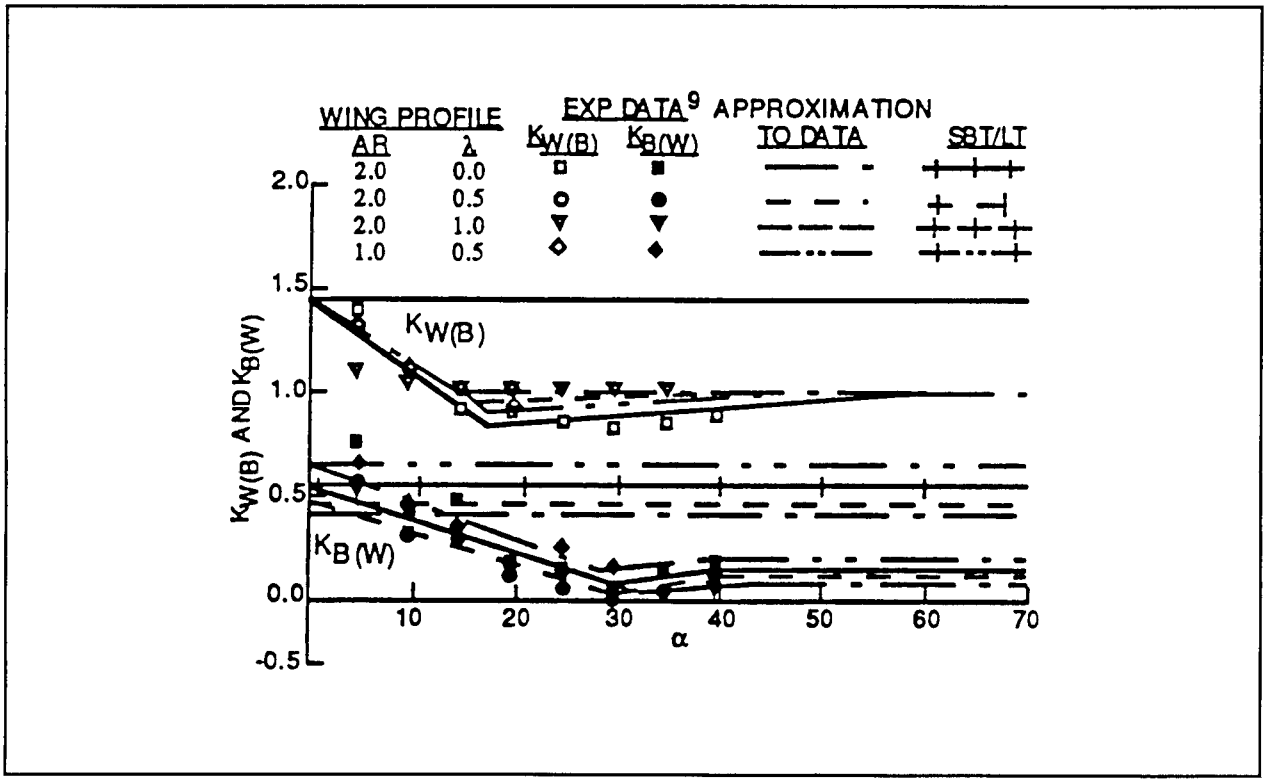

FIGURE 26. WING-BODY AND BODY-WING INTERFERENCE FACTORS AS A FUNCTION OF AOA ($M_\infty = 2.5$)

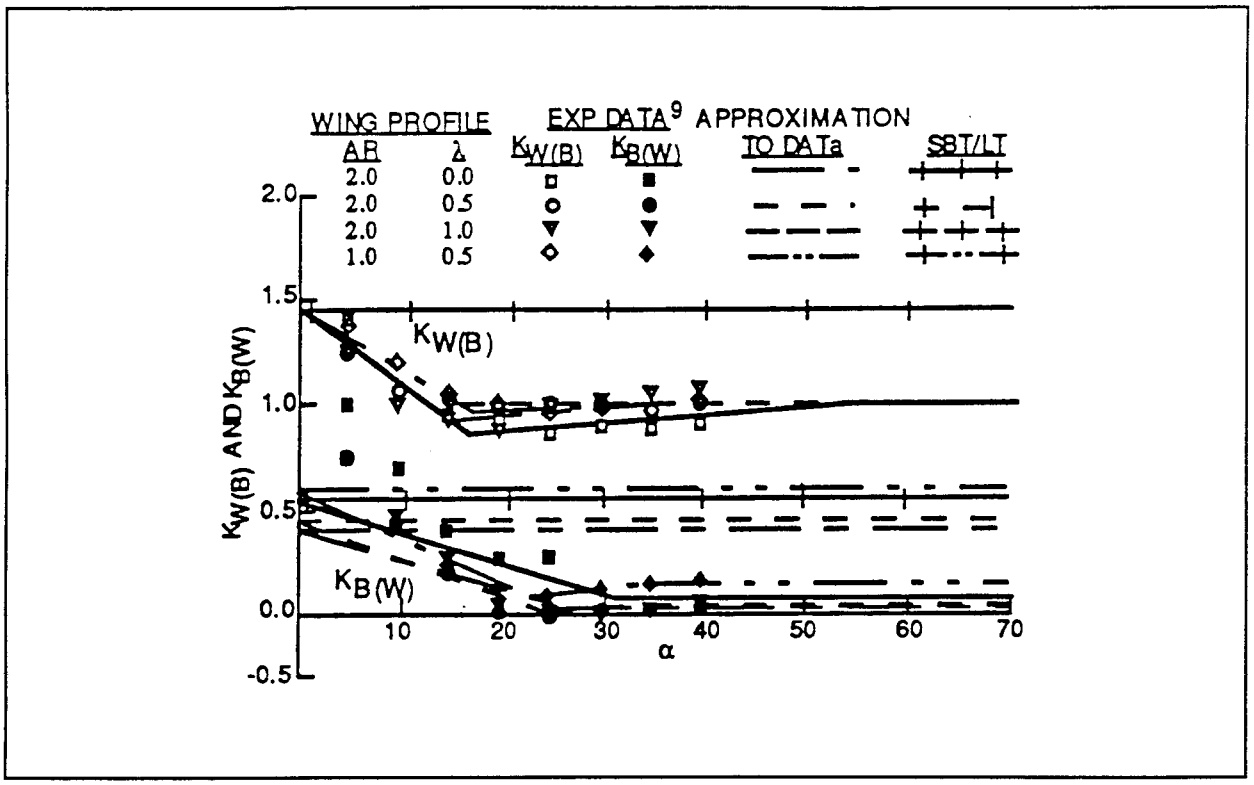

FIGURE 27. WING-BODY AND BODY-WING INTERFERENCE FACTORS AS A FUNCTION OF AOA ($M_\infty = 3.0$)

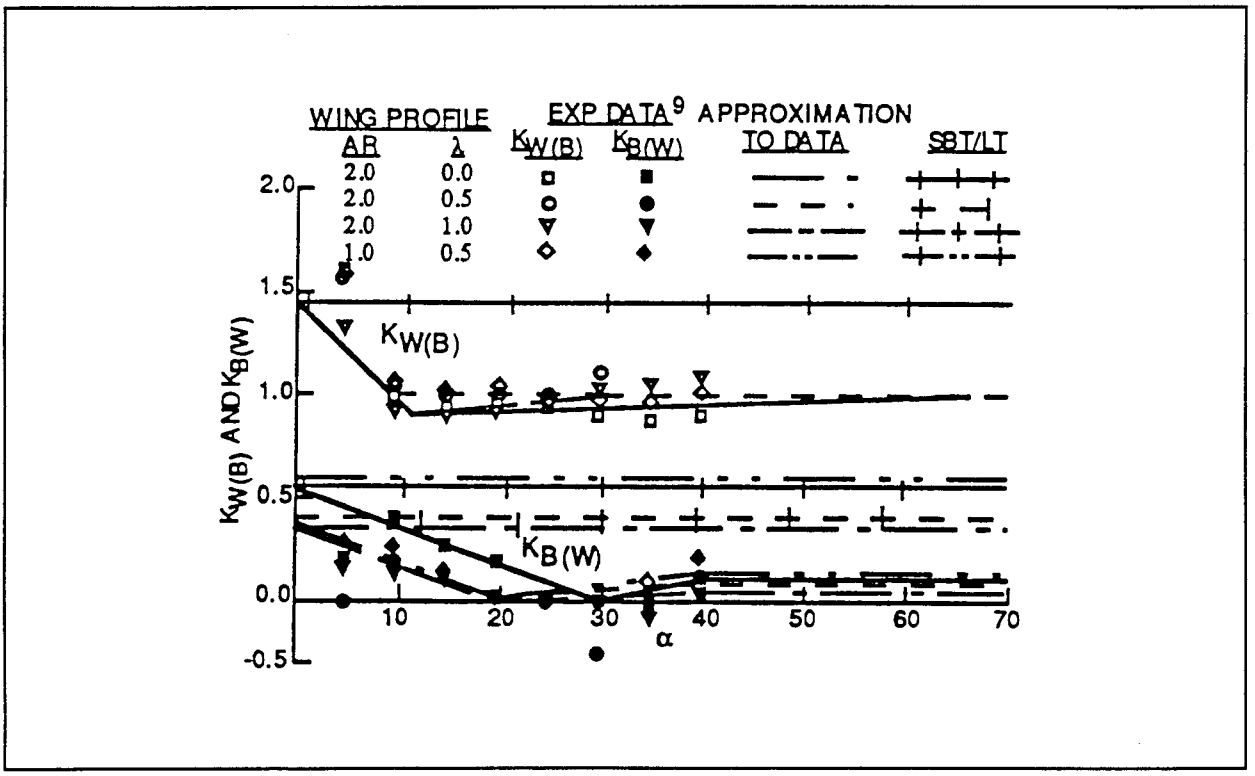

FIGURE 28. WING-BODY AND BODY-WING INTERFERENCE FACTORS AS A FUNCTION OF AOA ($M_\infty = 3.5$)

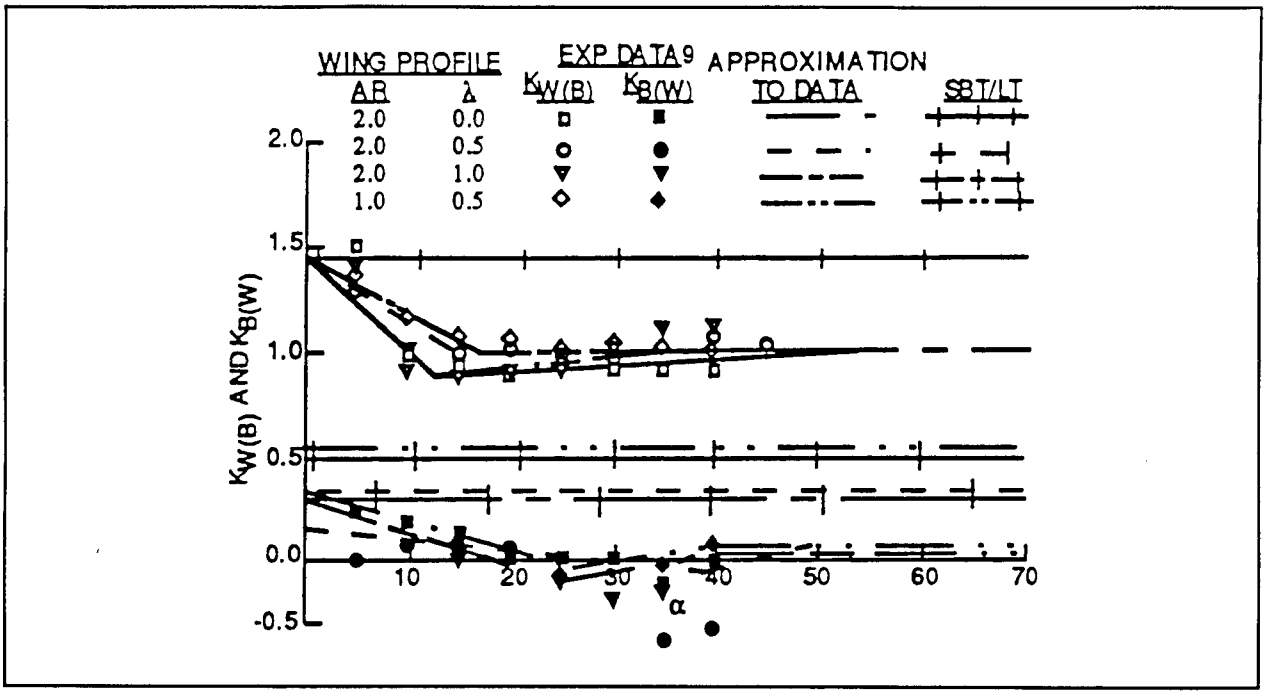

FIGURE 29. WING-BODY AND BODY-WING INTERFERENCE FACTORS AS A FUNCTION OF AOA ($M_\infty = 4.5$)

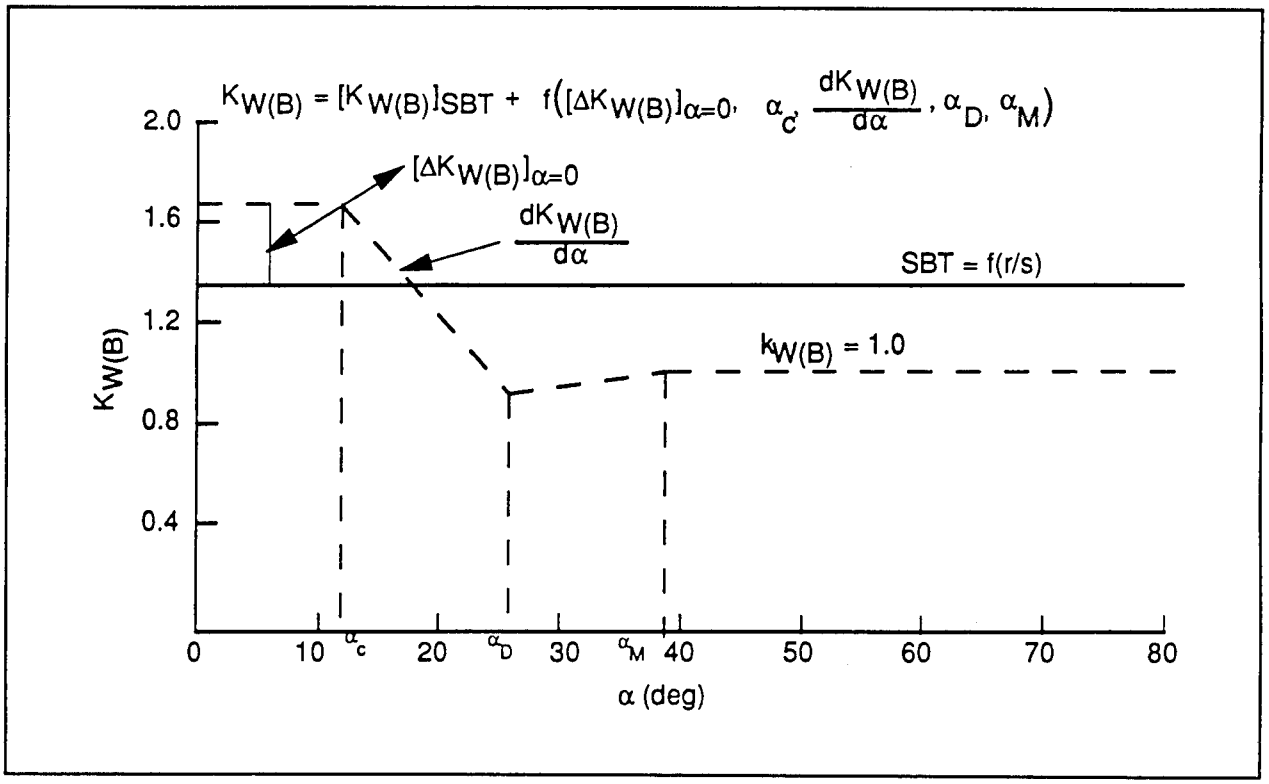

FIGURE 30. GENERIC REPRESENTATION OF $K_{W(B)}$ WITH AOA ($\Phi = 0°$)

TABLE 5. DATA FOR $\left[\Delta K_{W(B)}\right]_{\alpha=0}$

MACH NUMBER												
ASPECT RATIO	TAPER RATIO	≤0.1	0.6	0.8	1.2	1.5	2.0	2.5	3.0	3.5	4.5	≥5.0
≤0.25	0, 0.5, 1.0	−.30	0	0	0	0	0	0	0	0	0	0
0.5	0.5	.30	.27	.23	.05	0	0	0	0	0	0	0
1.0	0.5	.54	.25	.10	0	0	0	0	0	0	0	0
≥2.0	0.5	0	.20	.20	.10	0	0	0	0	0	0	0
0.5	0	.30	.35	.42	.18	0	0	0	0	0	0	0
1.0	0	.54	.29	.16	.06	0	0	0	0	0	0	0
≥2.0	0	0	.20	.20	.10	0	0	0	0	0	0	0
0.5	1.0	.30	.27	.29	.05	0	0	0	0	0	0	0
1.0	1.0	.54	.31	.19	.06	0	0	0	0	0	0	0
≥2.0	1.0	0	.20	.20	.10	0	0	0	0	0	0	0

TABLE 6. DATA FOR α_c (deg)

MACH NUMBER												
ASPECT RATIO	TAPER RATIO	≤0.1	0.6	0.8	1.2	1.5	2.0	2.5	3.0	3.5	4.5	≥5.0
≤0.25	0, 0.5, 1.0	0	22.0	22.0	0	0	0	0	0	0	0	0
0.5	0.5	30.0	17.3	11.5	10.0	0	0	0	0	0	0	0
1.0	0.5	30.0	15.0	11.0	10.0	0	0	0	0	0	0	0
≥2.0	0.5	10.0	20.0	20.0	15.0	0	0	0	0	0	0	0
0.5	0	30.0	12.0	10.0	10.0	0	0	0	0	0	0	0
1.0	0	30.0	13.0	10.0	10.0	0	0	0	0	0	0	0
≥2.0	0	10.0	20.0	20.0	15.0	0	0	0	0	0	0	0
0.5	1.0	30.0	17.3	15.0	10.0	0	0	0	0	0	0	0
1.0	1.0	30.0	15.0	12.5	10.0	0	0	0	0	0	0	0
≥2.0	1.0	10.0	20.0	20.0	15.0	0	0	0	0	0	0	0

TABLE 7. DATA FOR $\left[K_{W(B)}\right]_{\alpha=\alpha_D}$

MACH NUMBER												
ASPECT RATIO	TAPER RATIO	≤0.1	0.6	0.8	1.2	1.5	2.0	2.5	3.0	3.5	4.5	≥5.0
≤0.25	0, 0.5, 1.0	1.0	1.0	1.0	1.0	1.0	1.0	1.0	1.0	1.0	1.0	1.0
0.5	0.5	1.0	1.0	1.0	.90	.90	1.0	.95	1.0	.97	1.0	1.0
1.0	0.5	1.0	1.0	1.0	.95	1.0	1.0	1.0	1.0	1.0	1.0	1.0
≥2.0	0.5	1.0	1.0	.95	.95	1.0	1.0	1.0	1.0	1.0	1.0	1.0
0.5	0	1.0	1.0	1.0	1.05	.90	.90	.90	.90	.90	.90	1.0
1.0	0	1.0	1.0	1.0	.95	1.0	1.0	1.0	1.0	1.0	1.0	1.0
≥2.0	0	1.0	1.0	.95	1.0	1.0	1.0	1.0	1.0	1.0	1.0	1.0
0.5	1.0	1.0	1.0	1.0	1.0	1.0	1.0	1.05	1.15	1.13	1.15	1.0
1.0	1.0	1.0	1.0	1.0	.95	.95	.95	1.0	1.0	1.0	1.0	1.0
≥2.0	1.0	1.0	1.0	1.0	1.0	1.0	1.0	1.0	.93	.90	.95	1.0

TABLE 8. DATA FOR α_D (deg)

MACH NUMBER												
ASPECT RATIO	TAPER RATIO	≤0.1	0.6	0.8	1.2	1.5	2.0	2.5	3.0	3.5	4.5	≥5.0
≤0.25	0, 0.5, 1.0	44.0	40.0	38.0	35.0	30.0	25.0	16.3	15.1	13.9	13.1	12.3
0.5	0.5	50.0	33.0	31.4	27.5	30.0	16.8	17.8	17.0	15.0	15.0	14.0
1.0	0.5	50.0	32.5	39.0	22.0	20.0	22.5	17.5	18.0	10.0	17.0	15.0
≥2.0	0.5	42.0	35.0	35.0	30.0	25.0	16.5	17.0	16.0	10.0	17.0	15.0
0.5	0	50.0	30.0	30.0	21.2	25.0	15.0	14.0	15.0	15.0	12.0	11.5
1.0	0	50.0	31.0	39.0	20.0	18.0	21.5	16.0	17.0	11.0	13.0	13.0
≥2.0	0	42.0	35.0	35.0	30.0	25.0	20.0	17.7	17.0	12.0	12.6	11.5
0.5	1.0	50.0	33.0	34.2	26.0	30.0	14.2	17.0	13.4	11.8	12.2	11.5
1.0	1.0	50.0	33.0	40.0	21.0	20.0	22.0	17.0	16.0	9.0	14.0	12.0
≥2.0	1.0	42.0	35.0	35.0	30.0	25.0	18.0	15.0	15.5	12.0	12.6	11.5

TABLE 9. DATA FOR $\propto_M$ (deg)

MACH NUMBER												
ASPECT RATIO	TAPER RATIO	≤0.1	0.6	0.8	1.2	1.5	2.0	2.5	3.0	3.5	4.5	≥5.0
≤0.25	0, 0.5, 1.0	50.0	45.0	45.0	40.0	44.0	38.0	50.0	46.0	50.0	50.0	46.0
0.5	0.5	50.0	33.0	31.4	40.0	50.0	17.0	40.0	17.0	40.0	15.0	14.0
1.0	0.5	50.0	33.0	39.0	45.0	50.0	50.0	50.0	36.0	33.0	17.0	17.0
≥2.0	0.5	50.0	43.0	45.0	30.0	50.0	50.0	50.0	36.0	33.0	17.0	17.0
0.5	0	50.0	30.0	30.0	40.0	50.0	48.0	50.0	50.0	50.0	50.0	50.0
1.0	0	50.0	31.0	40.0	50.0	42.0	50.0	50.0	50.0	44.0	40.0	40.0
≥2.0	0	50.0	43.0	45.0	45.0	50.0	50.0	50.0	50.0	50.0	50.0	35.0
0.5	1.0	50.0	33.0	34.2	50.0	31.0	50.0	50.0	50.0	50.0	50.0	50.0
1.0	1.0	50.0	33.0	40.0	50.0	42.0	50.0	50.0	50.0	44.0	40.0	40.0
≥2.0	1.0	50.0	43.0	45.0	45.0	25.0	18.0	15.0	36.0	33.0	37.0	30.0

The mathematical model for $K_{W(B)}$ is then:

For $\propto \leq \propto_C$,

$$K_{W(B)} = [K_{W(B)}]_{SBT} + [\Delta K_{W(B)}]_{\propto = 0} \tag{17}$$

For $\propto_C < \propto \leq \propto_D$,

$$K_{W(B)} = [K_{W(B)}]_{SBT} + \left\{ [\Delta K_{W(B)}]_{\propto = 0} + \left(\frac{dK_{W(B)}}{d\propto} \right)_1 (\propto - \propto_C) \right\} \tag{18}$$

For $\propto_D < \propto \leq \propto_M$,

$$K_{W(B)} = 1 - \left(\frac{\propto_M - \propto}{\propto_M - \propto_D} \right) \left(1 - [K_{W(B)}]_{\propto = \propto_D} \right) \tag{19}$$

For $\propto > \propto_M$,

$$K_{W(B)} = 1 \tag{20}$$

It should be noted that the nonlinear term of Equations (17) through (19) does not contain the r/s factor that was used in AP93. This was done to eliminate this assumption from the mathematical model. Hence, the parameters of Tables 5 through 9 may be slightly different than they would be if this term were included. Also, comparing the absolute values of $[K_{W(B)}]_{\alpha=\alpha_D}$ from Figures 11 through 29 with Table 7 shows the figure values to be lower than Table 7 values in many cases. This may be partly because of the r/s not being included, but may also be the result of errors in the data bases. In other words, Tables 5 through 9, like Tables 2 through 4, have been adjusted somewhat based on complete missile configuration comparisons.

Turning now to the model for $K_{B(W)}$, recall that this model was defined[19] by

$$K_{B(W)} = [K_{B(W)}]_{SBT}^{LT} + \frac{r/s}{0.5}\left\{[\Delta K_{B(W)}]_{\alpha=0} + |\alpha|\frac{dK_{B(W)}}{d\alpha}\right\} \tag{21}$$

with constraints $0 \leq K_{B(W)} \leq 2.0$. The terms $[\Delta K_{B(W)}]_{\alpha=0}$ and $dK_{B(W)}/d\alpha$ of Equation (21) were defined in tables as functions of M_∞, AR, and λ. Of course this model was for $\alpha \leq 30$ deg. Based on Figures 11 through 29, a more refined and complicated model is developed to allow α up to 90 deg for AOA. Figure 31 is a qualitative way to represent $K_{B(W)}$ as a function of α that will cover all conditions presented in Figures 11 through 29. Unfortunately, as illustrated in Figure 31, three additional parameters are required to define $K_{B(W)}$. The two that were the same as presented in the Moore, Hymer, and Devan work[19] were modified to account for the more recent Meyer[16] data. Two of the new parameters were defined as tables and only one was defined in an equation form.

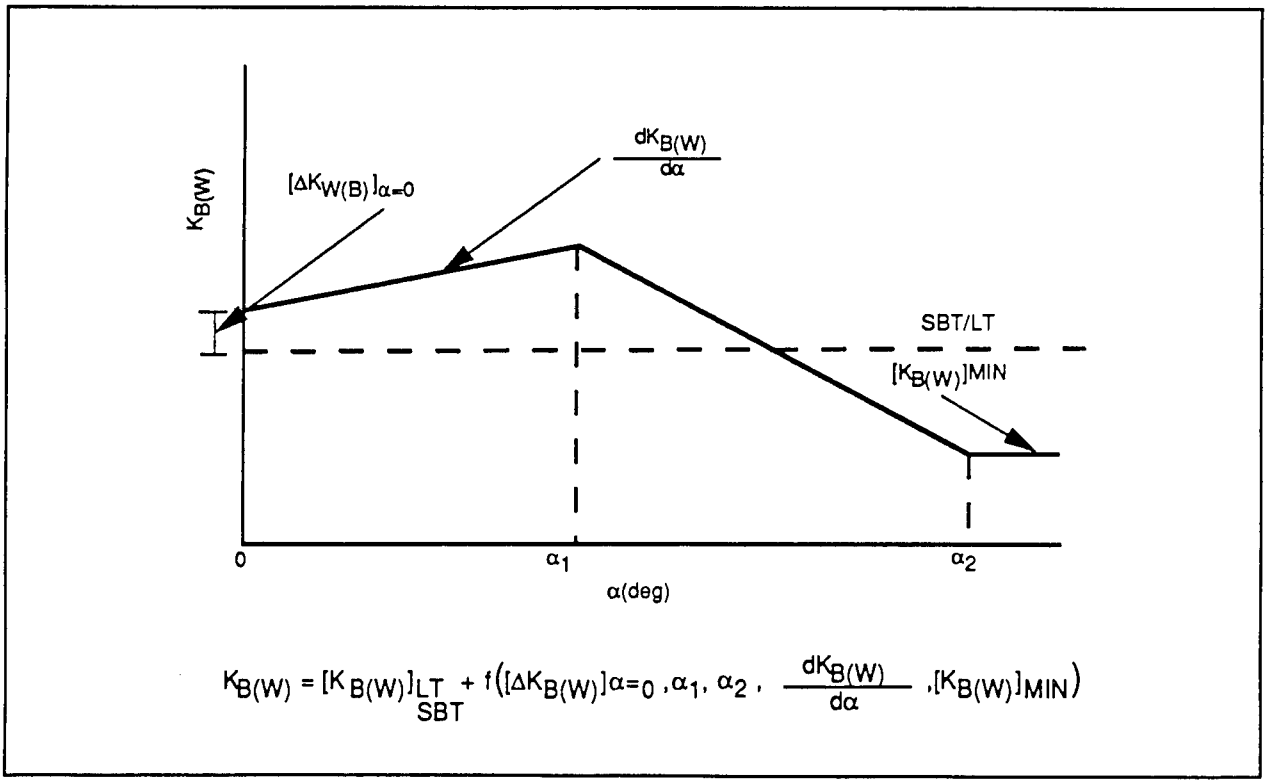

FIGURE 31. GENERIC REPRESENTATION OF $K_{B(W)}$ WITH AOA ($\Phi = 0°$)

Definitions of the parameters in Figure 31 are given as follows:

$[K_{B(W)}]_{\alpha=0}$ = difference between SBT/LT and average of experimental data at $\alpha = 0$

α_1 = AOA where first slope $\frac{dK_{B(W)}}{d\alpha}$ changes sign

$\frac{dK_{B(W)}}{d\alpha}$ = change in $K_{B(W)}$ as a function of α between $\alpha = 0$ and $\alpha = \alpha_1$
(If $\alpha = \alpha_1 = 0$, this parameter is zero.)
Computed from value of $K_{B(W)}$ at $\alpha = \alpha_1$ and $\alpha = 0$.

α_2 = AOA where $K_{B(W)}$ reaches its final value

$[K_{B(W)}]_{MIN}$ = minimum value of $K_{B(W)}$ as a percent of SBT or LT at $\alpha = \alpha_2$

The specific mathematical model for $K_{B(W)}$ is given by Equations (22) through (24).

For $\alpha \leq \alpha_1$,

$$K_{B(W)} = [K_{B(W)}]_{\substack{LT \\ SBT}} + [\Delta K_{B(W)}]_{\alpha=0} + |\alpha|\frac{dK_{B(W)}}{d\alpha} \tag{22}$$

For $\alpha_1 < \alpha \leq \alpha_2$,

$$K_{B(W)} = [K_{B(W)}]_{\alpha=\alpha_1} + \left(\frac{\alpha_1 - \alpha}{\alpha_2 - \alpha_1}\right)\left\{[K_{B(W)}]_{\alpha=\alpha_1} - [K_{B(W)}]_{MIN}\right\} \tag{23}$$

For $\alpha > \alpha_2$,

$$K_{B(W)} = [K_{B(W)}]_{MIN} \tag{24}$$

Equations (22) through (24) also have the constraint that $K_{B(W)} \leq 2.0$, analogous to SBT. As with the $K_{W(B)}$ term, these equations have eliminated the assumption of linear variations with r/s. Tables 10 through 13 define the parameters $[\Delta K_{B(W)}]_{\alpha=0}$, α_1, $dK_{B(W)}/d\alpha$, and α_2. The term $[K_{B(W)}]_{MIN}$ is shown in Figure 32. This figure was arrived at by the combination of Figures 11 through 29 and comparisons with complete missile configurations. As seen in Figure 32, the decrease of $K_{B(W)}$ to zero does not occur nearly as fast in terms of Mach number as implied from Figures 11 through 29. This is assumed to be entirely because of the lack of accurate data at high Mach number and AOA for the $\Delta C_{N_{B(W)}}$ component of force. Linear interpolation also is used for $K_{B(W)}$ for values of M_∞, AR, and λ between any of those presented in the Tables 10 through 13.

TABLE 10. DATA FOR $\left[\Delta K_{B(W)}\right]_{\alpha=0}$

MACH NUMBER												
ASPECT RATIO	TAPER RATIO	≤0.1	0.6	0.8	1.2	1.5	2.0	2.5	3.0	3.5	4.5	≥5.0
≤0.25	0, 0.5, 1.0	0.0	0.0	0.0	0.0	0.0	0.0	0.0	0.0	0.0	0.0	0.0
0.5	0.5	0.0	-.28	-.15	.16	.10	-.02	0.0	0.0	0.0	0.0	0.0
1.0	0.5	0.0	-.20	-.20	.15	.20	.05	0.0	0.0	0.0	0.0	0.0
≥2.0	0.5	0.0	-.20	-.07	.17	.18	.10	0.0	0.0	0.0	0.0	0.0
0.5	0	0.0	-.33	-.30	.28	.20	.10	.08	0.0	0.0	0.0	0.0
1.0	0	0.0	-.24	-.25	.13	.28	.05	0.0	0.0	0.0	0.0	0.0
≥2.0	0	0.0	-.20	-.07	.17	0.0	.05	0.0	0.0	0.0	0.0	0.0
0.5	1.0	0.0	-.28	-.15	.25	0.0	.10	0.0	0.0	0.0	0.0	0.0
1.0	1.0	0.0	-.20	-.20	.22	.10	.05	0.0	0.0	0.0	0.0	0.0
≥2.0	1.0	0.0	-.20	-.07	.17	.20	.10	.15	0.0	0.0	0.0	0.0

TABLE 11. DATA FOR $dK_{B(W)}/d\alpha$ (per deg)

MACH NUMBER												
ASPECT RATIO	TAPER RATIO	≤0.1	0.6	0.8	1.2	1.5	2.0	2.5	3.0	3.5	4.5	≥5.0
≤0.25	0, 0.5, 1.0	0.0	0.0	0.0	0.0	0.0	0.0	-.007	-.014	-.015	-.016	-.020
0.5	0.5	.006	.023	.023	-.009	-.012	-.010	-.015	-.014	-.015	-.016	-.020
1.0	0.5	.006	.012	.011	-.003	-.003	-.005	-.006	-.008	-.010	-.012	-.015
≥2.0	0.5	0.0	.012	.011	0.0	0.0	-.001	-.012	-.014	-.015	-.016	-.020
0.5	0	.006	.043	.058	0.0	0.0	0.0	-.004	-.014	-.015	-.016	-.020
1.0	0	.006	.020	.0225	-.003	-.003	-.005	-.006	-.008	-.010	-.012	-.015
≥2.0	0	0.0	.012	.011	0.0	0.0	-.002	-.012	-.014	-.015	-.016	-.020
0.5	1.0	.006	.038	.033	-.013	-.012	-.010	-.015	-.014	-.015	-.016	-.020
1.0	1.0	.006	.007	.005	-.003	-.010	-.010	-.015	-.016	-.016	-.016	-.018
≥2.0	1.0	0.0	.012	.011	0.0	-.002	-.007	-.012	-.014	-.015	-.016	-.020

TABLE 12. DATA FOR $\propto_1$ (deg)

MACH NUMBER												
ASPECT RATIO	TAPER RATIO	≤0.1	0.6	0.8	1.2	1.5	2.0	2.5	3.0	3.5	4.5	≥5.0
≤0.25	0, 0.5, 1.0	30.0	21.1	16.5	45.0	37.0	33.3	23.3	20.5	20.5	20.0	20.0
0.5	0.5	30.0	22.2	16.7	62.0	43.0	40.0	25.0	25.0	25.0	20.0	20.0
1.0	0.5	30.0	25.0	20.0	70.0	30.0	25.0	28.6	23.0	20.4	26.0	26.0
≥2.0	0.5	30.0	25.0	20.0	40.0	66.0	58.0	30.0	24.0	20.4	26.0	26.0
0.5	0	30.0	24.2	17.2	25.0	25.0	20.0	20.0	10.0	27.0	20.0	20.0
1.0	0	30.0	25.0	20.0	70.0	61.0	18.0	27.0	18.0	24.0	24.0	24.0
≥2.0	0	30.0	25.0	20.0	40.0	48.5	49.0	30.0	32.0	30.0	26.0	26.0
0.5	1.0	30.0	17.0	15.5	48.5	43.0	40.0	25.0	26.5	21.6	20.0	20.0
1.0	1.0	30.0	25.0	20.0	70.0	54.0	22.0	29.5	23.5	18.0	22.0	22.0
≥2.0	1.0	30.0	25.0	20.0	40.0	48.0	47.0	32.0	26.0	20.0	26.0	26.0

TABLE 13. DATA FOR $\propto_2$ (deg)

MACH NUMBER												
ASPECT RATIO	TAPER RATIO	≤0.1	0.6	0.8	1.2	1.5	2.0	2.5	3.0	3.5	4.5	≥5.0
≤0.25	0, 0.5, 1.0	90.0	80.0	65.0	63.4	45.0	43.3	42.5	31.5	37.3	40.0	40.0
0.5	0.5	90.0	80.0	65.0	62.0	43.0	41.0	42.5	25.0	42.0	40.0	40.0
1.0	0.5	90.0	80.0	80.0	80.0	65.0	46.0	40.0	36.0	40.0	40.0	40.0
≥2.0	0.5	90.0	80.0	80.0	80.0	90.0	90.0	42.0	40.0	40.0	40.0	40.0
0.5	0	90.0	80.0	80.0	80.0	49.0	47.8	42.5	43.0	26.5	40.0	40.0
1.0	0	90.0	80.0	80.0	80.0	59.0	46.0	40.0	40.0	34.0	40.0	40.0
≥2.0	0	90.0	80.0	80.0	80.0	90.0	90.0	41.0	35.0	40.0	43.0	43.0
0.5	1.0	90.0	80.0	53.2	48.7	43.0	41.0	42.5	26.5	43.5	40.0	40.0
1.0	1.0	90.0	80.0	74.0	72.0	55.0	46.0	40.0	32.0	40.0	40.0	40.0
≥2.0	1.0	90.0	80.0	80.0	80.0	90.0	90.0	45.0	30.0	40.0	43.0	43.0

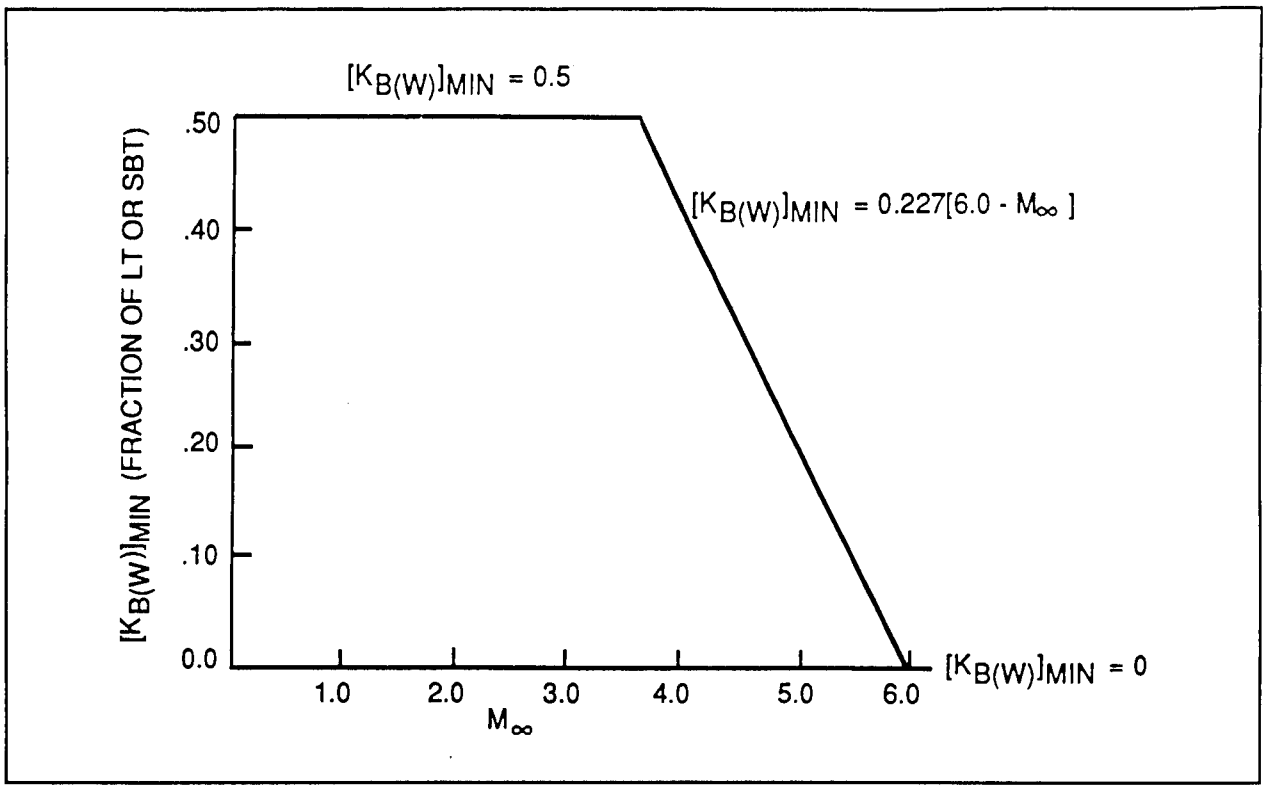

FIGURE 32. MINIMUM VALUE OF BODY-WING INTERFERENCE FACTOR AT HIGH AOA

In examining the nonlinear models for $K_{W(B)}$ and $K_{B(W)}$, it is instructive to try to correlate the mathematical models with the physics of the flow. The wing-body interference factor is somewhat easier to understand than the body-wing interference. The wing-body experimental data show that at low Mach number, SBT slightly underpredicts the experimental data. As AOA is increased, $K_{W(B)}$ starts decreasing and in some cases decreases below its wing-alone value. As AOA increases, $K_{W(B)}$ approaches its wing-alone value. As Mach number increases, the positive interference lift on the wing, caused by the presence of the body, is lost faster and faster as AOA increases. That is, the wing-alone solution is recovered much faster at high Mach number, as AOA increases, than at low Mach number. This is believed to be the result of the Newtonian Impact mechanism where, at high Mach number, the momentum of the air particle is lost almost entirely upon direct impact on a surface, as opposed to wrapping around the surface and carrying some of the momentum with it, as at low Mach numbers.

The $K_{B(W)}$ model contains body vortex effects, nose- and wing-to-wing shock effects, as well as the usual added dynamic pressure of the body caused by the presence of the wing. While some of the trends in Tables 10 through 13 and Figure 32 can be rationalized, others cannot, except in light of these combination effects. The stronger variations in Tables 10 through 13 than in Tables 5 through 9 are caused in part by trying to approximately model all three of these phenomena simultaneously. The alternative is to try to estimate the effects of the body vortices and nose- and wing-shock interactions and subtract them. This process not only complicates the methodology, but adds additional inherent errors because these effects cannot be easily and accurately estimated. The present approach neglects some of the scale effects caused by the position of the wing on the body. However, this error is probably smaller than approximating

analytically the other effects, subtracting them, and then adding them again for a different geometrical configuration.

In general, $K_{B(W)}$ actually increases with AOA at low Mach numbers to a certain point, where it starts decreasing analogous to $K_{W(B)}$. However, a certain amount of lift or force enhancement is gained all the way to $\propto$ = 90 deg for low Mach numbers as shown in Figure 11. This phenomenon is assumed to occur all the way to M = 6.0 based on extrapolated data from the point where experimental data end, which is AOA of 25 to 40 deg depending on Mach number, to $\propto$ = 90 deg shown in Figures 12 through 29 and represented in Figure 32 as $[K_{B(W)}]_{MIN}$.

Additional higher AOA data above $\propto$ = 40 deg is needed for both $K_{W(B)}$ and $K_{B(W)}$ to modify the assumed extrapolations of the models for $K_{W(B)}$ and $K_{B(W)}$ at high AOA. However, until additional data are available, the approximate nonlinear models for $K_{W(B)}$ and $K_{B(W)}$ can be used to estimate aerodynamics for engineering use. This statement will be validated for a limited set of flight conditions in a later section.

2.3.5 Interference Factor Due to Control Deflection and Wing-Tail Interference

The AP93 developed a nonlinear model for the interference factor resulting from control deflection ($k_{W(B)}$) and the wing-tail interference ($C_{N_{T(V)}}$) simultaneously, from data available on wing-body-tail configurations.[1] This approach was taken because many of the wings deflected in the Langley data base[9] were quite small. This made it difficult to get accurate data to differentiate the effects of control deflection from AOA. As a result, AOA nonlinear interference factors were defined based on the Langley data base, and the nonlinear model for control deflection and wing-tail interference was defined based on SBT and data different from the Langley study.

The AP93 method will also be used here, except some refinements will be made in the equations based on the extension of the methodology past 30 deg AOA.[1] The refinements are primarily slight adjustments to several of the constants, primarily at high AOA and Mach number, where upper limits are required on the methodology. The model for $k_{W(B)}$ and $C_{N_{T(V)}}$ is defined by Equations (25) and (26).

$$k_{W(B)} = C_1(M)[k_{W(B)}]_{SBT} + C_2(|\propto_W|, M) \tag{25}$$

$$C_{N_{T(V)}} = \frac{(C_{N_\propto})_W (C_{N_\propto})_T [K_{W(B)}\sin\propto + Fk_{W(B)}\sin\delta_W] i (s_T - r_T) A_W}{2\Pi(AR)_T(f_W - r_W) A_{REF}} \tag{26}$$

where $F = C_3(M, |\propto_W|)$.

Equations (25) and (26) are identical to those used in AP93. The difference in AP93 and AP95 is in the constants (C_1, C_2, and C_3) used to define the nonlinearities of the equations. These modified constants are included in Figure 33. Note that the $k_{B(W)}$ term is still computed with SBT only. Because of the way the method is derived, separating the nonlinearity in $k_{B(W)}$ from that in $k_{W(B)}$ is not possible. Hence, all the nonlinearity and errors associated with the use of SBT to predict $k_{W(B)}$ and $k_{B(W)}$ are attributed to the $k_{W(B)}$ term.

2.3.6 Treatment of Linear Aerodynamics at High AOA

Most nonlinear aerodynamics methods discussed in the preceding sections are based on the combination of a linear and a nonlinear term. In the AP93, the linear term was assumed to vary linearly with AOA up to the maximum AOA of 30 deg or in some cases a lower AOA. As to how to treat the linear terms above AOA of 30 deg, each term is treated differently and careful judgment is required for the decision process because of lack of data. The terms considered are base axial force, skin-friction axial force, wave-drag axial force, normal force coefficient derivative of the body alone, and center of pressure of the body alone. The linear term of the wing alone is automatically incorporated into the new fourth-order method discussed previously.

Figure 34 presents a summary of how each of the terms in question is treated. As seen in the figure, most of the terms are assumed to vary linearly between their value at AOA of 30 deg, and zero at AOA of 90 deg. An exception to this is the center-of-pressure treatment of the body alone. Several factors were considered including aerodynamic nonlinearities, in addition to the change in the center of pressure caused by the assumption of a constant center of pressure for the linear term of normal force. All these effects are combined in Table 1.

2.4 NONLINEARITIES NOT MODELED COMPLETELY

Several aerodynamic nonlinearities are either not modeled or modeled only partially. These include asymmetrically shed body vortices (which can be important primarily for $M \leq 2.0$ and $\alpha > 25$ deg), internal shock interactions, and cross coupling of the aerodynamics resulting from roll. Each of these will be briefly discussed.

The physical mechanism that causes asymmetric body vortices is still not completely understood even after many years of research. The general consensus of the research appears to be that the asymmetric shedding arises from one or more of the following: nonuniform surface roughness, nosetip geometry, or body motion.[8] The magnitude of the side force generated as a result of asymmetric vortex shedding is Reynolds-number dependent, with both the maximum and minimum occurring in the critical Reynolds-number range. The critical Reynolds number can vary considerably from wind tunnel to wind tunnel. As a result of these unknowns and the inability to predict the direction of the side force, no attempt is made to model the out-of-plane side force.

MACH	NONLINEAR MODEL
$M \leq 0.8$	If $\lvert\alpha_w\rvert \leq 4.0 \rightarrow k_{W(B)} = 1.4[k_{W(B)}]_{SB}$ If $\lvert\alpha_w\rvert > 24.0 \rightarrow k_{W(B)} = 1.4[0.000794\lvert\alpha_w\rvert^2 - 0.0933\lvert\alpha_w\rvert + 2.71]$ $F = 1.1$
$M = 1.1$	If $\lvert\alpha_w\rvert \leq 15.0 \rightarrow k_{W(B)} = 1.3[k_{W(B)}]_{SB}$ If $\lvert\alpha_w\rvert > 15.0 \rightarrow k_{W(B)} = 1.3[0.00087\lvert\alpha_w\rvert^2 - 0.0825\lvert\alpha_w\rvert + 1.98]$ $F = 1.1$
$M = 1.5$	If $\lvert\alpha_w\rvert \leq 10.0 \rightarrow k_{W(B)} = 1.0[k_{W(B)}]_{SB}$ If $\lvert\alpha_w\rvert > 10.0 \rightarrow k_{W(B)} = 1.0[k_{W(B)}]_{SB} - 0.005[\lvert\alpha_w\rvert - 10.0]$ If $\lvert\alpha_w\rvert \leq 20.0 \rightarrow F = 0.8$ If $\lvert\alpha_w\rvert > 20.0 \rightarrow F = 0.8 + 0.10[\lvert\alpha_w\rvert - 20.0]$
$M = 2.0$	If $\lvert\alpha_w\rvert \leq 10.0 \rightarrow k_{W(B)} = 0.9[k_{W(B)}]_{SB}$ If $\lvert\alpha_w\rvert > 10.0 \rightarrow k_{W(B)} = 0.9[k_{W(B)}]_{SB} - 0.003[\lvert\alpha_w\rvert - 10.0]$ If $\lvert\alpha_w\rvert \leq 20.0 \rightarrow F = 0.8$ If $\lvert\alpha_w\rvert > 20.0 \rightarrow F = 0.8 + 0.17[\lvert\alpha_w\rvert - 20.0]$
$M = 2.3$	If $\lvert\alpha_w\rvert \leq 40.0 \rightarrow k_{W(B)} = 0.9[k_{W(B)}]_{SB}$ If $\lvert\alpha_w\rvert > 40.0 \rightarrow k_{W(B)} = 0.9[k_{W(B)}]_{SB} + 0.005[\lvert\alpha_w\rvert - 40.0]$ If $\lvert\alpha_w\rvert \leq 30.0 \rightarrow F = 0.9$ If $\lvert\alpha_w\rvert > 30.0 \rightarrow F = 0.9 + 0.15[\lvert\alpha_w\rvert - 30.0]$
$M = 2.87$	If $\lvert\alpha_w\rvert \leq 40.0 \rightarrow k_{W(B)} = 0.9[k_{W(B)}]_{SB}$ If $\lvert\alpha_w\rvert > 40.0 \rightarrow k_{W(B)} = 0.9[k_{W(B)}]_{SB} + 0.005[\lvert\alpha_w\rvert - 40.0]$ If $\lvert\alpha_w\rvert \leq 30.0 \rightarrow F = 0.9$ If $\lvert\alpha_w\rvert > 30.0 \rightarrow F = 0.9 + 0.17[\lvert\alpha_w\rvert - 30.0]$
$M = 3.95$	If $\lvert\alpha_w\rvert \leq 20.0 \rightarrow k_{W(B)} = 0.8[k_{W(B)}]_{SB}$ If $\lvert\alpha_w\rvert > 20.0 \rightarrow k_{W(B)} = 0.8[k_{W(B)}]_{SB} + 0.007[\lvert\alpha_w\rvert - 20.0]$ If $\lvert\alpha_w\rvert \leq 30.0 \rightarrow F = 0.9$ If $\lvert\alpha_w\rvert > 30.0 \rightarrow F = 0.9 + 0.2[\lvert\alpha_w\rvert - 30.0]$
$M \geq 4.6$	If $\lvert\alpha_w\rvert \leq 20.0 \rightarrow k_{W(B)} = 0.75[k_{W(B)}]_{SB}$ If $\lvert\alpha_w\rvert > 20.0 \rightarrow k_{W(B)} = 0.75[k_{W(B)}]_{SB} + 0.013[\lvert\alpha_w\rvert - 20.0]$ If $\lvert\alpha_w\rvert \leq 35.0 \rightarrow F = 0.9$ If $\lvert\alpha_w\rvert > 35.0 \rightarrow F = 0.9 + 0.2[\lvert\alpha_w\rvert - 35.0]$
Where $\alpha_w = \alpha + \alpha$ and $k_{B(W)} = [k_{B(W)}]_{SB}$	

FIGURE 33. NONLINEAR WING-BODY INTERFERENCE MODEL FOR CONTROL DEFLECTION

PARAMETER	MACH RANGE			
	$M < 0.6$	$0.6 \leq M < 1.2$	$1.2 \leq M <$ ALIMIT	$M \geq$ ALIMIT
C_{A_B}	Data based $\propto$ effects to 15°; extrapolated to $\propto$ = 30°; linearly goes to zero from $\propto$ = 30° to $\propto$ = 90°			
C_{A_F}	Independent of $\propto$ to 30°; linearly goes to zero from $\propto$ = 30° to $\propto$ = 90°			
C_{A_W}	zero	Semi empirical esitmate independent of $\propto$ to 30°; linearly goes to zero at $\propto$ = 90°	SOVD estimate to $\propto$ = 15°; held constant to $\propto$ = 30°; linearly goes to zero from $\propto$ = 30° to $\propto$ = 90°	SOSE estimate to $\propto$ = 30°; linearly goes to zero from $\propto$ = 30° to $\propto$ = 90°
$(C_{N_\propto})_B$	Empirical value constant to $\propto$ = 30° linearly goes to zero at $\propto$ = 90°			SOSE estimate to $\propto$ = 15°; held constant to $\propto$ = 30°; linearly goes to zero from $\propto$ = 30° to $\propto$ = 90°
C_{N_W}	Included in fourth order math model for all M + $\propto$			
$(X_{CP})_B$	Constant independent of $\propto$ correction made in Table 1 to attempt to compensate for this assumption			

FIGURE 34. LINEARIZED AERO TREATMENT AS $\propto$ INCREASES

The best way to deal with the asymmetric vortices for missiles that need to fly at high AOA at $M < 2$ is to use nose strakes with a slightly blunt nose. The strakes will force the vortices to be symmetric, and the side force is then approximately zero.

The Langley data base[9] also showed the normal force to vary by as much as 10 percent as a function of roll position when $\alpha \geq 25$ deg and $M < 1.2$. In the AP93 development, the experimental data were averaged over roll so that no roll dependence was shown. This in itself introduced some error in comparing the data to theory. However, this level of accuracy is believed acceptable for a semiempirical aeroprediction code. A key in developing an engineering aeroprediction code, however, is understanding the physics and being able to mathematically model the physics. As concerns asymmetric vortex shedding, neither of these prerequisites is at a level that is satisfactory for an engineering code. Only the maximum absolute value of the side force can be satisfactorily modeled.

The asymmetric shedding of vortices also causes the center of pressure of the body to shift toward the nose. This movement is partially accounted for in Table 1 based on the Baker data base.[11]

The second nonlinearity that is only partially modeled is internal shock interactions. Internal shock interactions can come from the wing or tail shock intersecting the bow shock, a wing shock intersecting another wing, or a wing shock intersecting the tail. Figure 35 illustrates some of these shock interactions. The data base used primarily in the present analysis had only one set of lifting surfaces present and these were located in the mid to aft part of the body.[9] Hence, wing-to-tail shocks are not modeled. Also the bow shock intersecting the wing shock is at best only partially modeled. This second nonlinearity, unlike the asymmetric vortex, is better understood physically and mathematically. However, additional work remains to adequately model these shock interactions that tend to occur primarily for $M > 2$ and $\alpha > 30$ deg.

Another nonlinearity not modeled is the out-of-plane aerodynamics. These aerodynamics are intentionally not modeled for the following two reasons. First, a primary use of out-of-plane aerodynamics is to conduct six-degree-of-freedom trajectory analysis. In most cases, for this detailed trajectory analysis, the accuracy provided by semiempirical aerodynamic prediction codes is unacceptable, and more accurate wind tunnel data or numerical codes are required. Second, many out-of-plane effects (such as induced roll, for example) can be fairly small, and accurate data sets or acceptable sets of numerical computations are needed. Once again, the small size of many control fins in the Langley data base[9] makes this difficult.

On the positive side, the physics of the out-of-plane aerodynamics (with the exception of the asymmetric vortices) are well understood. With adequate data or computations, an accurate out-of-plane aerodynamics semiempirical model may be possible. The only semiempirical method at present that attempts to calculate out-of-plane aerodynamics is the so-called equivalent AOA approach.[20]

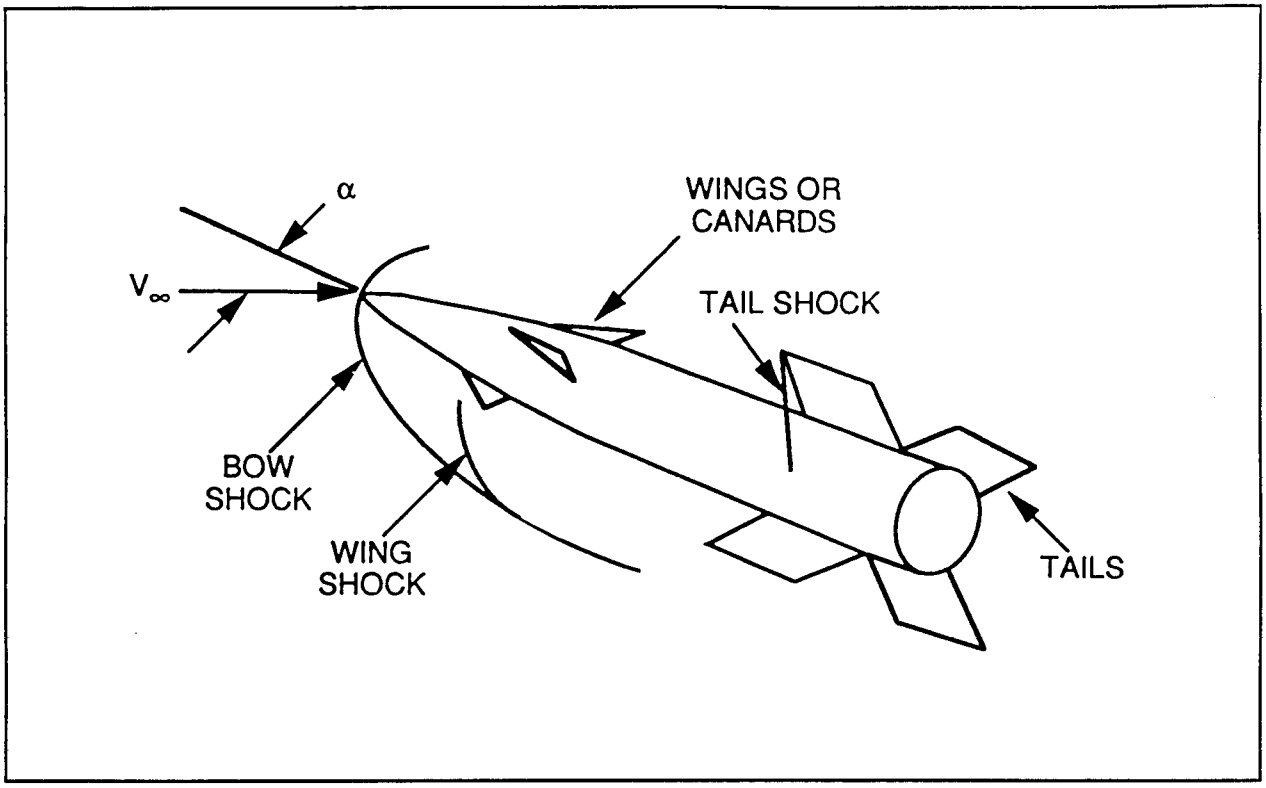

FIGURE 35. ILLUSTRATION OF SOME INTERNAL SHOCK INTERACTIONS

A final nonlinearity modeled only in the approximate sense is in the transonic flow region. Here, the mathematical model is nonlinear at small AOA and as a result, increases the computational difficulty in getting solutions. The approach here is to use more sophisticated numerical codes to estimate aerodynamics as a function of geometric and freestream parameters, and then use table look-up procedures to estimate aerodynamics on a configuration other than those computed. Table 1 includes body-alone center-of-pressure shifts that are also partly a result of this nonlinearity.

3.0 RESULTS AND DISCUSSION

Results of the new methodology extended to AOA greater than 30 deg will be presented both within and outside the data base used to define the nonlinear terms associated with the normal force coefficient and interference lift terms of Equation (1).

The first criterion of accuracy must be in how well the new methodology duplicates aerodynamics within the data bases used in the definition of the nonlinear terms. The second criterion is to determine if the new methodology is robust in the parametric definition of the nonlinear quantities so it will predict aerodynamics within the desired accuracy bounds outside the data base. These accuracy bounds are ±10 percent on average values of axial and normal force coefficient and ±4 percent of the body length on center of pressure. "Average values" means that each force and center-of-pressure prediction is compared to the measured value at a number of Mach numbers and AOA. These errors are then averaged over enough points to get a good statistical

average. In general, at least six data points (a data point is one AOA and one Mach number) should be used. The more data points used, the greater the confidence that can be placed on the accuracy predictions.

3.1 CONFIGURATIONS WITHIN THE DATA BASE

The primary data bases used in the definition of the nonlinear quantities of Equation (1) are the Langley[9] and the Stallings and Lamb,[10] with other data bases[6,11,13,16,21] playing a less significant role. The primary data bases are the most important to duplicate. The results of the AP95 methodology compared to the AP81, AP93, and Langley experimental data are shown in Figure 36. These results are for AOA of 10, 15, 20, 25, and 30 deg at Mach numbers 0.6, 0.8, 1.2, 1.5., 2.0, 2.5, 3.0, 3.5, and 4.5, and for wing planforms AR = 0.5, λ = 0, 0.5, 1.0; AR = 1.0, λ = 0.5; AR = 2.0, λ = 0, 0.5, 1.0; and AR = 4.0, λ = 0.5. Not all data were available at each AOA, so a total of 309 cases are available (numbers without parentheses in Figure 36). Comparisons have been previously made with the AP93 and AP81 for these same AOA, so a direct comparison of the AP95 improvements can be made with the AP93 and AP81 methodology. Also note that 5-deg AOA was excluded from the comparison because much of the data deviated slightly from going through $C_N = 0$ at $\alpha = 0$. Rather than going through a shift in data for several hundred cases, the error was smaller for AOA of 10 deg and greater than at AOA of 5 deg and smaller. The small AOA data were, therefore, not used. Even so, the data have some small errors that were not corrected.

COMPARISON WITH EXPERIMENTAL RESULTS
INSIDE DATA BASE

DATA BASE PARAMETERS

$0.6 \leq M_\infty \leq 4.6$
$0.25 \leq AR \leq 4$
$0 \leq \lambda \leq 1.0$
$r/s = 0.5$

BODY: 12.33 CALIBER OGIVE CYLINDER
3 CALIBER TAN OGIVE NOSE

COMPUTATIONAL RESULTS FOR 309 (403) BODY-TAIL CASES

α = 10, 15, 20, 25, 30, (35, 40)

	C_N			$\bar{X}_{cp}$		
ERROR	AP81	AP93	AP95	AP81	AP93	AP95
AVG ERROR	11.7%	5.6%	4.0% (4.1%)	.029L	.012L	.010L (.009L)
MAX ERROR	51.0%	20.0%	11.8% (11.8%)	.112L	.053L	.041L (.041L)

FIGURE 36. COMPARISON WITH EXPERIMENTAL RESULTS INSIDE DATA BASE

As seen in Figure 36, AP95 decreases the average normal force error for $\alpha \leq 30$ by almost 30 percent (4.0 percent versus 5.6 percent) and decreases the maximum normal force error by over 40 percent (11.8 percent versus 20 percent). The average center-of-pressure errors are

reduced by about 17 percent (0.010ℓ versus 0.012ℓ), with the maximum error reduced by almost 23 percent (0.041ℓ versus 0.053ℓ). Furthermore, when the higher AOA of 35 deg and 40 deg are considered, yielding 403 versus 309 cases, the average and maximum normal-force and center-of-pressure errors are about the same as for the $\alpha \leq 30$ deg cases.

The configuration of Figure 8[16] was considered for the wing B in the mid-position for AOA up to 80 deg and at M = 0.1. On average, the normal force and center-of-pressure errors were similar to those in Figure 36. More specifically, the configuration shown in Figure 8 was considered at M = 0.1 only, but for AOA from 0 to 80 deg. Averaging the errors in normal force coefficient and center of pressure every 10 deg in AOA gave an average error count of less than 8 percent and 4 percent, respectively, for C_N and X_{CP}/D. These errors are somewhat larger than those for the Langley[9] and Stallings and Lamb[10] data bases, but the errors for those data bases were averaged to 40-deg AOA only, whereas the errors for the Figure 8 data base were averaged to 80-deg AOA. The results of Figure 36 and the other configuration within the data base are encouraging. Most of the decrease in prediction error of the AP95 over the AP93 is the result of the new wing-alone model, the improved wing-body and body-wing interference models, and the addition of Reynolds number as a parameter to the body-alone cross-flow drag coefficient determination. The average errors of the normal-force coefficient and center-of-pressure predictions on configurations within the data base were significantly less than the maximum tolerance of ±10 percent on C_N and ±4 percent ℓ on center of pressure.

3.2 CONFIGURATIONS OUTSIDE THE DATA BASE

Several configurations have been selected for comparisons of predicted static aerodynamics with experimental data. The first of these configurations is shown in Figure 37A. This configuration is a body-alone wind tunnel model tested in the transonic and supersonic tunnels at Arnold Engineering and Development Center (AEDC) in Tullahoma, Tennessee. The configuration was tested without a transition trip, at Reynolds numbers varying from 1.8 X 10^6/ft to 5.3 X 10^6/ft, and at Mach numbers 0.6 to 4.0 and AOA from -6 to 14 deg. Interest here will focus on the zero AOA axial force comparison with various nose bluntness ratios. Only forebody axial force (wave plus skin friction) will be plotted since only this was given in the related report by Butler, Sears, and Pallas.[22]

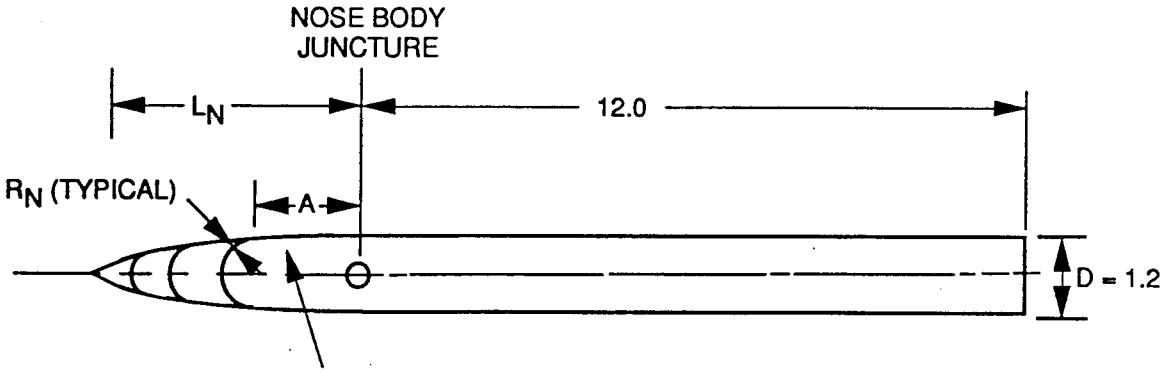

NOSE FINENESS RATIO L_N/D (CALIBER)	NOSE R_N/R_B	R_N (in.)	A (in.)	D (in.)	TOTAL LENGTH (in.)
2	0.00	0.00	2.40	1.2	14.4
2	0.25	0.15	2.06	1.2	14.06
2	0.50	0.30	1.67	1.2	13.67
2	0.75	0.45	1.17	1.2	13.17
4	0.00	0.00	4.80	1.2	16.80
4	0.25	0.15	4.15	1.2	16.15
4	0.50	0.30	3.38	1.2	15.38
4	0.75	0.45	2.38	1.2	14.38

FIGURE 37A. BUTLER, SEARS, AND PALLAS[22] WIND TUNNEL MODEL TESTED

Figures 37B and 37C give C_{A_F} as a function of M_∞ for the present theory and experiment for 2- and 3-cal tangent ogive noses, respectively, with various nose bluntness ratios. Only the supersonic results were given, and as seen in the figures, the present methodology gives very good predictions of forebody axial force for all nose bluntness ratios at all Mach numbers shown. This good agreement with experiment is attributed primarily to the second-order-accurate methods developed for calculating wave drag on blunt nose bodies of revelation.[1]

Figure 38A shows a second case considered. This case has the same body (12.33-cal tangent ogive cylinder with a 3-cal nose) as that tested at Langley.[9] However, dorsals of aspect ratio 0.1 and tail surfaces of aspect ratio 2.0 have been added. Mach numbers considered are 4.5 and 10.0. This case was originally defined[19] to allow computations to be performed with a full Euler solver[23] at high Mach number, since wind-tunnel data above Mach 4.6 appeared to be lacking. Figure 38B shows the comparison of the ZEUS[23] computations for normal force and center of pressure with the AP93 and AP95 results for the body-tail configuration. The AP95 results for normal force are slightly higher than the AP93 at M = 10.0, but quite similar at M = 4.5. Center of pressure results show the AP95 giving slight improvement over the AP93. This slightly high prediction is due to the fact the wing-alone data base was modified slightly from the tables in Moore and McInville.[4] The good agreement for C_N and X_{CP} with the ZEUS computations at M = 10 is particularly encouraging, as this Mach number is far outside the data base upon which the theory was based. This means the extrapolations and assumptions made in this Mach number region are at least reasonable.

Figure 38C shows the same comparisons as Figure 38B except for the dorsal-body-tail configuration. Results of AP95 comparisons to the ZEUS code and AP93 for the full configuration are similar to those of the body-tail case. In general, for the AOA range of 0 to 30 deg, the AP95 gives slightly improved results over the AP93 for the configuration of Figure 38A.

The next case considered is a wing-body-tail configuration tested by Jorgenson.[13] This case was also considered for AP95,[1] but only up to 30-deg AOA since that was the limit of that technology. The configuration is shown in Figure 39A. Note the very large wing surfaces and aspect ratios. These are much larger than most missile configurations would have and are quite similar to an aircraft. Figure 39B gives the normal-force coefficient comparison of AP95 with experiment for the wing-body case at Mach numbers 06., 0.9, 1.5 and 2.0. The AP93 results are also shown to AOA of 30 deg.

In general, the AP95 gives quite acceptable results for an engineering code for this configuration compared to data at all the Mach numbers considered. There is an apparent slight discontinuity in the slope of the C_N versus α curve at α = 35 deg AOA. This is caused by the fact that at subsonic Mach numbers, the wing basically stalls around AOA of 25 to 40 deg. The wing-alone method of the AP95 blends this discontinuous behavior out, and the fourth-order method for the wing tends to show a discontinuous slope of the C_N curve at low Mach number. If the configuration of Figure 39A were body-dominated, this behavior would not be as obvious, but since it is wing-dominated, the wing behavior is more prevalent.

Figure 39C gives the AP95 C_N and X_{CP} results at M = 0.6 and 2.0 for the full wing-body-tail configuration of Figure 39A.

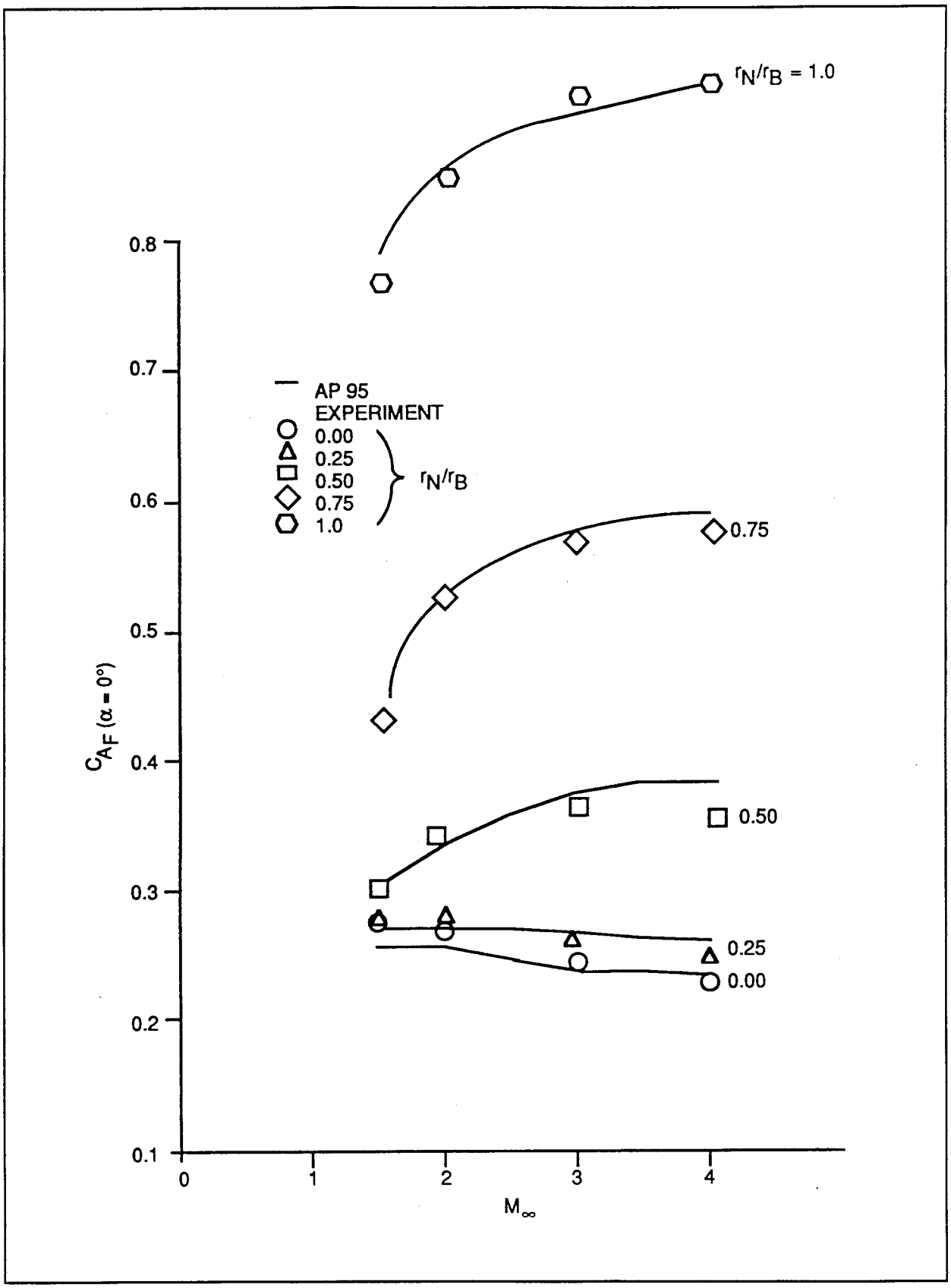

FIGURE 37B. VARIATION OF FOREBODY AXIAL FORCE COEFFICIENT WITH MACH NUMBER FOR VARIOUS NOSES ON 10-CAL AFTERBODY (R_N/ft = 1.8 X 10^6, ℓ_N = 2 cal)

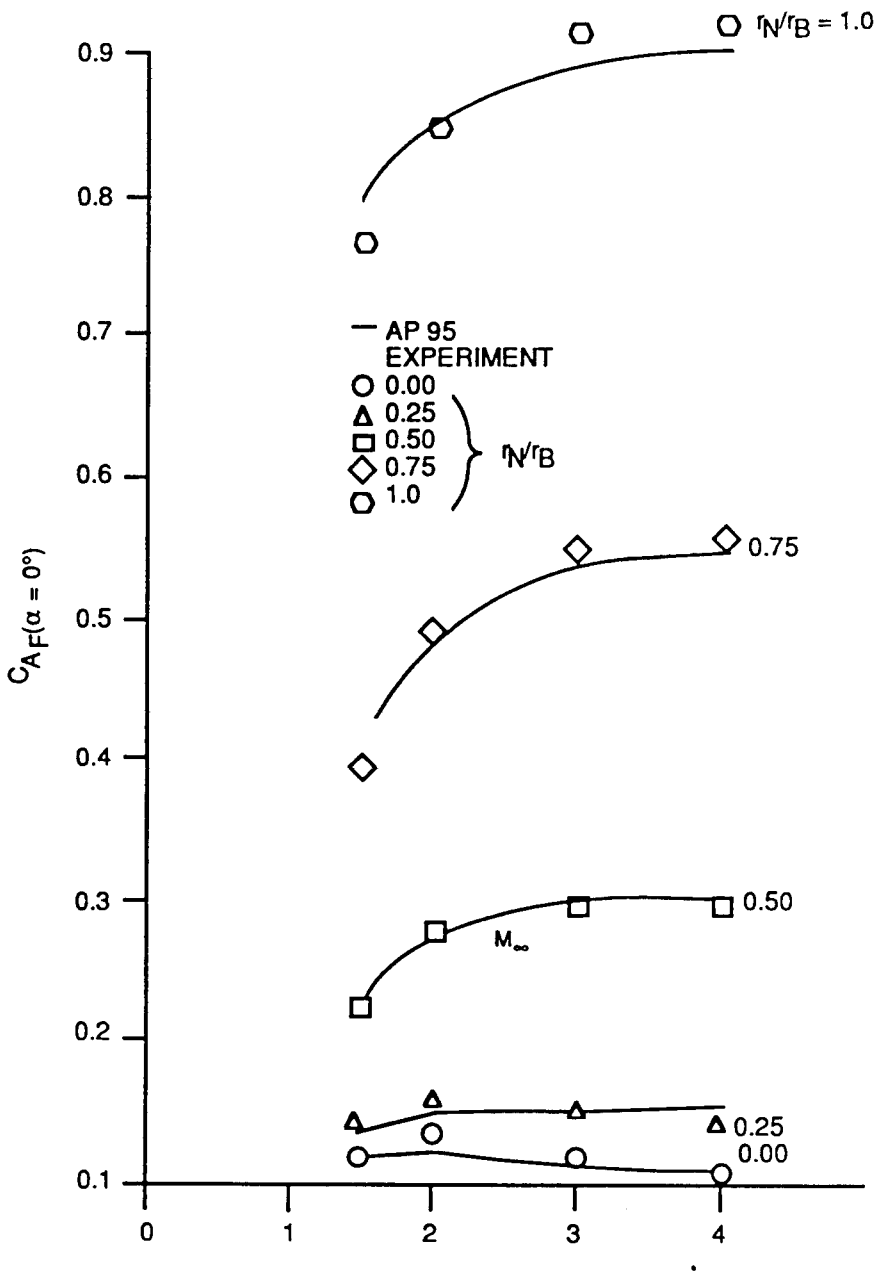

FIGURE 37C. VARIATION OF FOREBODY AXIAL FORCE COEFFICIENT WITH MACH NUMBER FOR VARIOUS NOSES ON 10-CAL AFTERBODY (R_N/ft 1.8 X 10^6, ℓ_N = 4 cal)

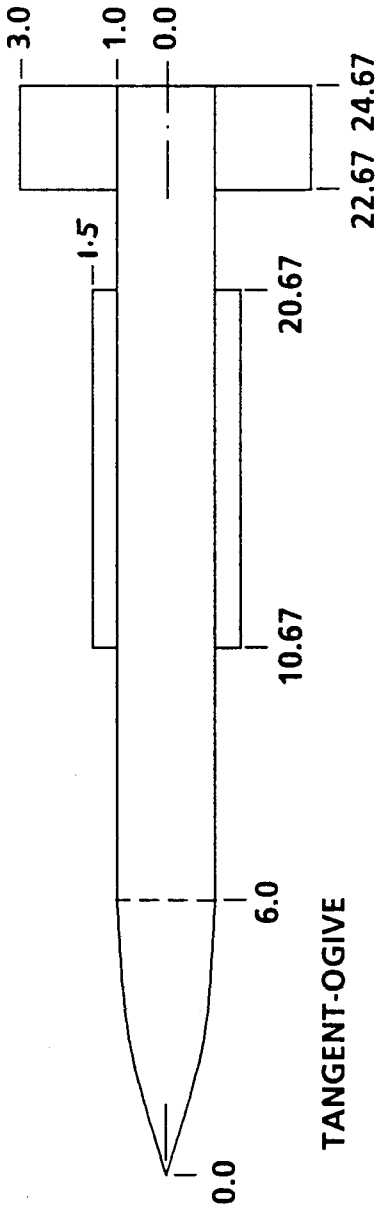

FIGURE 38A. BODY-DORSAL-TAIL CONFIGURATION
USED FOR COMPARING ZEUS, AP95, AND AP93 COMPUTATIONS

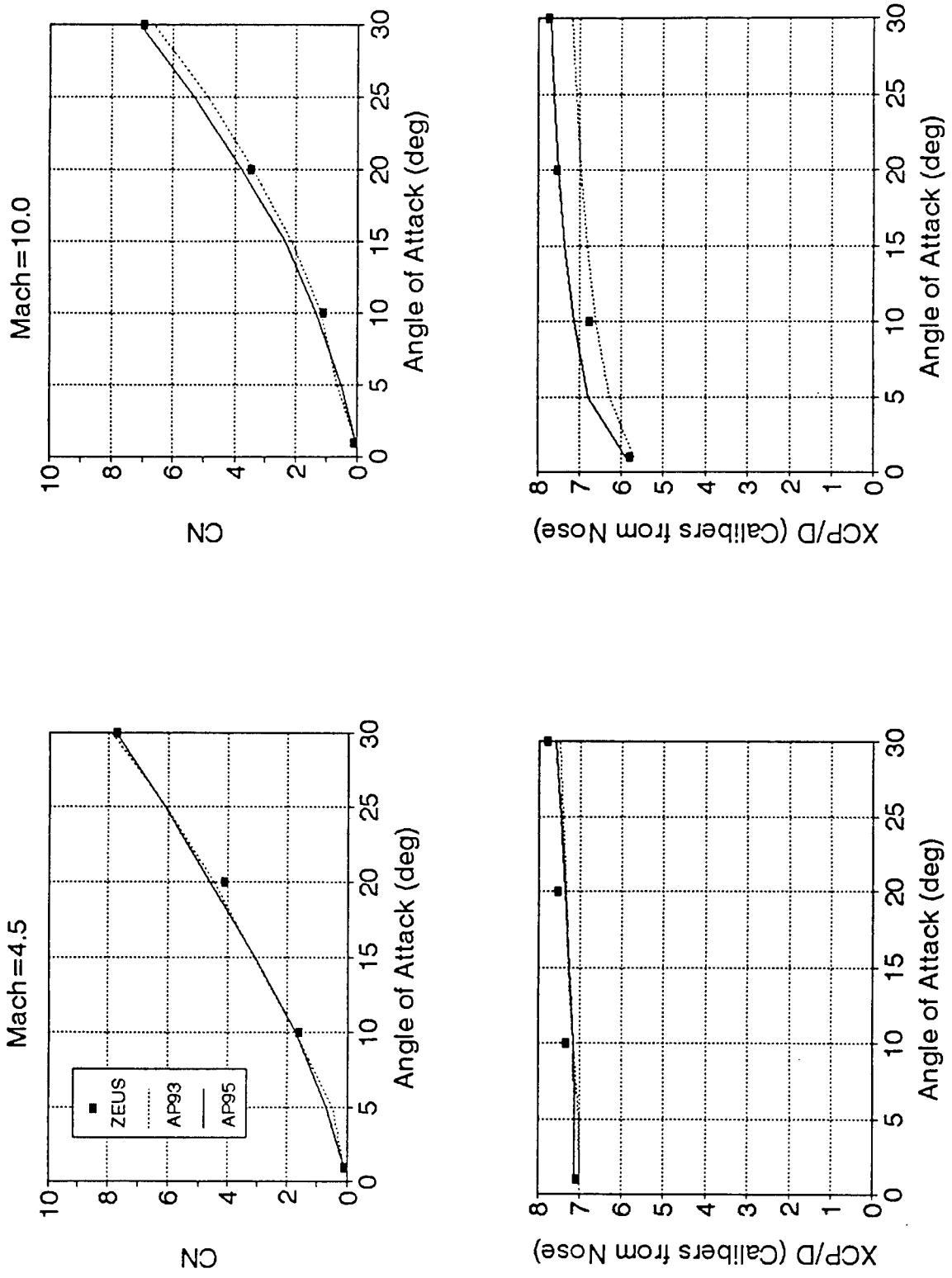

FIGURE 38B. NORMAL FORCE COEFFICIENT AND CENTER OF PRESSURE COMPARISONS OF THREE ANALYTICAL METHODS FOR BODY-TAIL OF FIGURE 38A

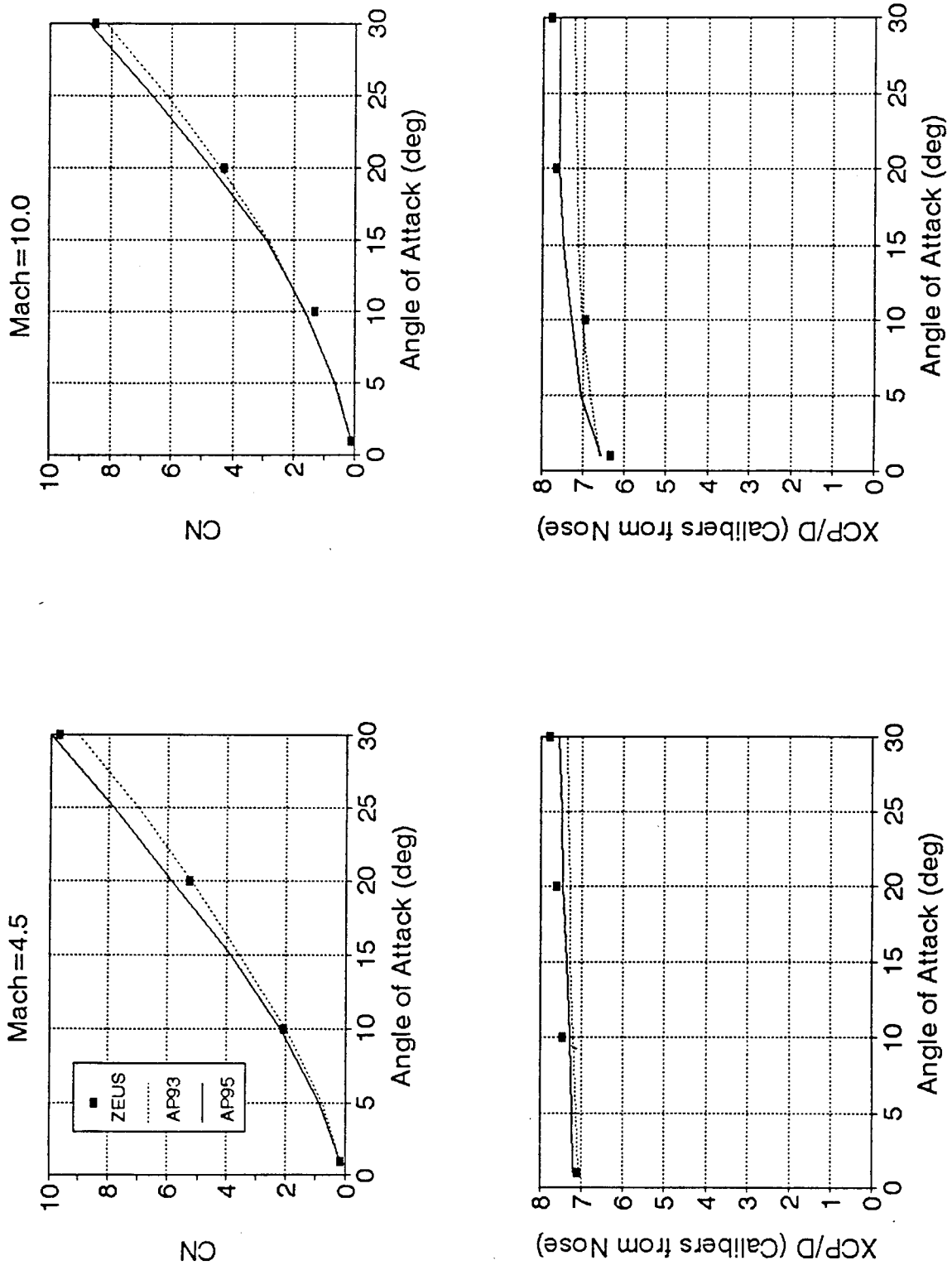

FIGURE 38C. NORMAL FORCE COEFFICIENT AND CENTER OF PRESSURE COMPARISONS OF THREE ANALYTICAL METHODS FOR CONFIGURATION OF FIGURE 38A

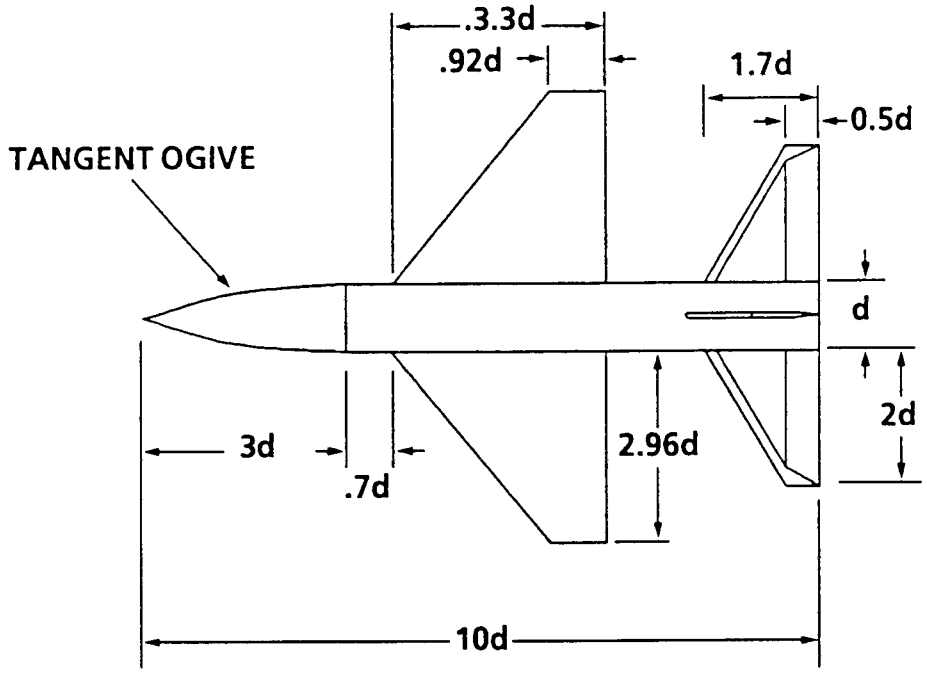

PARAMETERS

$(AR)_T = 3.64$	$\lambda_T = .29$	d = 2.6 in.
$(AR)_W = 2.81$	$\lambda_T = .28$	

FIGURE 39A. WING-BODY AND WING-BODY-TAIL CONFIGURATIONS USED FOR COMPARING AP95 TO EXPERIMENT AND AP93

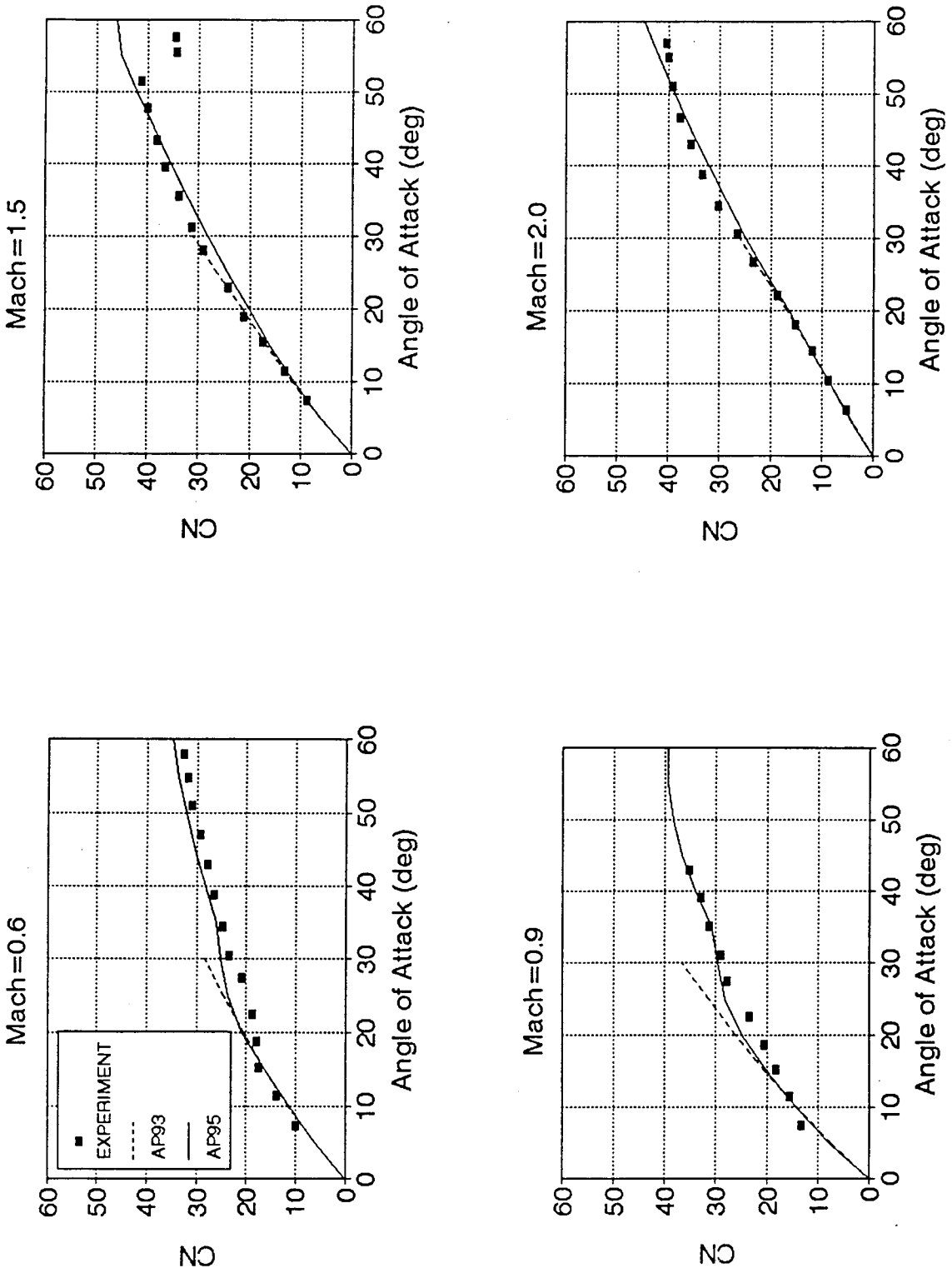

FIGURE 39B. NORMAL FORCE COEFFICIENT COMPARISONS FOR BODY-TAIL CONFIGURATION OF FIGURE 39A

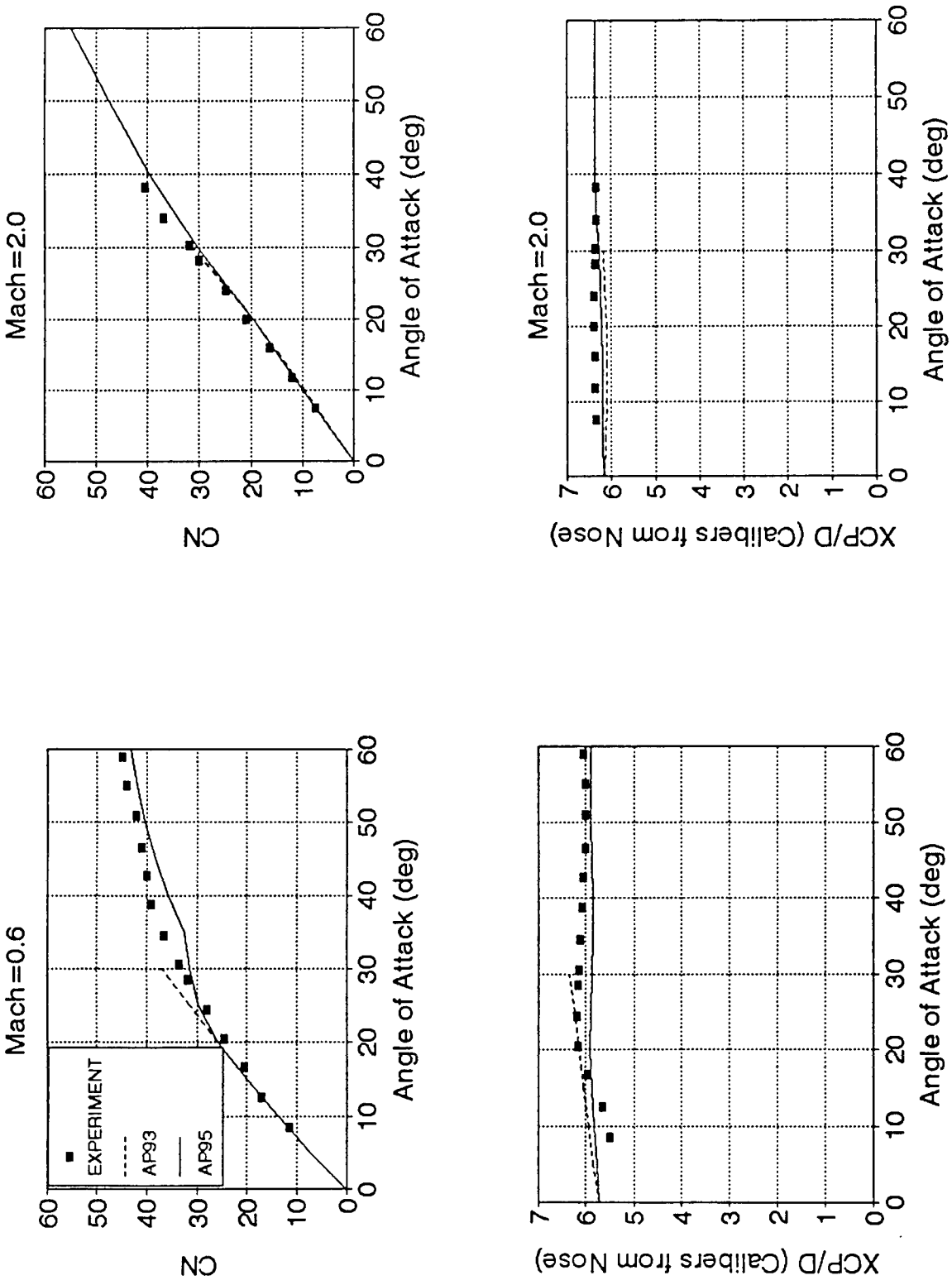

FIGURE 39C. NORMAL FORCE COEFFICIENT AND CENTER OF PRESSURE COMPARISONS FOR CONFIGURATION OF FIGURE 39A

The AP95 results are within the ±10 percent error goal for C_N, on average, as well as the ±4 percent ℓ goal for X_{CP}, all the way to 60-deg AOA at M = 0.6. For M = 2.0, experimental data were only given to about 40-deg AOA.[13]

The next three cases are low Mach number cases tested at the Naval Postgraduate School in Monterey. The first case is a canard-controlled configuration with aspect ratio 1.59 canard and 0.9 tail surfaces (see Figure 40A).[24] The body is 22.6 cal in length. Data are available for M = 0.2 up to 45-deg AOA and for control deflections of the canards of -20 deg, 0 deg and +20 deg. Axial force, normal force and pitching moment coefficients are shown in Figure 40B, for δ = -20 deg; Figure 40C, for δ = 0 deg; and Figure 40D for δ = +20 deg. Leading edge up is a positive control deflection. Shown on the figures are experimental data,[24] the AP95, and Missile DATCOM[7] results. The comparison of the AP95 with the data is quite encouraging for all three of the aerodynamic coefficients at all AOA. It should be pointed out that the C_N and C_M data for δ = 0 do not go through 0 at α = 0 and no attempt was made to try to correct the data. Also, the sting balance was chosen based on normal force loads, and the authors[24] point out that the axial force loads could have substantial error as a result of this decision. DATCOM also gives reasonable agreement with experiment to AOA of about 30 deg for both C_A and C_N, but appears to have more difficulty with pitching moments.[7]

The second low Mach number case is shown in Figure 41A, and the experimental results are documentated in a report by Smith, Salazar, Hebbar, and Platzer.[25] This configuration is 17.5 cal in length with a 1.88-cal tangent ogive nose. It has aspect ratio 1.38 wings located near the center of the missile and aspect ratio 1.56 tail surfaces located flush with the base.

Figure 41B presents the AP95 results for axial force, normal force and pitching moment coefficients compared to experiment and Missile DATCOM[7] where Missile DATCOM calculations were available from the Smith, Salazar, Hebbar, and Platzer work.[25] Results are shown for δ = 0 in all the figures, except for the one in the lower right-hand corner of Figure 41B, where pitching moments are given for control deflections of ±30 deg. The tail surface is deflected here. Again, acceptable agreement of the AP95 is obtained with the data for all the aerodynamic coefficients. Missile DATCOM[7] deviates substantially from the data above AOA of 20 to 25 deg.

The third of the low Mach number cases is shown in Figure 42, and the test data were given in a report by Howard and Dunn.[26] This configuration has dorsals that have an aspect ratio of 0.12 and tail surfaces that have an aspect ratio of 4.0. The exact configuration illustrated at the top of Figure 42 is not within the allowable constraints for fin planform required by the AP95. Therefore, a modified version of the fin planforms is required, one that meets the constraints of the AP95. This configuration is shown in the middle of Figure 42. Note that the parameters that were held constant for the fin planforms were area, aspect ratio, span, taper ratio, leading-edge sweep angle and location of the geometric centroid of the planform area. The Howard and Dunn[26] work only gave normal force as a function of AOA along with results from Missile DATCOM.[7] The AP95 results are also shown at the bottom of Figure 42. Quite acceptable agreement is obtained with the AP95 compared to experiment, even at high AOA. The AP95 is somewhat lower than the data suggest. However, part of this underprediction is suspected to be the tendency of a base-mounted sting to give larger-than-true normal forces at subsonic Mach numbers.[17,18] In making this statement, sting interference effects were assumed to be unaccounted for.

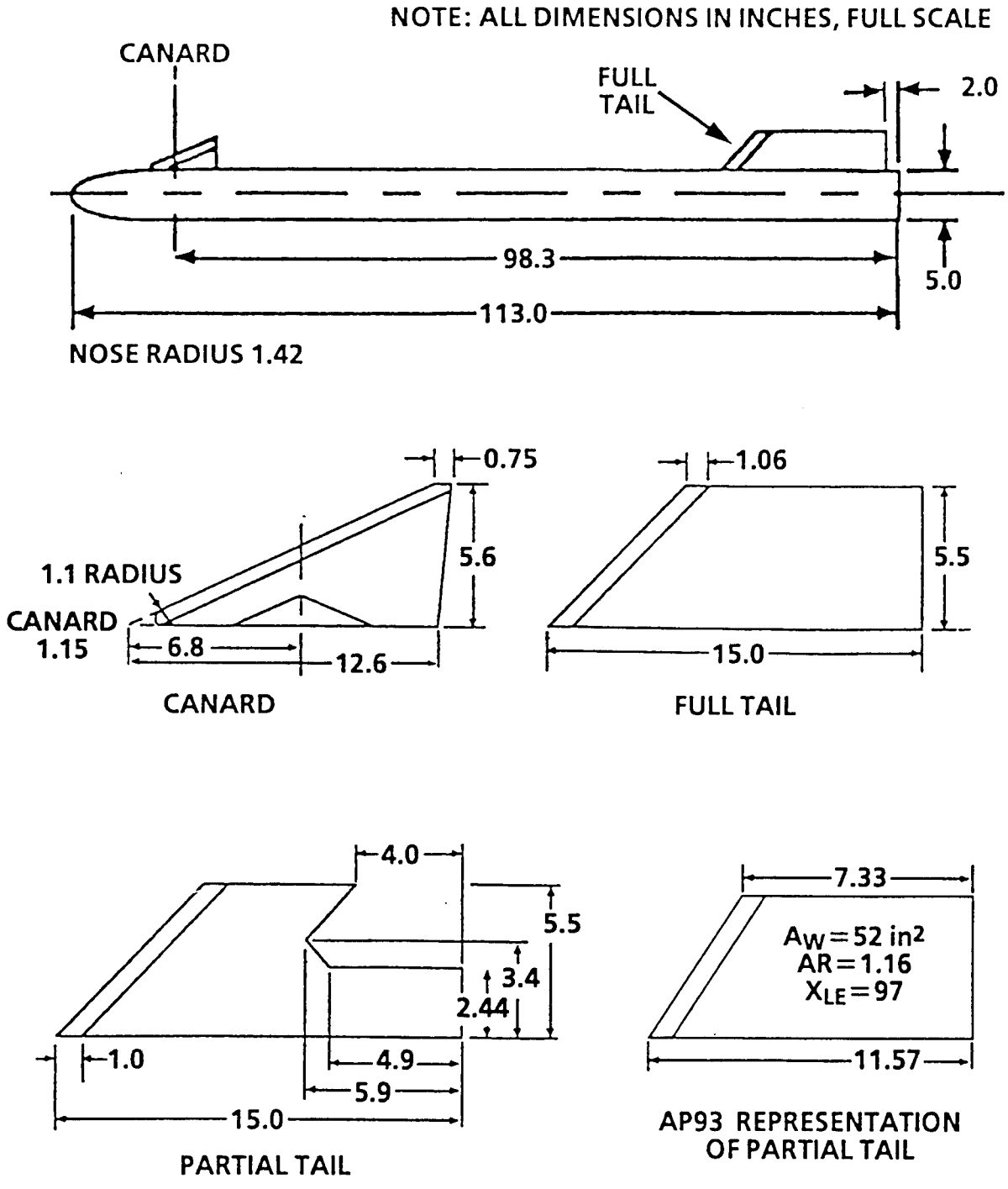

FIGURE 40A. CANARD-CONTROLLED MISSILE CONFIGURATION[24]

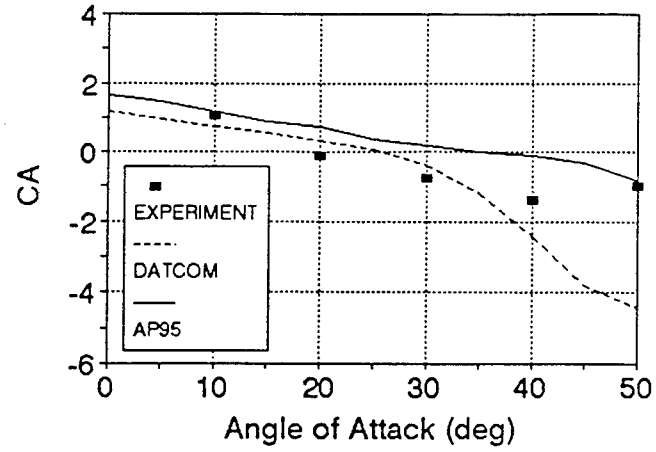

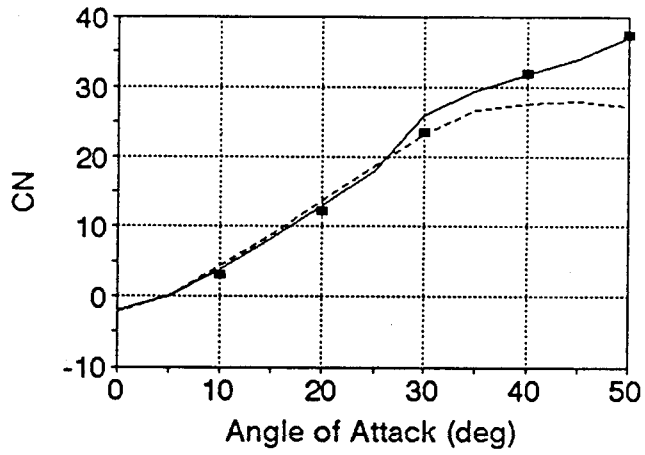

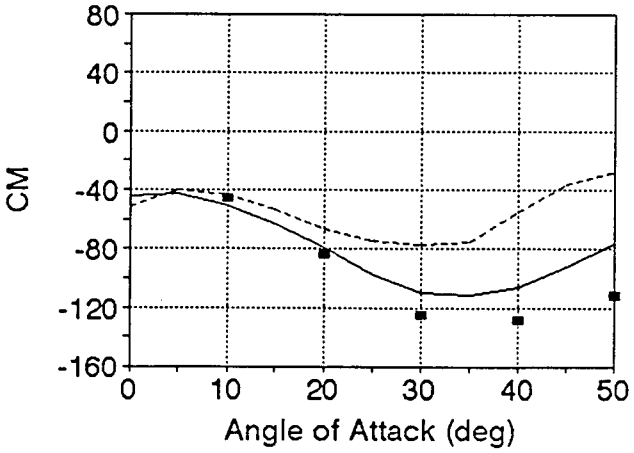

FIGURE 40B. COMPARISON OF AXIAL, NORMAL AND PITCHING MOMENT COEFFICIENTS BETWEEN EXPERIMENT, MISSILE DATCOM AND AP95 FOR FIGURE 40A CONFIGURATION (δ = -20°)

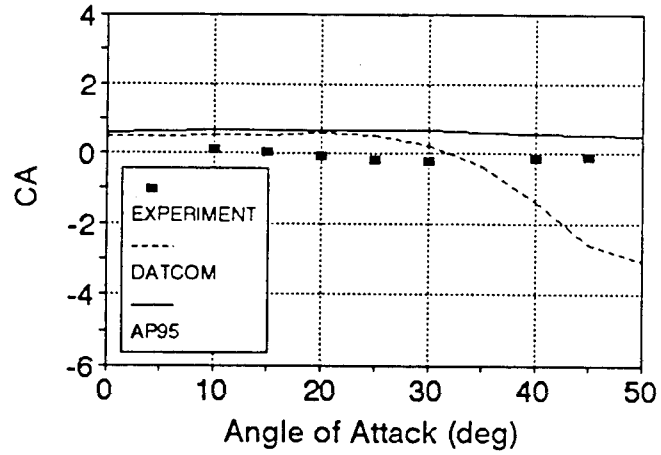

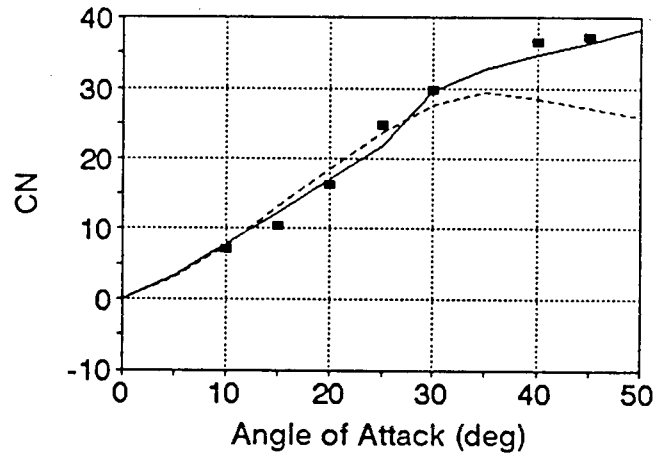

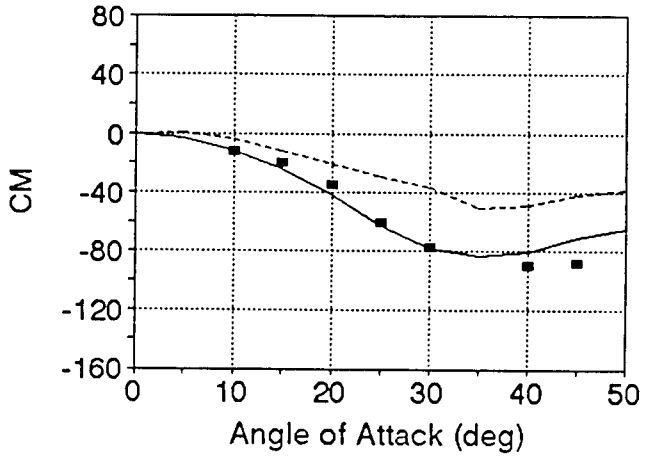

FIGURE 40C. COMPARISON OF AXIAL, NORMAL AND PITCHING MOMENT COEFFICIENTS BETWEEN EXPERIMENT, MISSILE DATCOM AND AP95 FOR FIGURE 40A CONFIGURATION ($\delta = 0°$)

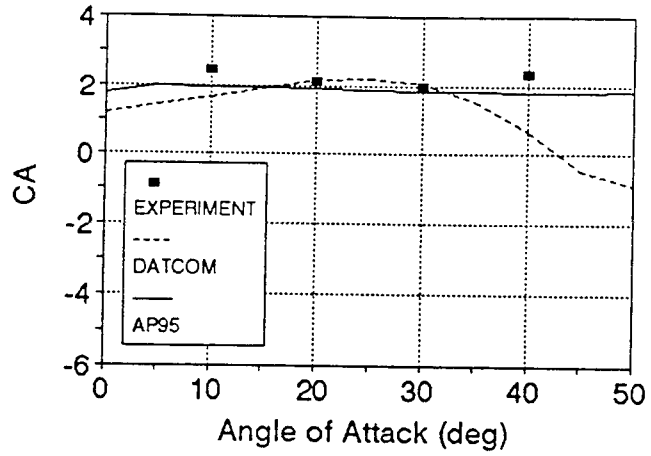

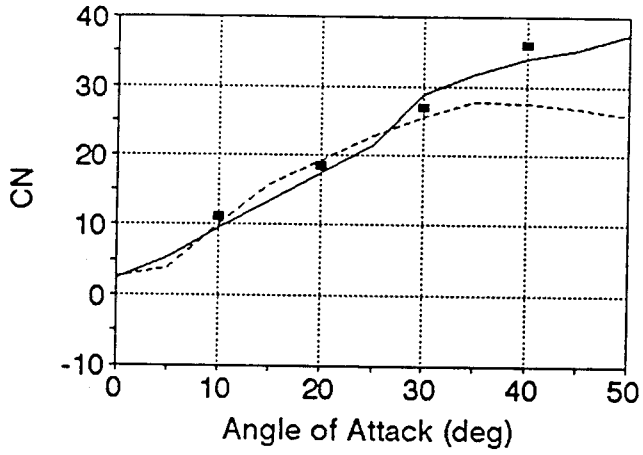

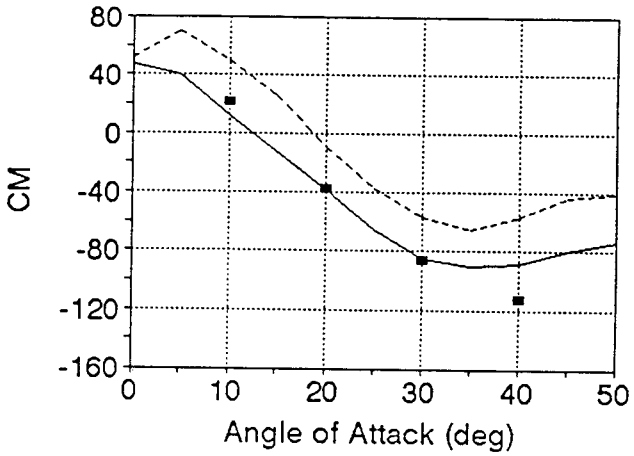

FIGURE 40D. COMPARISON OF AXIAL, NORMAL AND PITCHING MOMENT COEFFICIENTS BETWEEN EXPERIMENT, MISSILE DATCOM AND AP95 FOR FIGURE 40A CONFIGURATION ($\delta = +20°$)

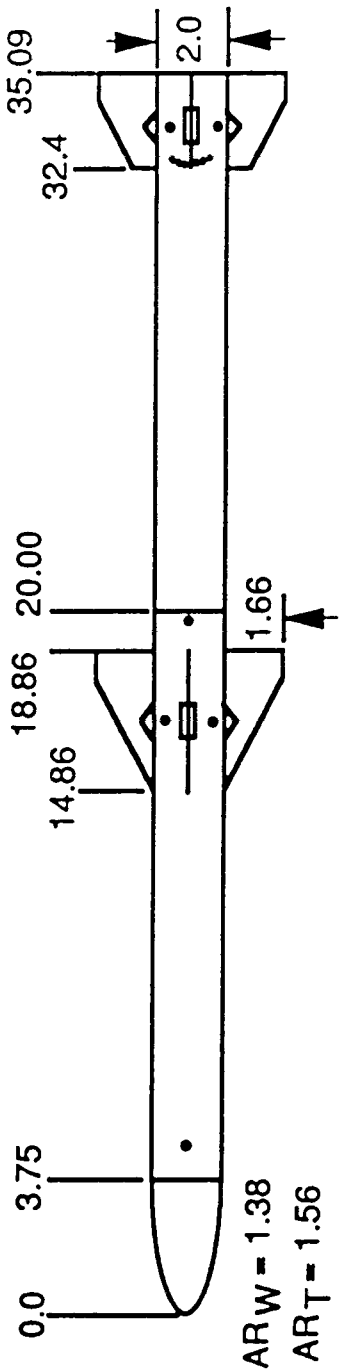

FIGURE 41A. MMPT CONFIGURATION TESTED AT $M_\infty = 0.2$ (FROM SMITH, SALAZAR, et al.[25])

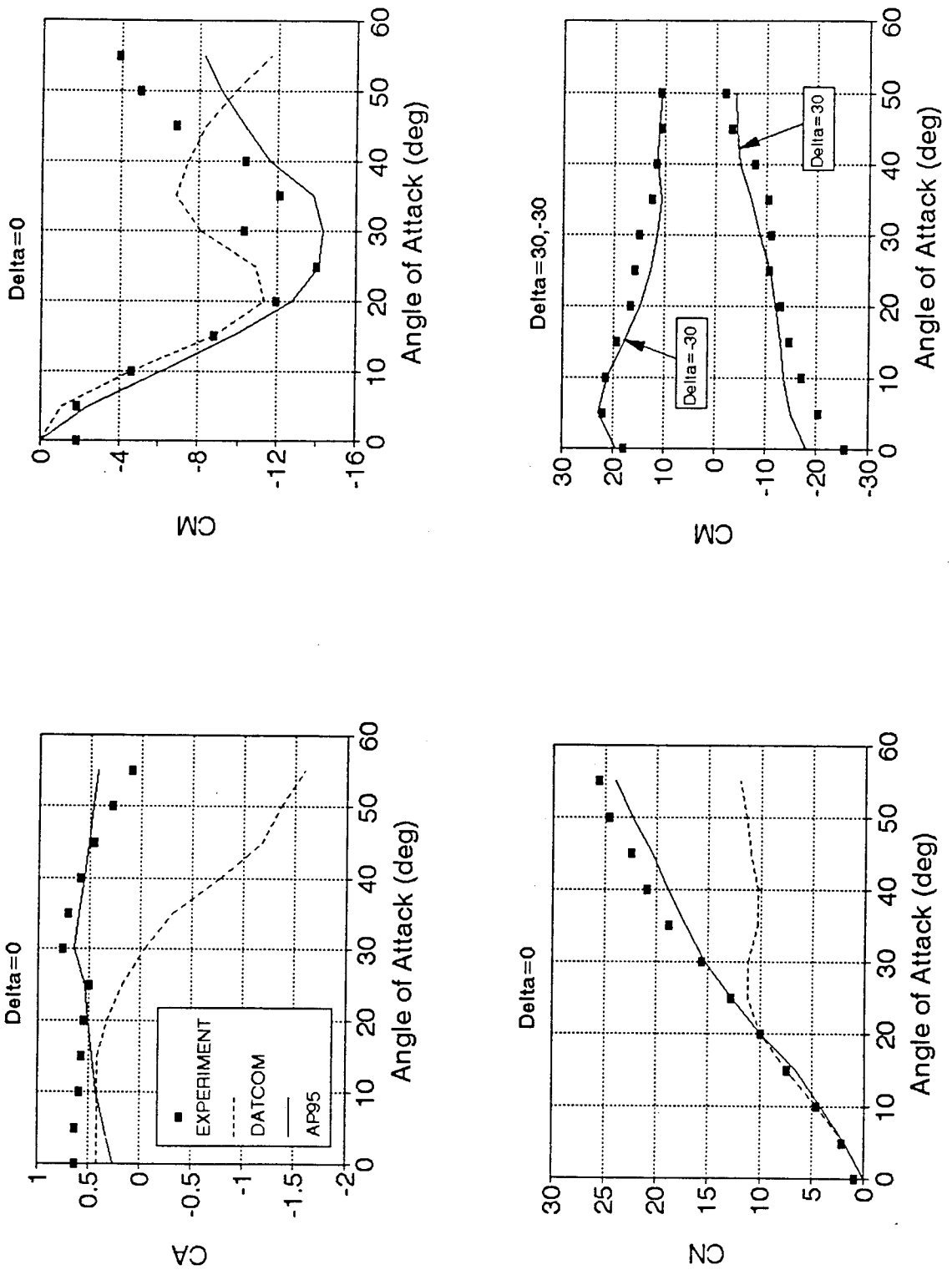

FIGURE 41B. COMPARISONS OF STATIC AERODYNAMIC COEFFICIENTS BETWEEN EXPERIMENT AND PREDICTIONS FOR CONFIGURATION OF FIGURE 41A

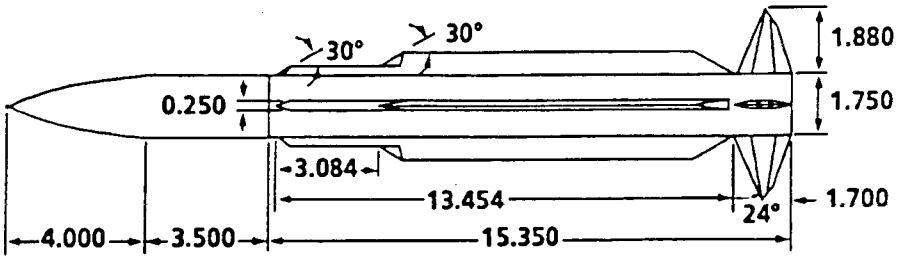

CONFIGURATION TESTED IN WIND TUNNEL (FROM REFERENCE 29 WHERE DIMENSIONS ARE IN INCHES)

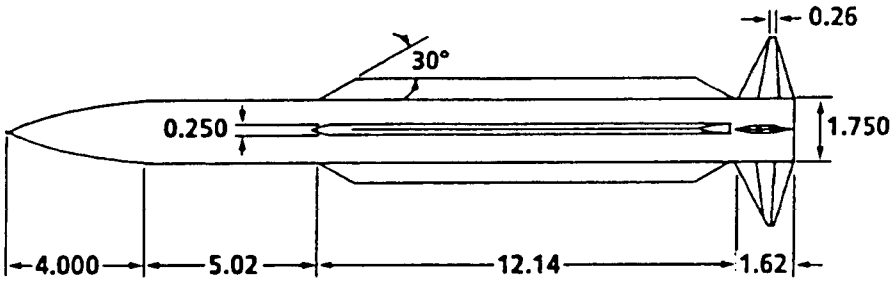

MODIFIED CONFIGURATION USED IN AEROPREDICTION COMPUTATIONS

PARAMETERSFOR BOTH MODELS

$(AR)_T = 4.0$	$b_t = 3.76$ in.	$\lambda_T = .16$	$(\Lambda_{LE})_T = 24°$	$A_T = 3.54$ in.^{2}
$(AR)_D = .12$	$b_D = 1.32$ in.	$\lambda_D = .77$	$(\Lambda_{LE})_D = 60°$	$A_D = 14.2$ in.^{2}

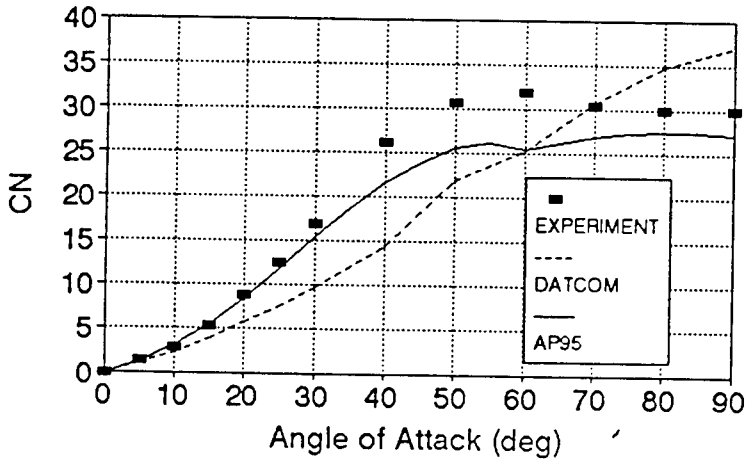

FIGURE 42. NORMAL FORCE COEFFICIENT COMPARISONS OF HOWARD AND DUNN[26] CONFIGURATION

The final validation case considered is a version of the SEASPARROW missile that has an extensive supersonic wind tunnel data base including AOA to 70 deg at some Mach numbers, and with control deflections to ±20 deg. The first data base includes AOA to 70 deg at Mach numbers of 2.3 and 4.6 only.[27] This configuration was tested with wiring tunnels on the exterior of the missile, which contributed somewhat to the aerodynamics. The other data base is more extensive in Mach number in that Mach numbers of 1.5, 2.0, 2.35, 2.87, 3.95 and 4.63 were tested, but AOA was limited to 45 deg.[28] In the comparisons that will be shown, the data at M = 2.3 and 2.35 and at M = 4.6, with and without wiring tunnels, will be shown on the same figures.

Figure 43A shows the external view of the configuration tested without the wiring tunnels.[28] The configuration is 18 cal in length with a 2.25-cal tangent ogive nose. It has wings with aspect ratio of 2.8 and tail surfaces of aspect ratio 2.6. The wings are used for control, and the pitching moments are referenced to a point 8.66 cal from the nose tip. Figures 43B through 43E present comparisons of C_N and C_M from the AP95 with experiment and the AP93 at M_∞ = 1.5, 2.0, 2.87, and 3.95, for control deflections of 0 and 10 or 20 deg depending on the availability of data. As mentioned earlier, the experimental data were on the configuration without wiring tunnels and were available only up to 45 deg AOA. Examining the figures shows that the AP95 gives quite good results for C_N at all α and δ. C_M is also predicted adequately at all α for M_∞ = 1.5, 2.0 and 2.87. However, at M_∞ = 3.95, nonlinearities associated with internal shock interactions of the bow and wing shocks and wing-to-tail shocks become important above AOA of 30 deg, and the predicted pitching moments deviate from the data by an increasing amount. This deviation occurs because the nonlinearity has been unaccounted for in a complete sense in the theoretical development of the AP95.

Figures 43F and 43G present the C_N and C_M comparisons of the AP95 with all data available at M = 2.3, 2.35 and 4.6. The data that extends to AOA = 70 deg has wiring tunnels present whereas the data without wiring tunnels only goes to 45 deg AOA. Note again that good agreement between the AP95 and data is obtained for all values of α and δ.

Pitching moments are also predicted fairly well at M = 2.3 for all α, because the internal shock interactions are not as severe. However, at Mach 4.6, the internal shock interactions are very severe and the AP95 does not predict the nonlinearities that occur between AOA of 30 and 60 deg. However, pitching moments are predicted quite well for AOA less than 30 deg and greater than 60 deg.

In trying to understand the phenomena occurring in Figures 43E and 43G, work by Agnone, Zakkay, and Tory was examined.[29] This work involved wind tunnel tests conducted at Mach number 2.7 on a wing-body configuration similar to the configuration in 43A without the tail surfaces. Body and wing pressure measurements, oil flow measurements and schlieren photographs were taken. The data showed that, even at a moderate supersonic Mach number of 2.7, the bow shock intersected the wing in the windward plane around AOA = 30 deg. When this occurred, a trailing shock was created behind the wing. Of course if a tail surface were present, this trailing shock would have the potential to interact with the tail surface. As Mach number increases, this trailing shock increases in strength, causing a much stronger impact on the tail surface. Since the tail surface is over 7 cal

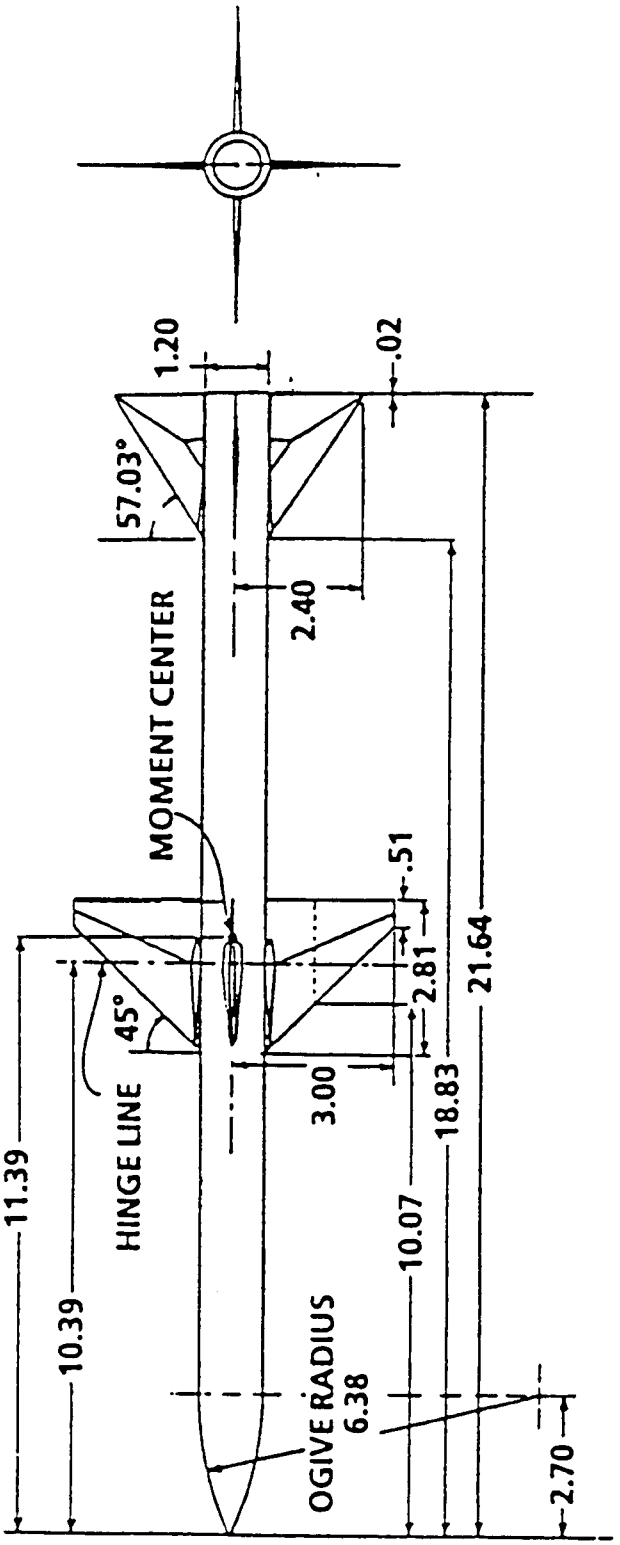

FIGURE 43A. AIR-TO-AIR MISSILE CONFIGURATION USED IN VALIDATION PROCESS[27,28]

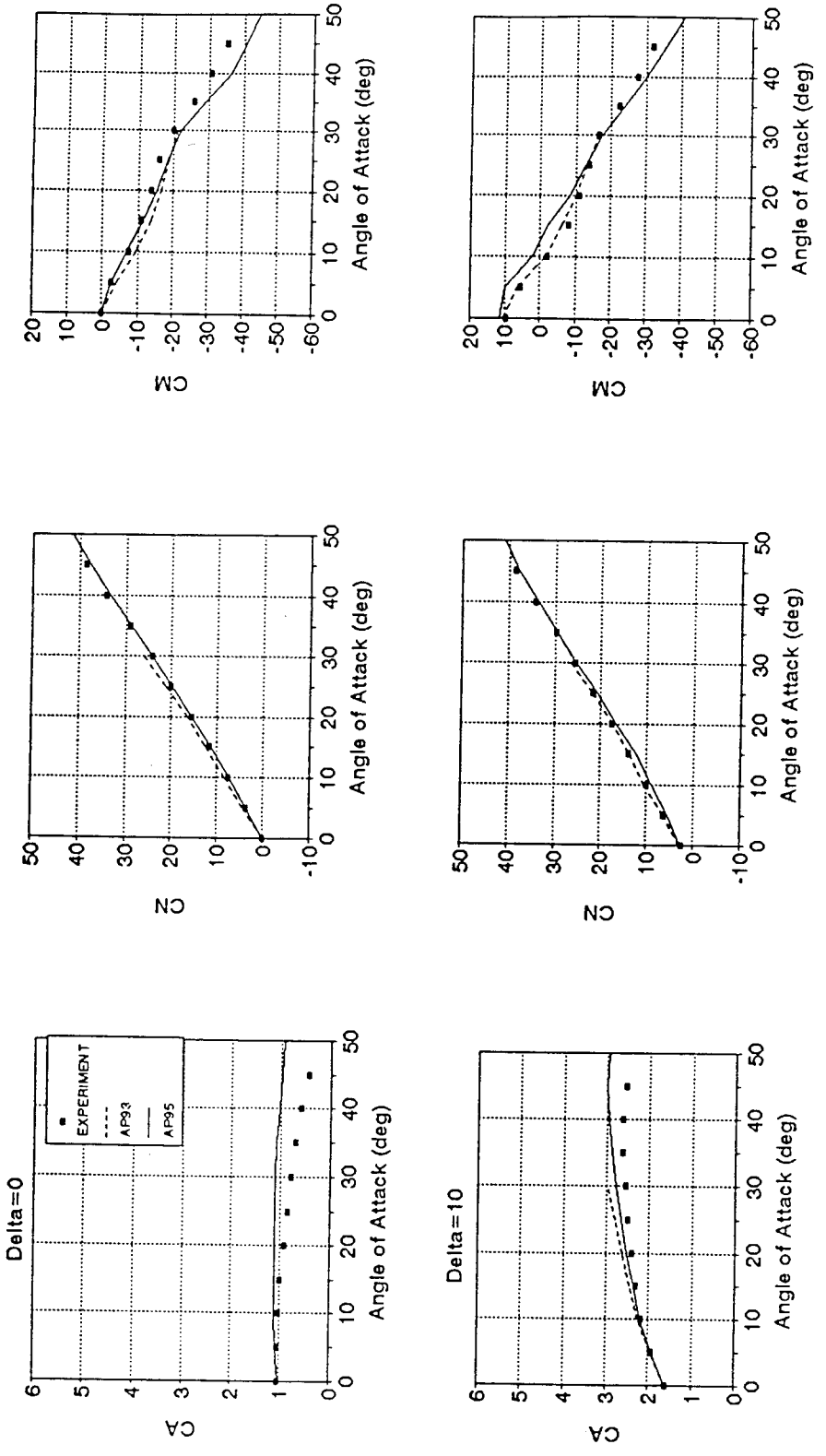

FIGURE 43B. STATIC AERODYNAMIC COEFFICIENT COMPARISONS FOR FIGURE 43A CONFIGURATION ($M_\infty = 1.5$)

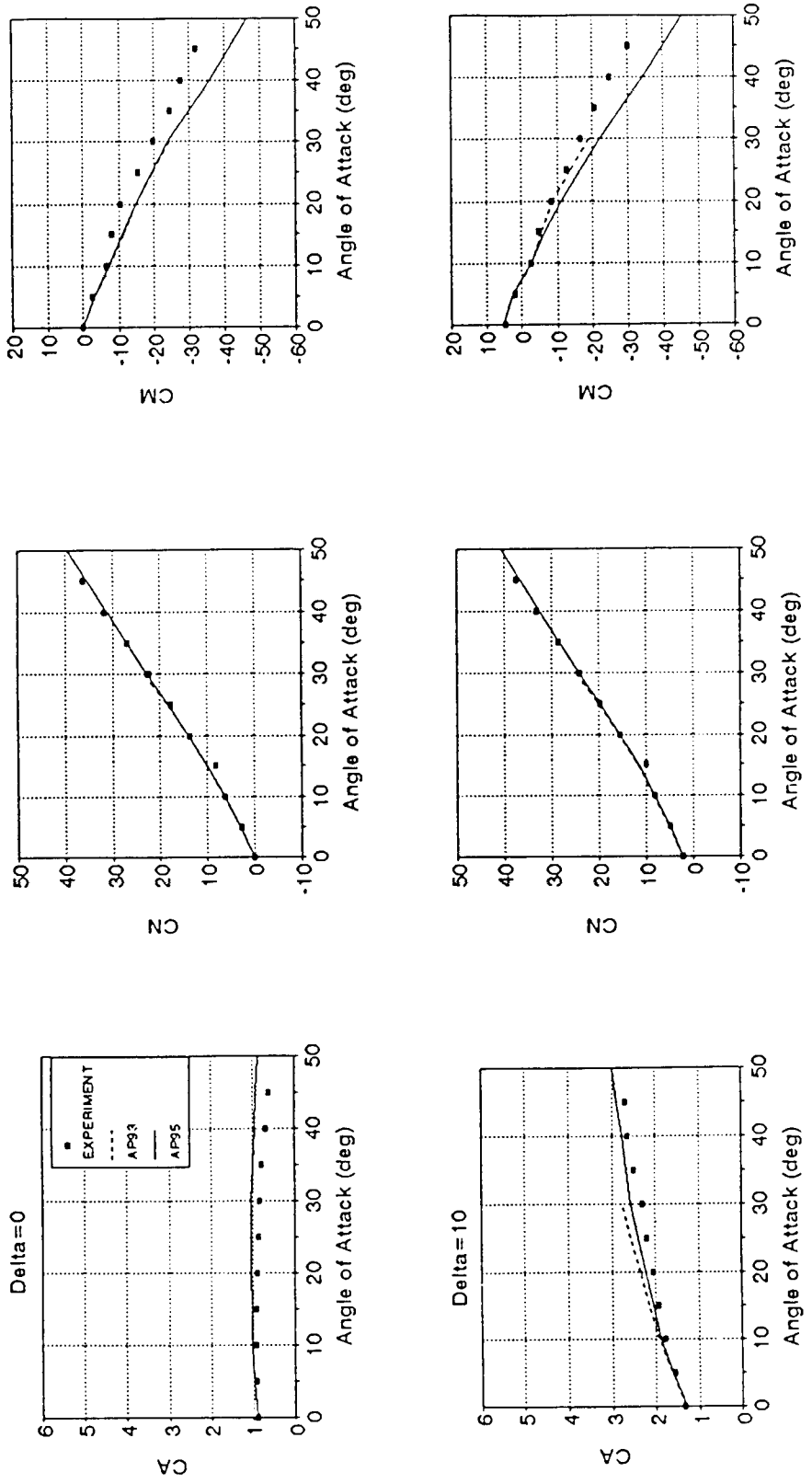

FIGURE 43C. STATIC AERODYNAMIC COEFFICIENT COMPARISONS FOR FIGURE 43A CONFIGURATION ($M_\infty = 2.0$)

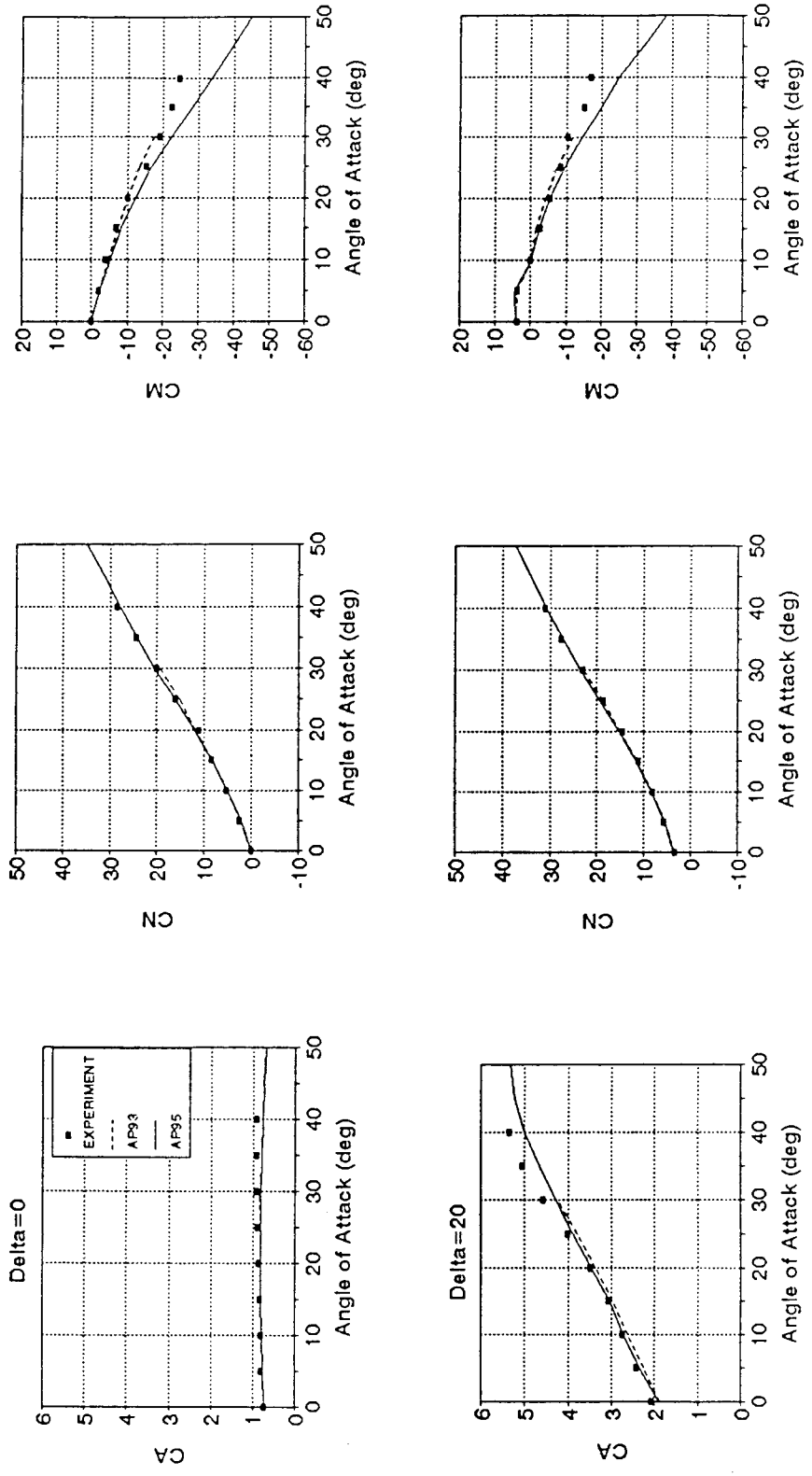

FIGURE 43D. STATIC AERODYNAMIC COEFFICIENT COMPARISONS FOR FIGURE 43A CONFIGURATION (M_∞ = 2.87)

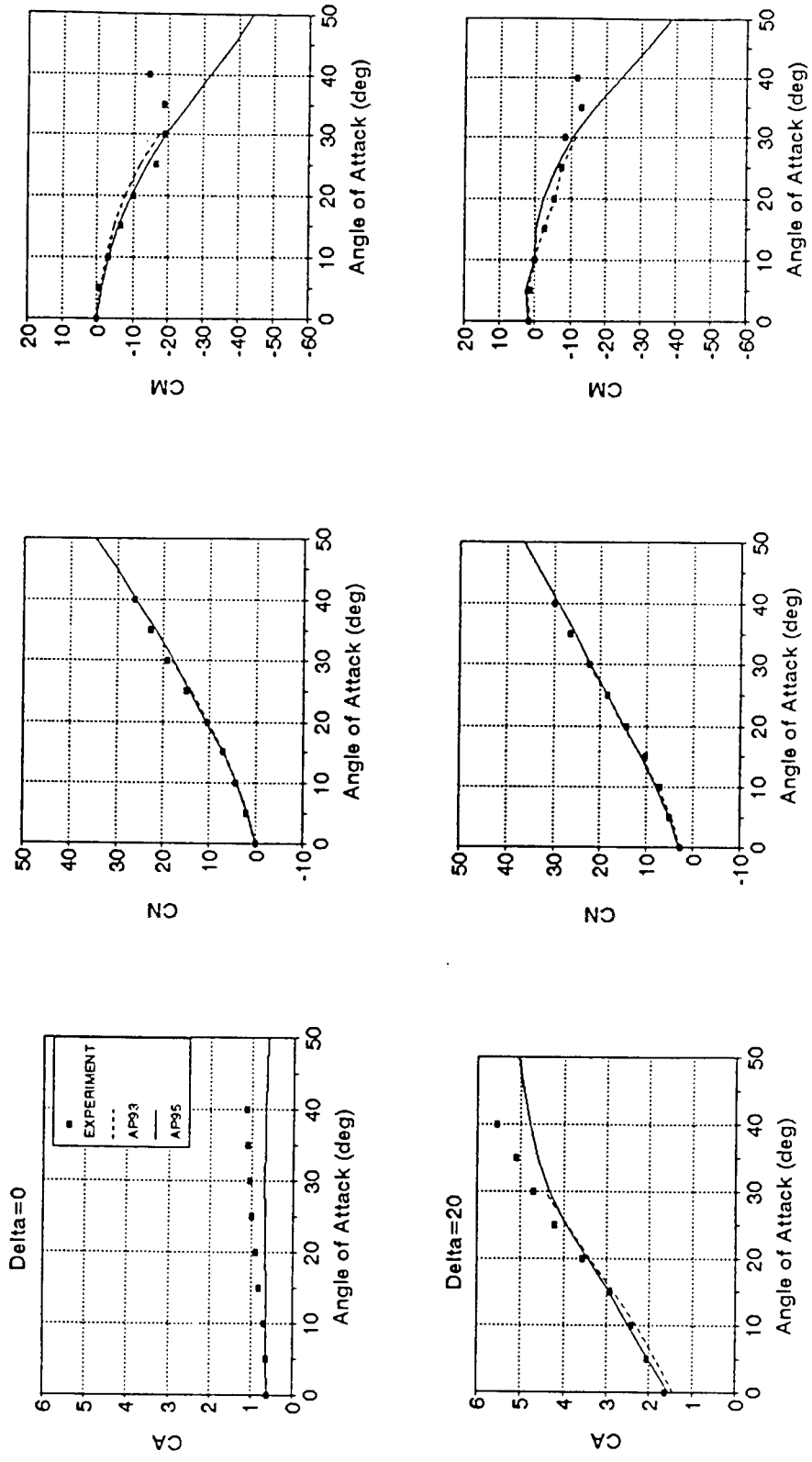

FIGURE 43E. STATIC AERODYNAMIC COEFFICIENT COMPARISONS FOR FIGURE 43A CONFIGURATION ($M_\infty = 3.95$)

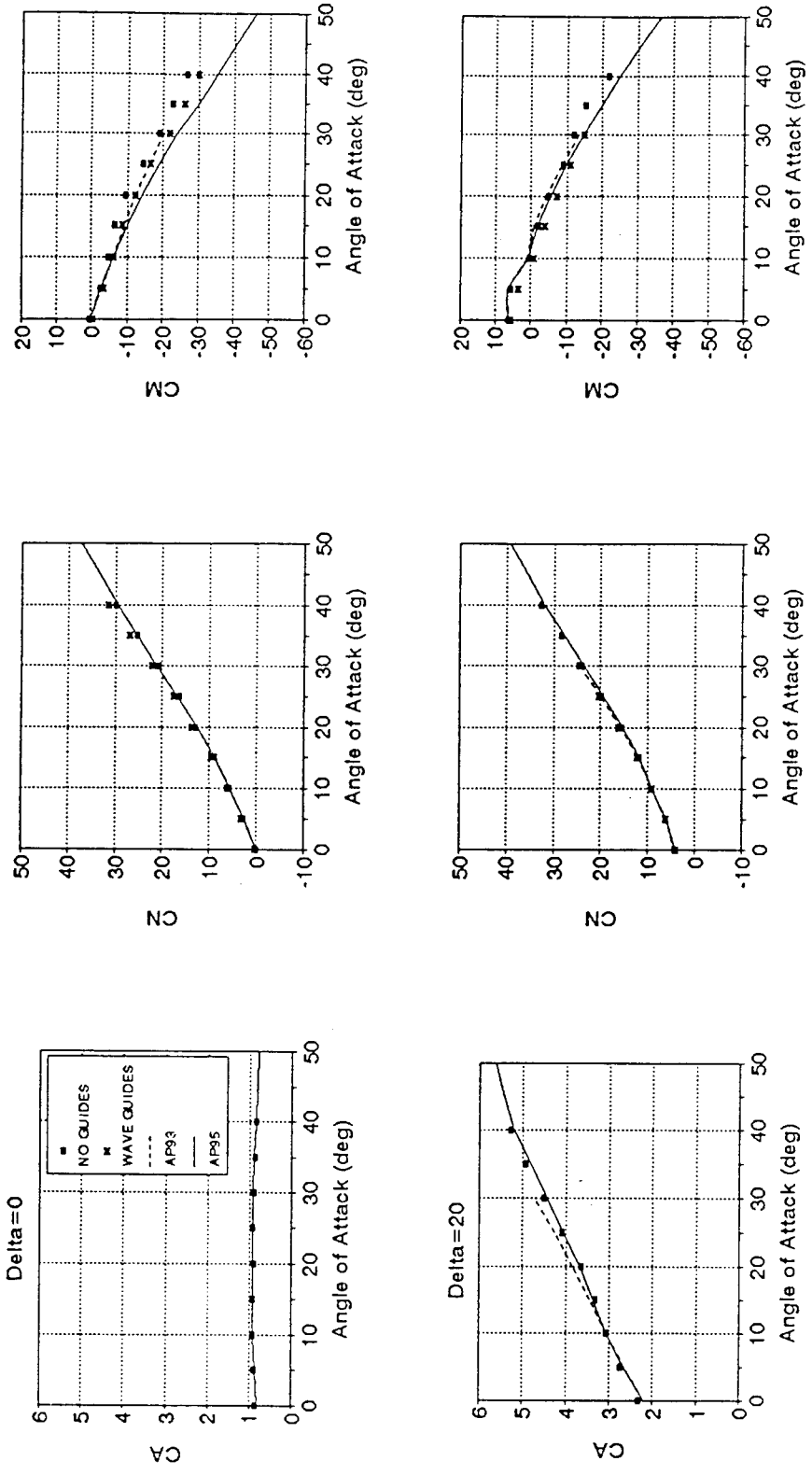

FIGURE 43F. STATIC AERODYNAMIC COEFFICIENT COMPARISONS FOR FIGURE 43A CONFIGURATION (M_∞ = 2.3)

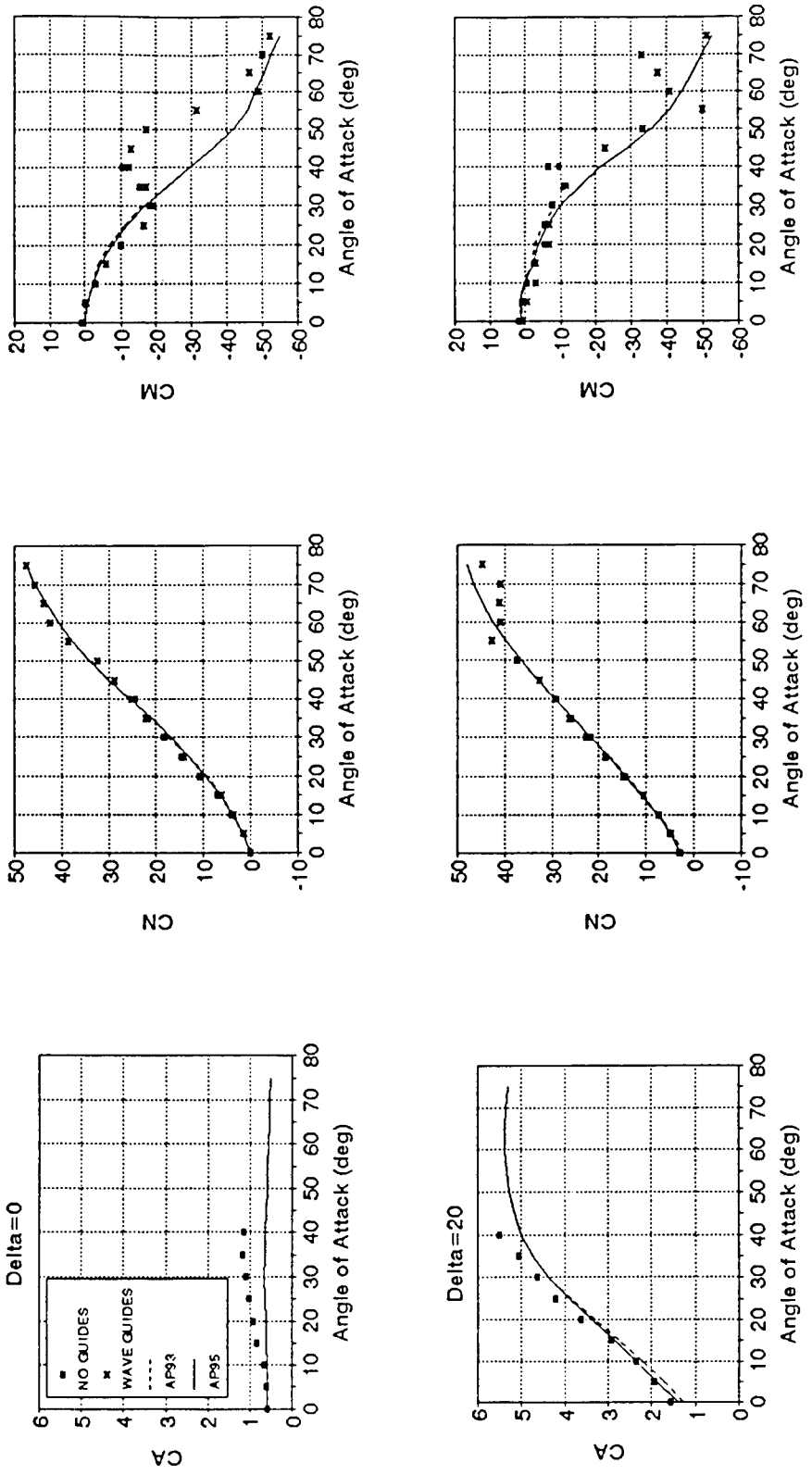

FIGURE 43G. STATIC AERODYNAMIC COEFFICIENT COMPARISONS FOR FIGURE 43A CONFIGURATION ($M_\infty = 4.6$)

from the moment center, a small change in tail normal force has a much larger impact on the pitching moment. The other physical phenomenon indicated was a fairly strong change in the pressure distribution of the carryover lift on the body.[29] Most likely, the center of pressure of this carryover lift also is affected, which also will change the pitching moment.

In summary, based on the validations conducted to date of the AP95 with experimental data and many missile configurations, it appears that an average accuracy goal of ±10 percent on C_A and C_N and ±4 percent ℓ for center of pressure has been met, except at high Mach number and high AOA on configurations with two sets of lifting surfaces. "Average accuracy" means average errors compared to data for several AOA and Mach numbers on a given configuration.

4.0 SUMMARY AND RECOMMENDATIONS

The technology has been developed to extend the 1993 version of the aeroprediction code (AP 93) to AOA above 30 deg. To accomplish this task, several data bases were used to estimate nonlinearities of the wing, body, and individual interference aerodynamic components separately. Extrapolations and engineering judgement were used where data were limited or not available. These new empirical estimates were combined with linearized and slender body theories to form estimates of aerodynamics for axisymmetric solid rocket configurations at all AOA and Mach numbers that missiles fly.

The new semiempirical model was then applied to several missile configurations outside the data base. Many of the component data bases had to be modified, presumably to correct out component measurement errors, to allow best estimate of aerodynamics and a near optimum semiempirical model for high AOA. Additional refinements could possibly improve the overall results even more.

New or improved technology developed includes a) extension of the wing-body and body-wing interference factor methodology above AOA = 30 deg for both zero and nonzero control deflections and b) refinements in body-alone center-of-pressure shift to account for transonic and asymmetric body-shed vortices.

Comparison of the AP95 methodology with data on many missile configurations showed (1) the AP95 to be slightly superior to the AP93 in estimating static aerodynamics over the AOA range of 0 to 30 deg, and (2) the goals of ±10 percent on C_A and C_N and ±4 percent ℓ for X_{CP} were met, on average, for AOA above 30 deg as well. The code is still limited to the $\Phi = 0$ deg or plus- fin roll orientation. Plans are to make the code applicable to the $\Phi = 45$ deg (or cross) fin roll orientation in the future.

While the AP95 has extended the state-of-the-art of semiempirical aeroprediction codes to AOA past 30 deg with good accuracy levels, many extrapolations of data were required. To improve upon the model and eliminate these extrapolations, additional component buildup data is required at AOA greater than 30 deg. These data should be obtained with fins mounted in the

middle of the missile configuration and with fin-to-body planform areas of at least 25 percent. Preferably, measurements of the wing in presence of the body and body in presence of the wing could be made simultaneously so as to avoid the error in $K_{B(w)}$ caused by subtraction of two numbers of the same magnitude.

To compute nonlinearities from internal shock interactions between two sets of lifting surfaces, a full Navier Stokes code may be appropriate to help define the shift in center of pressure on individual configuration force components, which occur as a result of these shock interactions at high AOA and Mach number.

5.0 REFERENCES

1. Moore, F. G.; Hymer, T. C.; McInville, R. M.; "Improved Aeroprediction Code: Part I - Summary of New Methods and Comparison with Experiment," NSWCDD/TR-93/91, May 1993, Dahlgren, VA.

2. Moore, F. G.; Hymer, T. C.; McInville, R. M.; "Improved Aeroprediction Code: Part II - Computer Program User's Guide and Listing," NSWCDD/TR-93/241, Aug 1993, Dahlgren, VA.

3. Moore, F. G.; Hymer, T. C.; McInville, R. M.; "A Planar Nonlinear Missile Aeroprediction Code for all Mach Numbers," AIAA paper 94-0026, 32nd Aerospace Sciences Meeting, Reno, NV, 10-13 Jan 1994.

4. Moore, F. G.; McInville, R. M.; "A New Method for Calculating Wing Alone Aerodynamics to Angle of Attack 180°," NSWCDD/TR-94/3, Mar 1994, Dahlgren, VA.

5. Devan, L.; Mason, L.; and Moore, F. G.; "Aerodynamics of Tactical Weapons to Mach Number 8 and Angle of Attack 180°," AIAA paper 82-0250, 20th Aerospace Sciences Meeting, Orlando, FL.

6. Nielsen, J. N.; Hemsch, M. H.; Smith, C. A.; "A Preliminary Method for Calculating the Aerodynamic Characteristics of Cruciform Missiles to High Angles of Attack Including Effects of Roll Angle and Control Deflections," Report ONR-CR215-216, 4F, Nov 1977, Office of Naval Research, 800 N. Quincy St., Arlington, VA 22217.

7. Vukelich, S. R. and Jenkins, J. E.; "Missile DATCOM: Aerodynamic Prediction on Conventional Missiles Using Component Build-Up Techniques," AIAA paper 84-0388, 1984, Reno, NV.

8. Ericsson, L. E. and Reding, J. P.; "Asymmetric Vortex Shedding from Bodies of Revolution," Tactical Missile Aerodynamics edited by M. J. Hemsch and J. N. Nielsen, Vol. 104, Progress in Astronautics and Aeronautics, AIAA, New York, 1986, pp. 243-296.

9. NASA Langley Research Center Tri-Service Missile Data Base, transmitted from NASA/LRC Jerry M. Allen to NSWCDD, 5 Nov 1991 (formal documentation of data base process).

10. Stallings, R. L., Jr., and Lamb, M.; "Wing-alone Aerodynamic Characteristics for High Angles of Attack at Supersonic Speeds," NASA Technical paper 1989, Jul 1981.

11. Baker, W. B., Jr.; "Static Aerodynamic Characteristics of a Series of Generalized Slender Bodies with and without Fins at Mach Numbers from 0.6 to 3.0 and Angles of Attack from 0 to 180°," AEDC-TR-75-124, Vols. I and II, May 1976, Tullahoma, TN.

12. Pitts, W. C.; Nielsen, J. N.; and Kaatari, G. E.; "Lift and Center of Pressure of Wing-Body-Tail Combinations at Subsonic, Transonic, and Supersonic Speeds," NACA TR 1307, 1957.

13. Jorgenson, L. H.; "Predictions of Static Aerodynamic Characteristics for Slender Bodies Alone and with Lifting Surfaces to Very High Angles of Attack," NASA TR R-474, Sep 1977.

14. Chin, S. S.; Missile Configuration Design, McGraw-Hill Book Co., Inc., New York, Copyright 1961.

15. Schlichting, H.; Boundary Layer Theory, McGraw Hill Book Company, Inc., 4th edition, New York, Copyright 1960.

16. Meyer, J.; "Effects of the Roll Angle on Cruciform Wing-Body Configurations at High Incidences," Journal of Spacecraft and Rockets, Vol. 31, No. 1, Jan-Feb 1994, pp. 113-122.

17. Dietz, W. E., Jr., and Altstatt, M. C.; "Experimental Investigation of Support Interference on an Ogive Cylinder at High Incidence," Journal of Spacecraft and Rockets, Vol. 16, No. 2, Mar-Apr 1979.

18. Canning, T. N. and Nielsen, J. N.; "Experimental Study of the Influence of Supports on the Aerodynamic Loads on a Ogive Cylinder at High Angles of Attack," AIAA paper 81-0007, 19th Aerospace Sciences Meeting, St. Louis, MO, 12-15 Jan 1981.

19. Moore, F. G.; Hymer, T.; Devan, L.; "New Methods for Predicting Nonlinear Lift, Center of Pressure, and Pitching Moment on Missile Configurations," NSWCDD/TR-92/217, Jul 1992.

20. Hemsch, M. J. and Nielsen, J. N.; "Equivalent Angle-of-Attack Method for Estimating Nonlinear Aerodynamics of Missile Fins," JSR, Vol. 20, No. 4, Jul-Aug 1983.

21. Maynes, R. D. and Gebert, G. A.; "An Investigation of High Angle of Attack Aerodynamics on a Finned and Finless Body with a Fineness Ratio of 20.0," AIAA Paper No. 94-0724, 32nd Aerospace Sciences Meeting, Reno, NV, 10-13 Jan 1994.

22. Butler, C. B.; Sears, E. S.; and Pallas, S. G.; "Aerodynamic Characteristics of 2-, 3- and 4-Caliber Tangent-Ogive cylinders with Nose Bluntness Ratios of 0.00, 0.25, 0.50 and 0.75 at Mach Numbers from 0.6 to 4.0," AFATL-TR-77-8, Jan 1977 (Eglin Air Force Base, FL 32542).

23. Wardlaw, A. B. Jr.; Baltakis, F. P.; Martin, F. M. and Priolo, F. J.; "A Godunov Method for Supersonic Tactical Missiles," Journal of Spacecraft and Rockets, Vol-24, No. 1, 1987, pp 40-47.

24. Smith, E. H.; Hebbar, S. K. and Platzer, M.; "Aerodynamic Characteristics of a Canard-Controlled Missile at High Angles of Attack," AIAA Paper No. 93-0763, presented at 31st Aerospace Sciences meeting, Reno, NV, 11-14 Jan 1993.

25. Smith, E. H.; Salazar, M. E.; Hebbar, S. K. and Platzer, M.; "Aerodynamic Characteristics of the MMPT ATD Vehicle at High Angles of Attack," AIAA Paper No. 93-3493, Aug 1993.

26. Howard, R. M. and Dunn, Archibald; "Missile Loads at High Angles of Attack," Engineering Note in Journal of Spacecraft and Rockets, Vol. 28, No. 1, Jan-Feb 1991.

27. McKinney, R. L.; "Longitudinal Stability and Control Characteristics of an Air-to-Air Missile Configuration at Mach Numbers of 2.3 and 4.6 and Angles of Attack from -45° to 90°, NASA TMX-846, 1972.

28. Monta, W. J.; "Supersonic Aerodynamic Characteristics of a Sparrow III Type Missile Model with Wing Controls and Comparison with Existing Tail-Control Results," NASA TP 1078, Nov 1977.

29. Agnone, A. M.; Zakkay, V. and Tory, E.; "Aerodynamics of Slender Finned Bodies at Large Angles of Attack," AIAA Paper 77-666, Fluid and Plasma Dynamics Conference, Albuquerque, NM, 27-29 Jun 1977.

6.0 SYMBOLS AND DEFINITIONS

AOA	Angle of Attack
APC	Aeroprediction Code

AP81	Aeroprediction 1981
AP93	Aeroprediction 1993
AP95	Aeroprediction 1995
AR	Aspect Ratio = b^2/A_W
LT	Linear Theory
NASA/LRC	National Aeronautics and Space Administration/Langley Research Center
NSWCDD	Naval Surface Warfare Center, Dahlgren Division
SB, SBT	Slender Body, Slender-body Theory
a	Speed of Sound (ft/sec)
a_0, a_1, a_2, a_3, a_4	Constants used in nonlinear wing-alone model
A_P	Planform area of the body or wing in the crossflow plane (ft^2)
A_{REF}	Reference area (maximum cross-sectional area of body, if a body is present, or planform area of wing, if wing alone)(ft^2)
A_W, S_W	Planform area of wing in crossflow plane (ft^2)
A_{WETTED}	Area of body or wing which flow touches
b	Wing span (not including body)(ft)
C_A	Axial force coefficient
$C_{A_B}, C_{A_F}, C_{A_W}$	Base, skin-friction, and wave components, respectively, of axial force coefficient
C_{D_C}	Crossflow drag coefficient
C_{F_ℓ}, C_{F_T}	Laminar and turbulent skin friction coefficients respectively
C_M	Pitching moment coefficient (based on reference area and body diameter, if body present, or mean aerodynamic chord, if wing alone)
C_N	Normal force coefficient

C_{N_B}	Normal force coefficient of body alone
$C_{N_{B(V)}}$	Negative afterbody normal-force coefficient due to canard or wing-shed vortices
$C_{N_{B(W)}}$, $C_{N_{B(T)}}$	Normal-force coefficient on body in presence of wing or tail
$\Delta C_{N_{B(W)}}$	Additional normal-force coefficient on body due to presence of the wing
C_{N_L}	Linear component of normal-force coefficient
$C_{N_{LOSS}}$	Loss of normal force on wing or body in transonic flow
$C_{N_{NL}}$	Nonlinear component of normal-force coefficient
$C_{N_{T(V)}}$	Negative normal-force coefficient component on tail due to wing or canard-shed vortex
C_{N_W}	Normal force coefficient of wing alone
$C_{N_{W(B)}}$	Normal-force coefficient of wing in presence of body
C_{N_α}	Normal-force coefficient derivative
C_P	Pressure coefficient $\left(\frac{p-p_\infty}{1/2\rho_\infty V_\infty^2}\right)$
c_r	Root chord (ft)
c_t	Tip chord (ft)
cal	Caliber(s) (one body diameter)
d	Body diameter (ft)
d_{ref}	Reference body diameter (ft)
$\frac{dK_{W(B)}}{d\alpha}$	Rate at which $K_{W(B)}$ decreases
deg	Degree(s)
F, C_1, C_2, C_3	Dimensionless empirical factors used in nonlinear models of $k_{W(B)}$ and $C_{N_{T(V)}}$ to approximate effects due to high AOA or control deflection.
f_W, f_T	Lateral location of wing or tail vortex (measured in feet from body center line)
i	Tail interference factor

$K_{B(W)}$, $K_{B(T)}$	Ratio of additional body normal-force coefficient in presence of wing, or tail to wing, or tail alone normal-force coefficient at $\delta = 0$ deg
$k_{B(W)}$, $k_{B(T)}$	Ratio of additional body normal-force coefficient due to presence of wing or tail at a control deflection to that of wing or tail alone
$[K_{B(W)}]_{MIN}$	Minimum value of $K_{B(W)}$ as percent of slender-body theory value
$K_{W(B)}$, $K_{T(B)}$	Ratio of normal-force coefficient of wing or tail in presence of body to that of wing or tail alone at $\delta = 0$ deg
$k_{W(B)}$, $k_{T(B)}$	Ratio of wing or tail normal-force coefficient in presence of body due to a control deflection to that of wing or tail alone
$[\Delta K_{W(B)}]_{\alpha=0}$ and $[\Delta K_{B(W)}]_{\alpha=0}$	Amount that the experimental values of $K_{W(B)}$ and $K_{B(W)}$ exceed slender body theory at $\alpha = 0°$
ℓ	Length (ft)
ℓ_N	Nose Length (can be in calibers or feet)
M	Mach number = V/a
M_C	Normal Mach number to body axis = M sin α
p	Pressure (lb/ft^2)
r	Radius of body (ft)
r_N	Radius of nose tip (ft)
r_W, r_T	Radius of body at wing or tail locations
Re	Reynolds number = $\frac{\rho V \ell}{\mu}$
Re_{CRIT}	Critical Reynolds number where flow transitions from separating on the forward part of a circular cylinder to the rear part
Re_D	Reynolds number based on diameter of body
Re_{EFF}	Reynolds number defined to better correlate values of C_{D_c} versus Reynolds number
s	Wing or tail semispan plus the body radius in wing-body lift methodology

t/c_r	Tail thickness to its root chord
t/d	Tail thickness to body diameter
TW	Bevel length on leading edge of wind tunnel model
V	Velocity (ft/sec)
x	Distance along the axis of symmetry measured positive aft of nose tip (ft or cal)
X_{CP}	Center of pressure (in feet or calibers from some reference point that can be specified)
$(X_{CP})_L$, $(X_{CP})_{NL}$	Center of pressure of linear and nonlinear terms of normal force.
α	Angle of attack (deg)
α_C	Angle of attack where wing-body interference factor starts decreasing from its slender-body theory value (deg)
α_D	Angle of attack where the wing-body interference factor reaches a minimum (deg)
α_M	Angle of attack where $K_{W(B)}$ reaches its limiting value
α_W, α_T	Local angle of attack of wing or tail ($\alpha + \delta_w$ or $\alpha + \delta_T$, respectively, in degrees)
α_1, α_2	Angles of attack used in nonlinear model for $K_{B(W)}$
δ	Control deflection (deg)
δ_W, δ_T	Deflection of wing or tail surfaces (deg), positive leading edge up
η	Parameter used in viscous crossflow theory for nonlinear body normal force (in this context, it is the normal force of a circular cylinder of given length-to-diameter ratio to that of a cylinder of infinite length)
λ	Taper ratio of a lifting surface = c_t/c_r
Λ	Leading edge sweep angle of wing or tail (deg)
μ	Viscosity of air (slug/ft-sec)
Φ	Circumferential position around body where $\Phi = 0$ is leeward plane (deg)

ρ	Density of air (slug/ft^3)
θ	Average cone half angle of a nose (deg)
∞	Free-stream conditions

DISTRIBUTION

	Copies
DOD ACTIVITIES (CONUS)	
ATTN CODE 04 (BISSON)	1
CODE 44 (ZIMET)	1
CODE 4425 (SIEGEL)	1
CODE 332FD (LEKOUDIS)	1
CODE 442 (WOOD)	1
CHIEF OF NAVAL RESEARCH	
BALLSTON TOWER 1	
800 N QUINCY ST BCT #1	
ARLINGTON VA 22217-5660	
ATTN CODE CL372 (LOFTUS)	1
CODE C2771 (SMITH)	1
CODE C2891 (PORTER)	1
CODE C2892 (STRUTZ)	1
CODE C2892 (HALTER)	1
CODE C2892 (GLEASON)	1
CODE C2894 (VAN DYKEN)	1
CODE C29B10	
TECHNICAL LIBRARY	1
COMMANDER	
NAVAL AIR WARFARE CENTER	
WEAPONS DIVISION	
CHINA LAKE CA 93555-6001	
ATTN TECHNICAL LIBRARY	1
COMMANDER	
NAVAL SEA SYSTEMS COMMAND	
WASHINGTON DC 20362-5160	
ATTN AIR 53012D (JOHNSON)	1
RM 904 JP 2	
TECHNICAL LIBRARY	1
COMMANDER	
NAVAL AIR SYSTEMS COMMAND	
WASHINGTON DC 20361-5120	
ATTN C KLEIN	1
TECHNICAL LIBRARY	1
COMMANDER	
NAVAL AIR WARFARE CENTER	
WEAPONS DIVISION	
POINT MUGU CA 93042-5000	
ATTN T C TAI	1
M J MALIA	1
TECHNICAL LIBRARY	1
COMMANDER	
NAVAL SHIP RESEARCH AND	
DEVELOPMENT CENTER	
WASHINGTON DC 20034	
ATTN R M HOWARD	1
TECHNICAL LIBRARY	1
SUPERINTENDENT	
US NAVAL POSTGRADUATE SCHOOL	
MONTEREY CA 93943-5000	
ATTN S GREENHALGH	1
C REITZ	1
TECHNICAL LIBRARY	1
COMMANDING OFFICER	
NAVAL AIR WARFARE CENTER	
AIRCRAFT DIVISION WARMINSTER	
WARMINSTER PA 18974-5000	
ATTN HEAD WEAPONS DEPT	1
HEAD SCIENCE DEPT	1
SUPERINTENDENT	
US NAVAL ACADEMY	
ANNAPOLIS MD 21402	
ATTN M KRUMINS	1
TECHNICAL LIBRARY	1
OFFICER IN CHARGE	
NAVAL INTELLIGENCE SUPPORT CENTER	
4301 SUITLAND ROAD	
WASHINGTON DC 20390 RM 810 CP5	
ALEXANDRIA VA 22217	
ATTN CODE 30	1
CHIEF OF NAVAL RESEARCH	
NAVY SDI	
2211 JEFFERSON DAVIS HWY	
ARLINGTON VA	

DISTRIBUTION (CONT.)

	Copies
ATTN DIAG DT 4T (PAUL MURAD) DEFENSE INTELLIGENCE AGENCY WASHINGTON DC 20546	2
ATTN CODE 50255 (WAGGONER) COMMANDER NAVAL SURFACE WARFARE CENTER CRANE DIVISION CRANE IN 47522-5000	1
ATTN CODE 5252P (KRAUSE) TECHNICAL LIBRARY COMMANDER NAVAL SURFACE WARFARE CENTER INDIAN HEAD DIVISION INDIAN HEAD MD 20640-5000	1 1
ATTN TECHNICAL LIBRARY COMMANDING GENERAL MARINE CORPS COMBAT DEVELOPMENT COMMAND QUANTICO VA 22134-5000	1
ATTN TECHNICAL LIBRARY AFATL (ADLRA) (DLGC) EGLIN AFB FL 32542-5000	1
ATTN E SEARS L E LIJEWSKI C COTTRELL TECHNICAL LIBRARY EGLIN AFB FL 32542	1 1 1 1
ATTN TECHNICAL LIBRARY USAF ACADEMY COLORADO SPRINGS CO 80912	1
ATTN TECHNICAL LIBRARY ADVANCED RESEARCH PROJECTS AGENCY DEPARTMENT OF DEFENSE WASHINGTON DC 20305	1
ATTN B BLAKE (BLD 146) D SHEREDA (BLD 450) J JENKINS (BLD 146) R SAMUELS (BLD 856) TECHNICAL LIBRARY COMMANDING OFFICER AFSC 2210 8TH STREET WRIGHT PATTERSON AFB OH 45433	1 1 1 1 1
ATTN J USSELTON W B BAKER JR TECHNICAL LIBRARY ARNOLD ENGINEERING DEVELOPMENT CENTER USAF TULLAHOMA TN 37389	1 1 1
ATTN H HUDGINS G FRIEDMAN TECHNICAL LIBRARY COMMANDING GENERAL ARRADCOM PICATINNY ARSENAL DOVER NJ 07801	1 1 1
ATTN C H MURPHY R M MCCOY W STUREK C NIETUBICZ A MIKHAIL P PLOSTINS TECHNICAL LIBRARY COMMANDING GENERAL BALLISTIC RESEARCH LABORATORY ABERDEEN PROVING GROUND ABERDEEN MD 21005-5066	1 1 1 1 1 1 1
ATTN CODE TNC (BLACKLEDGE) CDR A KOREJO DIRECTOR INTERCEPTOR TECHNOLOGY STRATEGIC DEFENSE INITIATIVE THE PENTAGON WASHINGTON DC 20350	1 1
ATTN SFAE SD ASP SFAE SD HED DEPUTY COMMANDER US ARMY STRATEGIC DEFENSE COMMAND P O BOX 1500 HUNTSVILLE AL 35807-3801	1 1

DISTRIBUTION (CONT.)

	Copies
ATTN D WASHINGTON	1
W WALKER	1
R KRETZSCHMAR	1
COMMAND GENERAL	
US ARMY MISSILE COMMAND	
AMSMI-RD-SS-AT	
REDSTONE ARSENAL AL 35898-5252	
DEFENSE TECHNICAL INFORMATION CENTER	12
CAMERON STATION	
ALEXANDRIA VA 22304-6145	
DEFENSE PRINTING SERVICE	1
WASHINGTON NAVY YARD	
WASHINGTON DC 20374	
ATTN CODE E29L	
TECHNICAL LIBRARY	1
COMMANDING OFFICER	
CSSDD NSWC	
6703 W HIGHWAY 98	
PANAMA CITY FL 32407-7001	
DOD ACTIVITIES (EX-CONUS)	
NONE	
NON-DOD ACTIVITIES	
THE CNA CORPORATION	1
P O BOX 16268	
ALEXANDRIA VA 22302-0268	
ATTN GIFT AND EXCHANGE DIVISION	4
LIBRARY OF CONGRESS	
WASHINGTON DC 20540	
GIDEP OPERATIONS OFFICE	1
CORONA CA 91720	
ATTN TECHNICAL LIBRARY	1
NASA AMES RESEARCH CENTER	
MOFFETT CA 94035-1099	
ATTN C SCOTT	1
D CURRY	1
NASA JOHNSON SPACE CENTER	
HOUSTON TX 77058	

	Copies
ATTN TECHNICAL LIBRARY	1
NASA	
WASHINGTON DC 20546	
ATTN W C SAWYER	1
B HENDERSON	1
D MILLER	1
J ALLEN	1
F WILCOX	1
TECHNICAL LIBRARY	2
NASA LANGLEY RESEARCH CENTER	
HAMPTON VA 23365	
ATTN D G MILLER	1
TECHNICAL LIBRARY	1
LAWRENCE LIVERMORE NATIONAL LABORATORY	
EARTH SCIENCES DIVISION	
UNIVERSITY OF CALIFORNIA	
P O BOX 808	
LIVERMORE CA 94550	
ATTN W RUTLEDGE (1635)	1
R LAFARGE	1
R EISLER	1
TECHNICAL LIBRARY	1
SANDIA NATIONAL LABORATORY	
P O BOX 5800	
ALBUQUERQUE NM 87185-5800	
ATTN LOUIS CHAN	1
INSTITUTE FOR AEROSPACE RESEARCH	
NATIONAL RESEARCH COUNCIL	
MONTREAL RD	
OTTAWA ON CANADA K1A0R6	
ATTN ASSISTANT DEFENSE COOPERATION ATTACHE	1
EMBASSY OF SPAIN	
WASHINGTON DC 20016	
ATTN CDR R TEMPEST	1
BRITISH NAVY STAFF	
WASHINGTON DC 20008	

DISTRIBUTION (CONT.)

	Copies
ATTN ASO LO IS ISRAEL AIR FORCE LIAISON OFFICER 700 ROBBINS AVE PHILADELPHIA PA 19111	1
ATTN GERMAN MILITARY REP US OA GMR TRAFFIC AND TRANSPORTATION DIVISION 10 SERVICES ROAD DULLES INTERNATIONAL AP WASHINGTON DC 20041	1
ATTN F D DEJARNETTE NORTH CAROLINA STATE UNIVERSITY DEPT OF MECHANICAL AND AEROSPACE ENGINEERING BOX 7921 RALEIGH NC 27695	1
ATTN PROF J A SCHETZ VIRGINIA POLYTECHNIC AND STATE UNIVERSITY DEPT OF AEROSPACE ENGINEERING BLACKSBURG VA 24060	1
ATTN J M WU C BALASUBRAMAYAN TECHNICAL LIBRARY THE UNIVERSITY OF TENNESSEE SPACE INSTITUTE TULLAHOMA TN 37388	1 1 1
ATTN R NELSON TECHNICAL LIBRARY UNIVERSITY OF NOTRE DAME DEPT OF AEROSPACE AND MECHANICAL ENGINEERING BOX 537 NOTRE DAME IN 46556	1 1
ATTN PROF F NELSON DEPT OF MECH AND AERO ENG UNIVERSITY OF MISSOURI ROLLA ROLLA MO 65401	1
ATTN DR DONALD SPRING AEROSPACE ENGINEERING DEPT AUBURN UNIVERSITY AL 36849-5338	1
ATTN ROBERT ENGLAR GEORGIA TECH RESEARCH INSTITUTE AEROSPACE SCIENCE AND TECHNOLOGY LAB ATLANTA GA 30332	1
ATTN E LUCERO L TISSERAND D FROSTBUTTER L PERINI TECHNICAL LIBRARY APPLIED PHYSICS LABORATORY JOHNS HOPKINS UNIVERSITY JOHNS HOPKINS ROAD LAUREL MD 20723-6099	1 1 1 1 1
ATTN B BROOKS R STANCIL R ELKINS LORAL VOUGHT SYSTEMS P O BOX 650003 M/S-EM-55 DALLAS TX 75265-0003	1 1 1
ATTN TECHNICAL LIBRARY MARTIN MARIETTA AEROSPACE P O BOX 5837 ORLANDO FL 32805	1
ATTN B OMILIAN CALSPAN ADVANCED TECHNOLOGY CENTER P O BOX 400 BUFFALO NY 14225	1
ATTN R CAVAGE ADVANCED SYSTEMS DESIGN DEPT 113 407 (GB14) ROCKWELL NORTH AMERICAN AIRCRAFT OPERATIONS P O BOX 92098 LOS ANGELES CA 90009	1
ATTN TECHNICAL LIBRARY HUGHES AIRCRAFT COMPANY MISSILE SYSTEMS SECTOR P O BOX 7928 CANOGA PARK CA 91304-7928	1

DISTRIBUTION (CONT.)

	Copies
ATTN M DILLENIUS NIELSEN ENGINEERING AND RESEARCH INC 510 CLYDE AVE MOUNTAIN VIEW CA 95043	1
ATTN J XERIKOS N CAMPBELL TECHNICAL LIBRARY MCDONNEL DOUGLAS ASTRONAUTICS CO (WEST) 5301 BOLSA AVE HUNTINGTON BEACH CA 92647	1 1 1
ATTN J WILLIAMS S VUKELICH J FIVEL R GERBSCH (CODE 1111041) TECHNICAL LIBRARY MCDONNELL DOUGLAS ASTRONAUTICS CO (EAST) BOX 516 ST LOUIS MO 63166-0516	1 1 1 1 1
ATTN TECHNICAL LIBRARY UNITED TECHNOLOGIES NORDEN SYSTEMS NORWALK CT 06856	1
ATTN T LUNDY D ANDREWS TECHNICAL LIBRARY LOCKHEED MISSILES AND SPACE CO INC P O BOX 1103 HUNTSVILLE AL 35807	1 1 1
ATTN R WYRICK BOEING COMPUTER SERVICES INC P O BOX 24346 SEATTLE WA 98124	1
ATTN W CHRISTENSON D WARNER MN 11 2920 ALLIANT TECHSYSTEMS INC 600 SECOND ST NE HOPKINS MN 55343	1 1
ATTN TECHNICAL LIBRARY B SALAMI J BOUDREAU RAYTHEON MISSILE SYSTEMS 50 APPLE HILL DR STOP T3TBB TEWKSBURY MA 01876-0901	1 1 1
ATTN LLOYD PRATT AEROJET TACTICAL SYSTEMS CO P O BOX 13400 SACRAMENTO CA 95813	1
ATTN JOWEPH ANDRZIJEWSKI MEVATEC CORP 1525 PERIMETER PARKWAY SUITE 500 HUNTSVILLE AL 35806	1
ATTN DR G S SCHMIDT LORAL DEFENSE SYSTEMS 1210 MASSILLAN ROAD AKRON OH 44315-0001	1
ATTN W NORDGREN 721 GOULD INC OSD 18901 EUCLID AVE CLEVELAND OH 44117	1
ATTN TECH LIBRARY AEROJET ELECTRONIC SYSTEMS P O BOX 296 III AZUSA CA 91702	1
ATTN L E ERICSSON P REDING G CHRUSCIEL TECHNICAL LIBRARY LOCKHEED MISSILES AND SPACE CO INC P O BOX 504 SUNNYVALE CA 94086	1 1 1 1
ATTN K C LEE ACCUREX CORP P O BOX 7040 520 CLYDE AVE MOUNTAIN VIEW CA 94039	1

DISTRIBUTION (CONT.)

	Copies
ATTN TECH LIBRARY FMC NAVAL SYSTEMS DIV 4800 E RIVER ROAD MINNEAPOLIS MN 55421-1402	1
ATTN L FRENCH TRACOR AEROSPACE AUSTIN INC 6500 TRACOR LANE AUSTIN TX 87825	1
ATTN DORIA GLADSTONE BATTELLE MEMORIAL INSTITUTE COLUMBUS DIVISION 505 KING AVE COLUMBUS OH 43201-2693	1
ATTN JAMES SORENSON ORBITAL SCIENCES 3380 SOUTH PRICE ROAD CHANDLER ARIZONA 85248	1
ATTN J FORKOIS KAMAN SCIENCES CORP 1500 GARDEN OF THE GODS ROAD P O BOX 7463 COLORADO SPRINGS CO 80933	1
ATTN FRED KAUTZ MIT LINCOLN LABORATORY LEXINGTON MA 02173-0073	1
ATTN D J GRIESE BOEING DEFENSE AND SPACE GROUP P O BOX 3999 MS 4C-61 SEATTLE WA 98124-2499	1
ATTN W J CLARK DYNA EAST CORPORATION 3132 MARKET ST PHILADELPHIA PA 19104	1
ATTN BRIAN WALKUP HERCULES AEROSPACE PRODUCT CO ALLEGHANY BALLISTIC LAB ROCKET CENTER WV 26726	1
ATTN B D PRATS MARTIN MARIETTA ASTROSPACE AEROTHERMOPHYSICS 230 E GODDARD BLVD KING OF PRUSSIA PA 19406	1
ATTN DR T LIN TRW ELECTRONICS AND DEFENSE SECTOR BLDG 527/RM 706 P O BOX 1310 SAN BERNADINO CA 92402	1
ATTN G VINCENT SPARTA INC 4301 CORPORATE DR HUNTSVILLE AL 35805	1
ATTN D P FORSMO TECHNICAL LIBRARY RAYTHEON COMPANY MISSILE SYSTEMS DIVISION HARTWELL RD BEDFORD MA 01730	1 1
ATTN M S MILLER BRIAN EST DYNETICS INC P O DRAWER B HUNTSVILLE AL 35814-5050	1 1
ATTN H A MCELROY GENERAL DEFENSE CORP P O BOX 127 RED LION PA 17356	1
ATTN R SEPLAK BRUNSWICK CORP DEFENSE DIVISION 3333 HARBOR BLVD COSTA MESA CA 92628-2009	1
ATTN J W MCDONALD GENERAL RESEARCH CORP ADVANCED TECHNOLOGY INC 5383 HOLLISTER AVE P O BOX 6770 SANTA BARBARA CA 93160-6770	1

DISTRIBUTION (CONT.)

	Copies
ATTN CAROL BUTLER OTI INTERNATIONAL 60 2ND ST SUITE 301 P O BOX 37 SHALIMAR FL 32579	1
ATTN ENGINEERING LIBRARY ARMAMENT SYSTEMS DEPT GENERAL ELECTRIC CO BURLINGTON VT 05401	1
ATTN H B ASLUND SAAB MILITARY AIRCRAFT 581 88 LINKOEPING SWEDEN	1
ATTN R BARDWELL DEFENSE SYSTEMS LTD THE GROVE, WARREN LANE STANMORE, MIDDLESEX UNITED KINGDOM	1
ATTN A BOOTH BRITISH AEROSPACE DEFENCE LTD MILITARY AIRCRAFT DIVISION, WARTON AERODROME WARTON PRESTON, LANCASHIRE PR4 1AX UNITED KINGDOM	1
ATTN R CAYZAC GIAT INDUSTRIES 7 ROUTE DE GUERCY 18023 BOURGES CEDEX FRANCE	1
ATTN MAJ F DE COCK ECOLE ROYALE MILITAIRE 30 AV DE LA RENAISSANCE 1040 BRUXELLES BELGIUM	1
ATTN J EKEROOT BOFORS MISSILES 691 80 KARLSKOGA SWEDEN	1
ATTN CH FRANSSON NATIONAL DEFENCE RESEARCH ESTABLISHMENT DEPT OF WEAPON SYSTEMS EFFECTS AND PROTECTION KARLAVAGEN 106B 172 90 SUNDBYBERG SWEDEN	1
ATTN M HARPER-BOURNE DEFENCE RESEARCH AGENCY Q134 BUILDING RAE FARNBOROUGH HAMPSHIRE QU14 6TD UNITED KINGDOM	1
ATTN A H HASSELROT FFA P O BOX 11021 161 11 BROMMA SWEDEN	1
ATTN B JONSSON DEFENCE MATERIAL ADMINISTRATION MISSILE TECHNOLOGY DIVISION 115 88 STOCKHOLM SWEDEN	1
ATTN P LEZEAUD DASSAULT AVIATION 78 QUAI MARCEL DASSAULT 92214 SAINT-CLOUD FRANCE	1
ATTN J LINDHOUT N L R ANTHONY FOKKERWEG 2 1059 CM AMSTERDAM THE NETHERLANDS	1
ATTN A MICKELLIDES GEC MARCONI DEFENCE SYSTEMS LTD THE GROVE WARREN LANE STANMORE MIDDLESEX UNITED KINGDOM	1

DISTRIBUTION (CONT.)

	Copies
ATTN K MOELLER BODENSEEWERK GERAETETECHNIK GMBH POSTFACH 10 11 55 88641 UBERLINGEN GERMANY	1
ATTN G MOSS ROYAL MILITARY COLLEGE AEROMECHANICAL SYSTEMS GROUP SHRIVENHAM SWINDON WILTS SN6 8LA UNITED KINGDOM	1
ATTN RIBADEAU DUMAS MATRA DEFENSE 37 AV LOUIS BREGUET BP 1 78146 VELIZY-VILLACOUBLAY CEDEX FRANCE	1
ATTN R ROGERS DEFENCE RESEARCH AGENCY BLDG 37 TUNNEL SITE CLAPHAM BEDS MK 41 6AE UNITED KINGDOM	1
ATTN S SMITH DEFENCE RESEARCH AGENCY Q134 BUILDING RAE FARNBOROUGH HAMPSHIRE QU14 6TD UNITED KINGDOM	1
ATTN J SOWA SAAB MISSILES AB 581 88 LINKOPING SWEDEN	1
ATTN D SPARROW HUNTING ENGINEERING LTD REDDINGS WOOD AMPTHILL BEDFORDSHIRE MK452HD UNITED KINGDOM	1
ATTN P STUDER DEFENCE TECHNOLOGY AND PROCUREMENT AGENCY SYSTEMS ANALYSIS AND INFORMATION SYSTEMS DIVISION PAPIERMUEHLESTRASSE 25 3003 BERNE SWITZERLAND	1
ATTN D WALLSTROM THE AERONAUTICAL RESEARCH INST OF SWEDEN P O BOX 11021 161 11 BROMMA SWEDEN	1
ATTN DR R G LACAU AEROSPATIALE - MISSILE DEPT E/ECN CENTRE DES GATINES 91370 VERRIERE LE BUISSON FRANCE	1
ATTN J M CHARBONNIER VON KARMAN INSTITUTE 72 CHAUSSEE DE WATERLOO 1640 RHODE-SAINT-GENESE BELGIUM	1
ATTN P CHAMPIGNY DIRECTION DE L'AERONAUTIQUE ONERA 29 AV DE LA DIVISION LECLERC 92320 CHATILLON-SOUS-BAGNEUX CEDEX FRANCE	1
ATTN DR P HENNIG DEUTSCHE AEROSPACE (DASA) VAS 414 ABWEHR AND SCHUTZ POSTFACH 801149 8000 MUENCHEN 80 GERMANY	1
ATTN DR P WEINACHT AERODYNAMICS BRANCH PROPULSION AND FLIGHT DIV WTD AMSRL-WT-PB US ARMY RESEARCH LAB ABERDEEN PROVING GROUND MD 21005-5066	1

DISTRIBUTION (CONT.)

	Copies
ATTN TECHNICAL LIBRARY OAYNE AERONAUTICAL 2701 HARBOR DRIVE SAN DIEGO CA 92138	1
ATTN WILLIAM FACINELLI ALLIED SIGNAL P O BOX 22200 MS 1230 21E TEMPE AZ 85285	1
ATTN T LIBRARY RAYTHEON COMPANY SPENCER LABORATORY BOX SL 7162 BURLINGTON MA 01803	1
ATTN NEILL S SMITH ARAP 1950 OLD GALLOWS ROAD SUITE 302 VIENNA VA 22180	1
ATTN DR T P SHIVANANDA TRW BMD P O BOX 1310 SAN BERNADINO CA 92402-1313	1
ATTN T R PEPITONE AEROSPACE TECHNOLOGY INC P O BOX 1809 DAHLGREN VA 22448	1
ATTN ERIC MOORE LOCKHEED SANDERS MAILSTOP MER 24-1281 P O BOX 868 NASHUA NH 03061	1
ATTN J EVANS DREV P O BOX 8800 COURCELETTE PQ CANADA GOA 1RO	1
ATTN DR BRIAN LANDRUM RI BLDG E33 PROPULSION RESEARCH CENTER UNIVERSITY OF ALABAMA HUNTSVILLE AL 35899	1

	Copies
ATTN BRUCE NORTON MAIL STOP BL-1 RAYTHEON 100 VANCE TANK RD BRISTOL TN 37620	1
ATTN JIM ROBERTSON RESEARCH SOUTH INC 555 SPARKMAN DRIVE SUITE 818 HUNTSVILLE AL 35816-3423	1
ATTN NEIL WALKER NICHOLAS RESEARCH CORPORATION MS-912 P O BOX 400002 4040 S MEMORIAL PKWY HUNTSVILLE AL 35801	1
ATTN H G KNOCHE DR GREGORIOU MESSERSCHMIDT BOLKOW BLOHM GMBH UNTERNEHMENSBEREICH APPARATE MUNCHEN 80 POSTFACH 801149 BAYERN FED REP OF GERMANY (DRF)	1 1
ATTN BOB WHYTE ARROW TECH ASSOCIATES INC 1233 SHELBURNE ROAD D8 SO BURLINGTON VT 05403	1
ATTN JUAN AMENABAR SAIC 1700 N MOORE ST STE 1820 ARLINGTON VA 22209	1
ATTN TECHNICAL LIBRARY TELEDYNE RYAN AERONAUTICAL 2701 HARBOR DRIVE SAN DIEGO CA 92138	1
INTERNAL	
B	1
B44	1
B44 (PRIOLO)	1
B44 (HSIEH)	1
B44 (WARDLAW)	1
C	1
D	1

DISTRIBUTION (CONT.)

	Copies
D4	1
A	1
B05 (STATON)	1
B51 (ARMISTEAD)	1
E231	3
E281 (SWANSBURG)	1
E282 (WAITS)	1
F	1
G	1
G02	1
G04	10
G05	1
G06	1
G20	1
G205	1
G23	1
G23 (CHADWICK)	1
G23 (DEVAN)	1
G23 (GRAFF)	1
G23 (HARDY)	1
G23 (HYMER)	50
G23 (MCINVILLE)	1
G23 (OHLMEYER)	1
G23 (ROWLES)	1
G23 (WEISEL)	1
G30	1
G40	1
G50	1
G60	1
G70	1
G73	1
K	1
K10	1
K20	1
K204	1
N	1
N74 (GIDEP)	1

REPORT DOCUMENTATION PAGE

Form Approved
OMB No. 0704-0188

1. AGENCY USE ONLY *(Leave blank)*	2. REPORT DATE	3. REPORT TYPE AND DATES COVERED
	February 1995	Final

4. TITLE AND SUBTITLE
The 1995 Version of the NSWC Aeroprediction Code: Part I-Summary of New Theoretical Methodology

5. FUNDING NUMBERS

6. AUTHOR(S)
Frank G. Morre, Roy M. McInville, Tom Hymer

7. PERFORMING ORGANIZATION NAME(S) AND ADDRESS(ES)
Naval Surface Warfare Center
Dahlgren Division, G04
17320 Dahlgren Road
Dahlgren, VA 22448-5100

8. PERFORMING ORGANIZATION REPORT NUMBER
NSWCDD/TR-94/379

9. SPONSORING/MONITORING AGENCY NAME(S) AND ADDRESS(ES)

10. SPONSORING/MONITORING AGENCY REPORT NUMBER

11. SUPPLEMENTARY NOTES

12a. DISTRIBUTION/AVAILABILITY
Approved for public release; distribution is unlimited.

12b. DISTRIBUTION CODE

13. ABSTRACT *(Maximum 200 words)*

The NSWC Aeroprediction Code has been extended to angles of attack (AOA) greater than 30 deg. To accomplish this, several data bases were used to approximate the nonlinearities in individual missile component aerodynamics. Theoretical aerodynamic methods are used at small AOA. The new semiempirical model was applied to several configurations and the empirical constants adjusted to eliminate some of the errors associated with wind tunnel measurements of individual missile component loads.

The new version of the code (AP95) was then applied to several other missile configurations and estimates compared to data and other aerodynamic code calculations. Comparisons were made for Mach numbers 0.1 to 10.0 and AOA of 0 to 90 deg (not all data were available on any single configuration). In general, average accuracy levels of ± 10 percent could be obtained for axial and normal force coefficient and ± 4 percent of body length for center of pressure, using the AP95. An exception to this was at AOA above 30 deg and at high supersonic Mach numbers, where nonlinearities caused by internal shock interactions were not accounted for. While these accuracy levels are very encouraging for a semiempirical code, improvements on the AP95 methodology could be made by additional missile-component wind-tunnel data at high AOA.

14. SUBJECT TERMS
Aeroprediction, Theoretical Methodology, slender-body theory, angles of attack, nonlinearities, missile component loads, aerodynamics, semiempirical, empirical, missile configuration, normal force coefficient, and wing-alone model

15. NUMBER OF PAGES
110

16. PRICE CODE

17. SECURITY CLASSIFICATION OF REPORT	18. SECURITY CLASSIFICATION OF THIS PAGE	19. SECURITY CLASSIFICATION OF ABSTRACT	20. LIMITATION OF ABSTRACT
UNCLASSIFIED	UNCLASSIFIED	UNCLASSIFIED	SAR

GENERAL INSTRUCTIONS FOR COMPLETING SF 298

The Report Documentation Page (RDP) is used in announcing and cataloging reports. It is important that this information be consistent with the rest of the report, particularly the cover and its title page. Instructions for filling in each block of the form follow. It is important to ***stay within the lines*** to meet ***optical scanning requirements***.

Block 1. Agency Use Only *(Leave blank)*.

Block 2. Report Date. Full publication date including day, month, and year, if available (e.g. 1 Jan 88). Must cite at least the year.

Block 3. Type of Report and Dates Covered. State whether report is interim, final, etc. If applicable, enter inclusive report dates (e.g. 10 Jun 87 - 30 Jun 88).

Block 4. Title and Subtitle. A title is taken from the part of the report that provides the most meaningful and complete information. When a report is prepared in more than one volume, repeat the primary title, add volume number, and include subtitle for the specific volume. On classified documents enter the title classification in parentheses.

Block 5. Funding Numbers. To include contract and grant numbers; may include program element number(s), project number(s), task number(s), and work unit number(s). Use the following labels:

C	- Contract	**PR**	- Project
G	- Grant	**TA**	- Task
PE	- Program Element	**WU**	- Work Unit Accession No.

BLOCK 6. Author(s). Name(s) of person(s) responsible for writing the report, performing the research, or credited with the content of the report. If editor or compiler, this should follow the name(s).

Block 7. Performing Organization Name(s) and address(es). Self-explanatory.

Block 8. Performing Organization Report Number. Enter the unique alphanumeric report number(s) assigned by the organization performing the report.

Block 9. Sponsoring/Monitoring Agency Name(s) and Address(es). Self-explanatory.

Block 10. Sponsoring/Monitoring Agency Report Number. *(If Known)*

Block 11. Supplementary Notes. Enter information not included elsewhere such as: Prepared in cooperation with...; Trans. of...; To be published in... . When a report is revised, include a statement whether the new report supersedes or supplements the older report.

Block 12a. Distribution/Availability Statement. Denotes public availability or limitations. Cite any availability to the public. Enter additional limitations or special markings in all capitals (e.g. NOFORN, REL, ITAR).

DOD	- See DoDD 5230.24, "Distribution Statements on Technical Documents."
DOE	- See authorities.
NASA	- See Handbook NHB 2200.2
NTIS	- Leave blank

Block 12b. Distribution Code.

DOD	- Leave blank.
DOE	- Enter DOE distribution categories from the Standard Distribution for Unclassified Scientific and Technical Reports.
NASA	- Leave blank.
NTIS	- Leave blank.

Block 13. Abstract. Include a brief ***(Maximum 200 words)*** factual summary of the most significant information contained in the report.

Block 14. Subject Terms. Keywords or phrases identifying major subjects in the report.

Block 15. Number of Pages. Enter the total number of pages.

Block 16. Price Code. Enter appropriate price code ***(NTIS only)***

Block 17.-19. Security Classifications. Self-explanatory. Enter U.S. Security Classification in accordance with U.S. Security Regulations (i.e., UNCLASSIFIED). If form contains classified information, stamp classification on the top and bottom of this page.

Block 20. Limitation of Abstract. This block must be completed to assign a limitation to the abstract. Enter either UL (unlimited or SAR (same as report). An entry in this block is necessary if the abstract is to be limited. If blank, the abstract is assumed to be unlimited.